ANALYSIS, MODIFICATION AND IMPROVEMENT OF PERFORMANCE

OF A CLOSED, REGENERATIVE, RECIPROCATING BRAYTON CYCLE ENGINE

by

KANGPIL LEE

B.S., Seoul National University
(1972)

S.M., Massachusetts Institute of Technology
(1974)

SUBMITTED IN PARTIAL FULFILLMENT

OF THE REQUIREMENTS FOR THE

DEGREE OF DOCTOR OF PHILOSOPHY

at the

MASSACHUSETTS INSTITUTE OF TECHNOLOGY

MAY, 1978

© MASSACHUSETTS INSTITUTE OF TECHNOLOGY 1978

Signature of Author...
Department of Mechanical Engineering, May 15, 1978

Certified by..
Thesis Supervisor

Accepted by...
Chairman, Departmental Committee on Graduate Students

ANALYSIS, MODIFICATION AND IMPROVEMENT OF PERFORMANCE
OF A CLOSED, REGENERATIVE, RECIPROCATING BRAYTON CYCLE ENGINE

by

KANGPIL   LEE

Submitted to the Department of Mechanical Engineering
in May, 1978 in partial fulfillment of the requirements
for the Degree of Doctor of Philosophy

ABSTRACT

The VHGE is a closed, regenerative, reciprocating Brayton
cycle engine using helium as the working gas. Preliminary
analysis shows that this engine is competitive with the Stirl-
ing engine in terms of low pollution, high efficiency, and
power density. The prototype one cylinder engine was built in
1972, and tested at low power. The causes of the low efficien-
cies achieved in the tests have been under investigation since
1972.

Piston ring leakage was first suspected as the cause, but
the tests and analyses reported in this thesis show that cyclic
heat transfer between the gas and the cylinder walls is the
dominant cause of the low efficiency. Compressor and expander
performance have been correlated with the magnitude of the

2

cyclic heat transfer. Modifications of the compressor configuration to decrease the cyclic heat transfer improved the compressor efficiency from 60% to 83% and the indicated engine efficiency from 21% to 33%.

The results indicate that indicated engine efficiency could approach the expected 47% by means of further reduction of cyclic heat transfer in both the expander and the compressor.

Thesis Supervisor

Joseph L. Smith, Jr.

Professor of Mechanical Engineering

3

TABLE OF CONTENTS

LIST OF TABLES

LIST OF FIGURES

ACKNOWLEDGEMENTS

I would like to thank the members of my thesis committee, Professor J.L. Smith, Professor D.G. Wilson, Professor J.B. Heywood, and Professor D.P. Hoult, for their guidance and adivice. Especially, my theis supervisor, Professor Smith has been very kind and willing to provide stimulus and encouragement to overcome various difficulties in the course of the study.

I would also like to thank my fellow students of the Cryogenics Laboratory for their helpful suggestions, and in particular, Mr. Henry Faulkner for his help during the engine tests. The technicians at the Cryogenics Laboratory, Mr. Karl Benner and Mr. Bob Gersten are thanked for the help with their expertise.

I would like to thank my wife, Jaeok, who has helped and encouraged me through the past four difficult years, and also typed the entire thesis.

During my study for this work, I was supported by a research assistantship from the Cryogenics Laboratory. I am deeply grateful to Professor Smith for the financial support.

GLOSSARY OF SYMBOLS

A	Heat transfer area
A_c	Compressor volume per unit displacement
A_w	Cross-section area of the thermocouple wire
b	h/k
C	Discharge coefficient for the orifice ; Celsius
c	Specific heat of the plate
C_d	Drag coefficient
c_p	Specific heat of gas at constant pressure
c_v	Specific heat of gas at constant volume
C_0	$(\gamma - 1)/\gamma$
C_1	C_0 / ξ_c
C_2	C_0 / ξ_e
c.v.	Control volume
D	Thermocouple bead diameter ; tube diameter
d	Thermocouple wire diameter ; diameter of the orifice
E	Total energy of the gas
E_f	Expansion factor of the gas due to compressibility
F	Radiation view factor
F_a	Thermal expansion factor of the orifice metal
F_{bead}	Drag force due to thermocouple bead
F_d	Drag force
F_{wire}	Drag force due to thermocouple wire
g_c	Gravitational proportionality constant

13

H	Total enthalpy ; heat stored in half a cycle
h	Specific enthalpy ; heat transfer coefficient
ΔH	Change of total enthalpy
I	Moment of inertia
I.D.	Inner diameter
j	$\sqrt{-1}$
K	Kelvin
k	Thermal conductivity ; wavelength constant
k_s	Average thermal conductivity of thermocouple wires
L	Length of the thermocouple wire exposed to the gas
L_c	Connecting rod length
L.P.	Low pressure
M	Mach No.
m	Mass of gas
$\dot{m}$	Mass flow rate
$\dot{m}_f$	Mass flow rate of the engine
M_{max}	Maximum bending moment
N_u	Nusselt No.
n_1, n_2	Polytropic index
O.D.	Outer diameter
P	Pressure
p	Acoustic pressure
$p(x,t)$	Acoustic pressure as a function of x,t
ΔP	Pressure difference
P_d	Mean discharge pressure
P_h	Expander inlet pressure

14

P_i	Mean intake pressure
P_L	Compressor inlet pressure
P_r	The ratio P_h/P_L
Pr_g	Prandtl No. for the gas
$P_{ref.}$	Reference pressure for entropy
$\dot{Q}$	Heat transfer rate
$q(x,t)$	Acoustic volume flow rate
$\dot{Q}_c$	Net heat transfer rate for the compressor
$\dot{Q}_e$	Net heat transfer rate for the expander
$\dot{Q}_{cooler}$	Cooling water heat removal rate of the cooler
Q_{cyclic}	Magnitude of cyclic heat transfer rate
$\dot{Q}_{environ,i}$	Rate or heat loss to the environment from control volume i
$\dot{Q}_{heater}$	Rate of electrical heat input to the heater
Q_{net}	Net heat input to the compressor per cycle
$\dot{Q}_{pm}$	Rate of heat transfer during process p for mass portion m
$\dot{Q}_{water}$	Cooling water heat removal rate
$\dot{Q}_+$	Rate of heat transfer into the gas
$\dot{Q}_-$	Rate of heat transfer out of the gas
R	Gas constant (PV / mT)
r	One half the engine stroke
Re_d	Reynolds No. based on d
R.H.Ex.	Regenerative heat exchanger
RPS	Engine revolution per second
S	Specific entropy
S_1, S_2	Cross-sectional area of the pressure tap chambers

15

T	Temperature of the gas
t	time
T.C.	Thermocouple
T_d	Mean discharge temperature of the compressor
T_{ei}	Effective intake temperature
T_{ed}	Effective discharge temperature
T_h	Expander intake temperature
T_{in}	Inlet temperature
T_j	Thermocouple junction temperature
T_L	Compressor inlet temperature
T_{out}	Outlet temperature
$T_{ref.}$	Reference temperature for entropy
T_w	Wall temperature
ΔT	Temperature difference
ΔT_c	Conduction error for thermocouple
$\Delta T_{comp.}$	Temperature difference between inlet and outlet compressor
$\Delta T_{exp.}$	Temperature difference between inlet and outlet expander
ΔT_r	Radiation error for thermocouple
ΔT_t	Transient error for thermocouple
ΔT_v	Velocity error for thermocouple
V	Volume of the gas
V_d	Discharge displacement
V_i	Intake displacement
$v_{p,max}$	Maximum piston velocity

$\dot{W}_{brake}$	Brake engine power
$\dot{W}_c$	Compressor indicated power
$\dot{W}_{c.v.}$	Rate of work transfer for control volume
$\dot{W}_{linkage}$	Linkage power loss of the engine
$\dot{W}_{nc}$	Reversible polytropic compressor power
$\dot{W}_{ne}$	Reversible polytropic expander power
$\dot{W}_{pm}$	Rate of work transfer during process p for mass portion m
$\dot{W}_{sc}$	Isentropic compressor power
$\dot{W}_{se}$	Isentropic expander power
α	Thermal diffussivity
β	Ratio orifice diameter d/ pipe diameter D
γ	Ratio of specific heats c_p/c_v
ε	Emissivity
η	Efficiency
η_c	Adiabatic efficiency of the compressor
η_e	Adiabatic efficiency of the expander
η_i	Indicated engine efficiency
η_{nc}	Polytropic efficiency of the compressor
η_{ne}	Polytropic efficiency of the expander
η_R	Regenerative heat exchanger effectiveness
η_v	Actual volumetric efficiency
θ	Temperature above average plate temperature
θ	Crank angle
θ_{ma}	Temperature amplitude of the medium
ξ_c	Polytropic coefficient of the compressor

17

ξ_e	Polytropic coefficient of the expander
ρ	Density of plate
ρ_g	Density of gas
σ	Normal stress
σ_{max}	Maximum normal stress
τ	Shear stress, time
τ_{max}	Maximum shear stress
τ_0	Characteristic response time for a thermocouple
ω	Angular speed

CHAPTER I. INTRODUCTION

1. History, Description of the Engine

The new valved hot-gas engine (VHGE) was constructed (1) at the Cryogenics Laboratory, M.I.T. in 1972 as a byproduct of many years of work in the laboratory on closed cycle engines and refrigerators. Studies on VHGE have been presented as theses (1,2,3,4) and a paper (5). The VHGE concept evolved from the idea of adding valves to the Stirling engine to overcome some of its practical limitations.*

The engine consists of a reciprocating expander/compressor, a heater, a cooler, and a regenerative heat exchanger as shown in Fig. I-1.** The compressor has spring-loaded check valves and the expander has cam-operated poppet valves.

The working gas undergoes a thermodynamic cycle close to ideal Brayton cycle. Ideally, the gas gets heated in the heater under constant-pressure followed by isentropic expansion in the expander, constant pressure regenerative cooling in the regenerative heat exchanger. The gas gets further cooled in the cooler under constant pressure, followed by isentropic compression and constant-pressure regenerative heating in the regenerative heat exchanger before the gas enters the heater to reach the maximum temperature (see Fig. I-2).

---

* For comparison between the VHGE and the Stirling engine, refer to reference 1.

** Taken from reference 1.

19

57.15 cm

8.89 cm

Heater

H_2O

Expander

8.26 cm

Regenerative
Heat Exchanger

12.7
cm

102.
cm

H_2O

H_2O

Cooler

Compressor

12.7cm

To
A

To low pressure
accumulator

63.5 cm

To high pressure
accumulator

To A
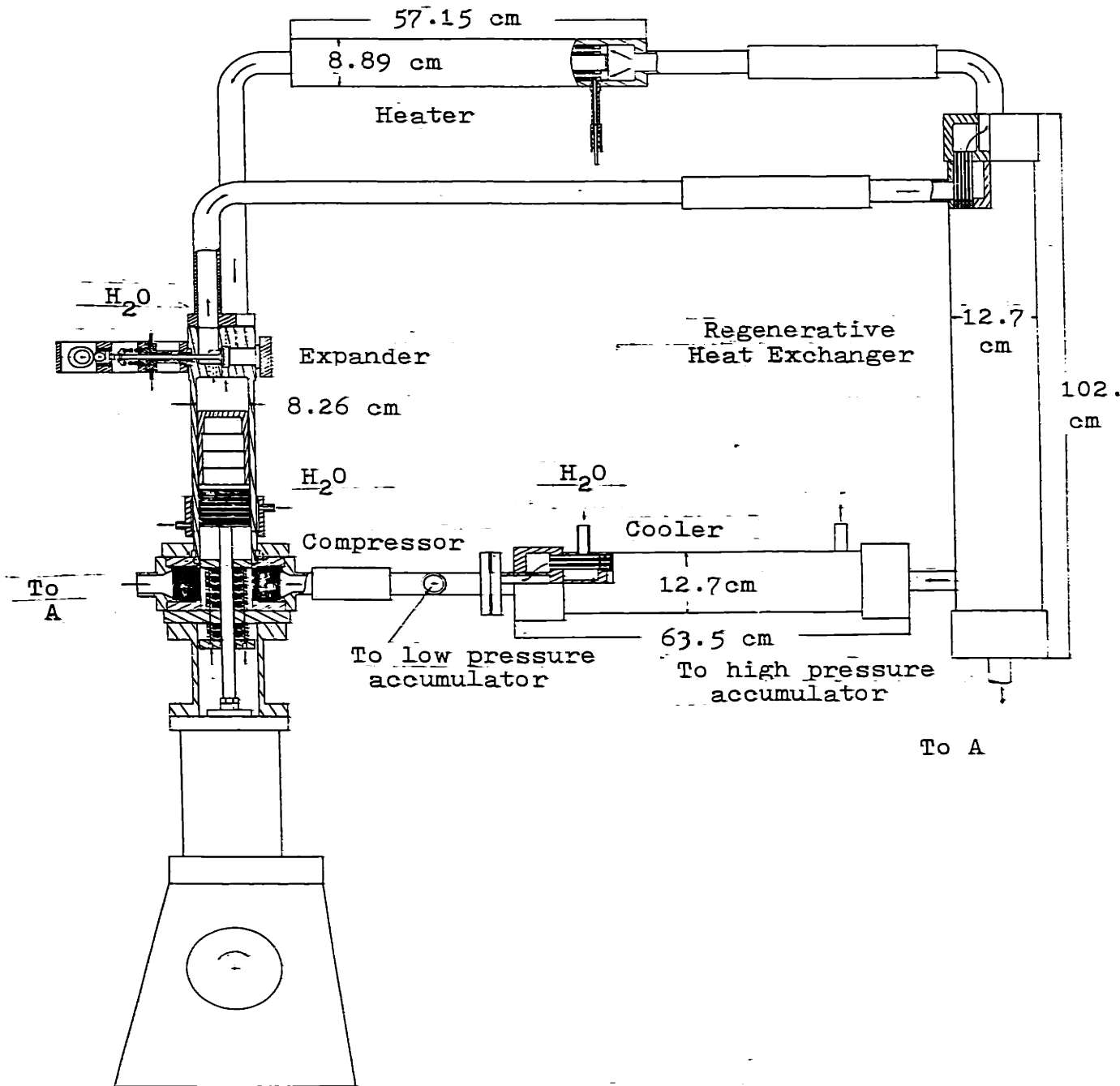
Fig. I-1 Prototype configuration of VHGE

20
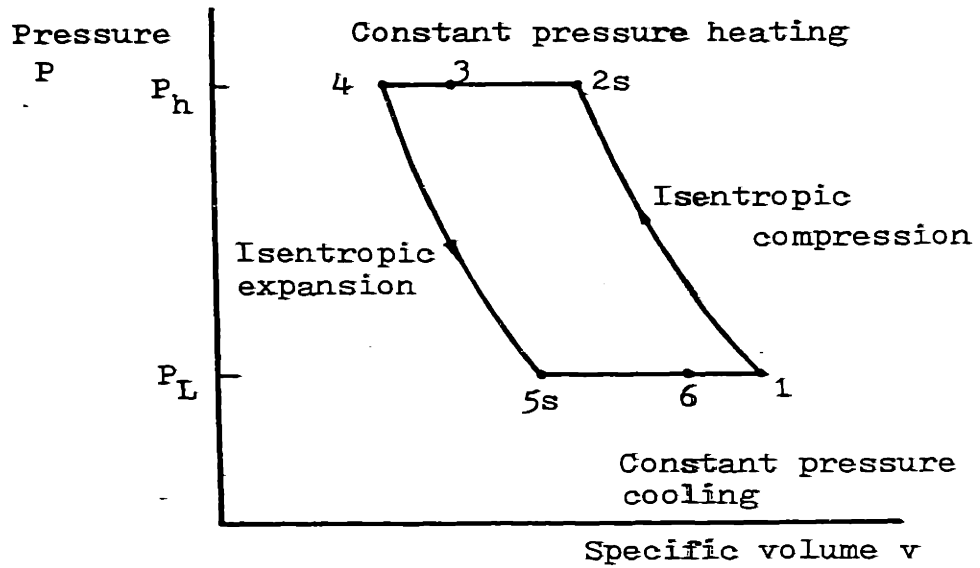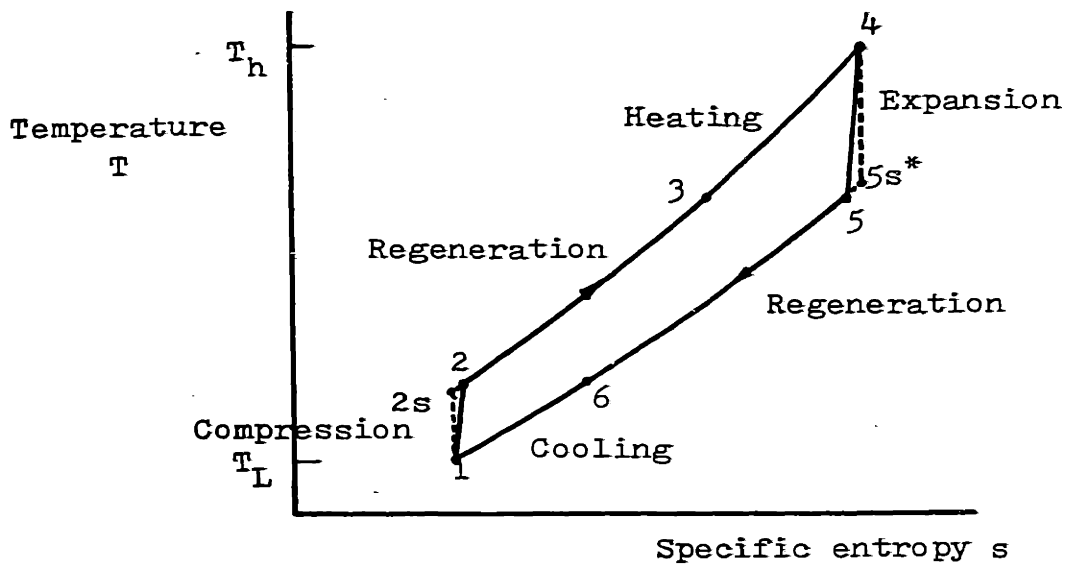
Fig. I-2   T-s, P-v diagram of VHGE

* s denotes isentropic process.

2. Objectives

The ultimate objective of this engine project is to realize the potential of the VHGE concept as a power plant for transportation vehicles or other energy conversion systems.

The immediate objective is to find the causes of low performance of the first generation VHGE and to improve the efficiency sufficiently to warrant further research on this type of external combustion engine, which seems to have a potential equal to the Stirling engine. It is hoped that careful documentation of the problems encountered in the work on this engine will be of benefit to others working on similar equipment.

3. Problems and Approaches

The low-power tests (12kW) showed consistently low efficiency* for a range of speeds, mean pressure, and temperature (2). The following symptoms were generally observed : (a) About 10% more heater power than expected was required to reach the designed operating conditions ; (b) the compressor power from the indicator diagram was about 1.8 times that expected; and (c) the compressor clearance volume had to be set at its minimum in order to reach the designed pressure ratio of 2:1. Further analysis of the data revealed the following : (d) about 10% of total heater power input could not be accounted for in the energy balance of the engine and (e) the "apparent mass

* η_i = 20.8% based on net heat input to the engine (Test #1)

22

flow rates" through the engine components differed from one
another significantly as shown in Table I-1.

Table I-1   Apparent Mass Flow Rates in terms of
           Cooler Flow Rate (Test #1, (1))

Expander intake	99%	Compressor intake	136%
Expander discharge	98%	Compressor discharge	148%
R.H.Ex. (H.P.)	111%	Heater	111%
R.H.Ex. (L.P.)	107%		

These mass flow rates are called as such because they
are not actual flow rates but the flow rates calculated using
average temperatures, pressures measured external to the com-
ponents, and for the expander and the compressor the volume
changes as well during intake and discharge. In the beginning,
the piston-ring leakage between the expander and the compressor
was suspected to be the main cause of the discrepancies in
apparent mass flow rates, and also of the low efficiency. But
a series of leakage tests showed that the leakage alone did
not account for the engine performance (1,3,4).

Measurements of the transient gas temperatures inside
cylinder showed significant spatial variation in the temperature.
The compressor head was cooled by a water jacket to show the
effect of internal heat transfer. The significant changes in
compressor and expander performance point to the internal heat

23

transfer as a very important factor.

In order to analyze the effect of heat transfer separately, the piston-ring leakage was eliminated by means of a temporary rubber O-ring piston seal. The zero-piston-ring-leakage test did not show any significant increase in compressor indicated efficiency. The compressor was found to be far from adiabatic, with a cyclic heat transfer at a rate on the order of the compressor power. In the expander, the cyclic heat-transfer rate was about half that of the compressor.

On the basis of this evidence, the compressor was modified to decrease the cyclic heat transfer inside compressor. The result was a drastic increase in compressor efficiency. Instantaneous mass flow rates were also measured at the compressor inlet and outlet during tests of the modified compressor. These more complete and accurate tests also corrected the energy balance and resolved the discrepancies in the apparent mass flow rates.

Chapter II PERFORMANCE EVALUATION AND IMPROVEMENT OF THE ENGINE

1. Experiments Performed

1) Leakage measurement

The aforementioned discrepancy in the apparent mass flow rates through engine components implied a significant gas leakage between expander and compressor past the polyimide piston rings. Static leakage rates past piston rings were measured to be about 5% of the engine mass flow rate (3). In order to simulate the reversal of the pressure difference during normal engine operation, the sign of ΔP across the piston was changed abruptly by pressurizing or depressurizing either the compressor or expander (4). The dynamic-leakage rate, estimated from the pressure-time trace, was on the order of 10% of the engine mass flow rate. Direct applicability of the result to the actual engine was questionable, however, because the pressure reversal occurs much faster during engine operation causing the piston rings to move rapidly across the grooves.

2) Transient gas-temperature measurement

After the inconclusive leakage tests, it was decided to take transient gas-temperature data inside the cylinder. Fast-response thermocouple probes of special design were fabricated using 25.4 μm O.D. chromel alumel wires, insulated with alumina ceramic tubes and protected by Inconel tubes. They were design-

ed to minimize the inherent errors due to conduction, radiation, velocity, and transients effect. The response time was less than a millisecond based on the flow conditions during the intake and discharge period. At first, four probes were inserted into the cylinder: one inside each expander port, and two inside the annular space of the compressor near each valve. (T.C. 1, T.C. 2 in Fig.II-1. (a)). Expander temperature data thus obtained show a significant temperature drop during the intake process, indicating significant negative heat transfer. Curiously, average compressor-inlet-and-exhaust temperature data do not show significant deviation from the isentropic case. However, it was the excessive compressor power (1.8 times the expected (1)), that was responsible for the low efficiency rather than the expander. Later tests with two additional probes (T.C. 3, T.C. 4 in Fig.II-1. (a)) into the edge of the main compressor space, revealed a significant spatial temperature variation inside the compressor (Fig.II-2) and a much higher temperature fluctuation in the main space than the annular space where the original two thermocouples were located. This information on cylinder gas temperature motivated further study of the internal heat-transfer problem.

3) Cooled-compressor test (Test #2)

During the measurements of the transient gas temperatures, additional performance data were obtained with a cooling-water jacket around the compressor block (Fig.II-1). The increased

26

(a)   (b)
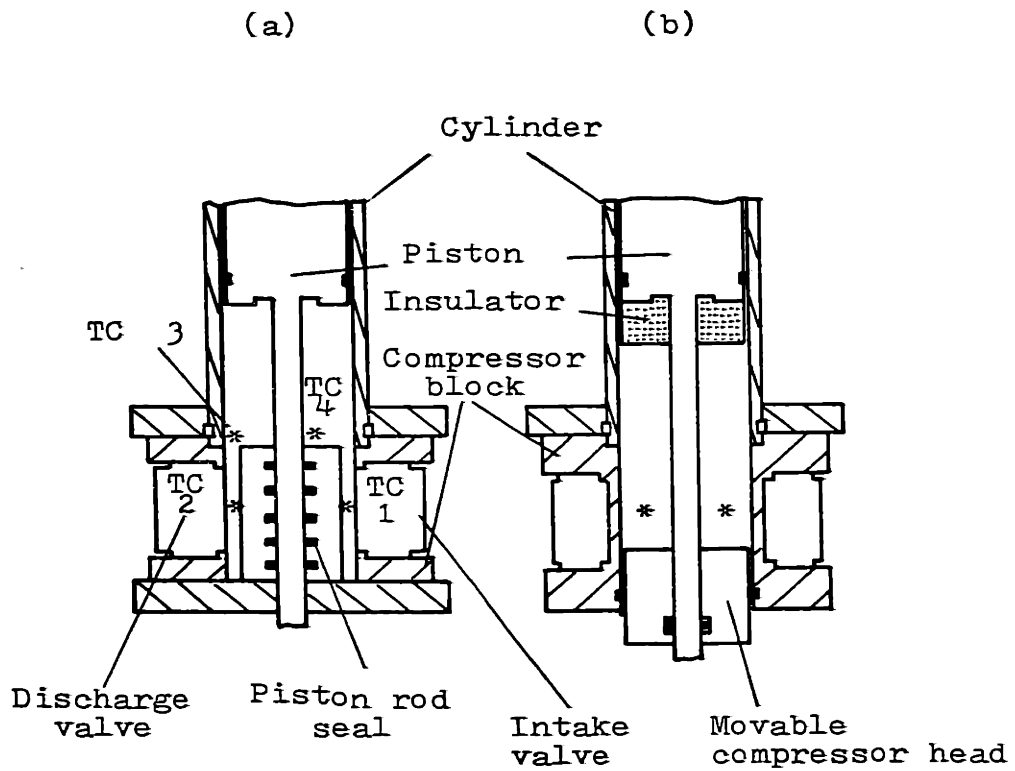
Fig. II-1 Compressor of VHGE before(a) and after(b)
           modification

* denotes location of thermocouples
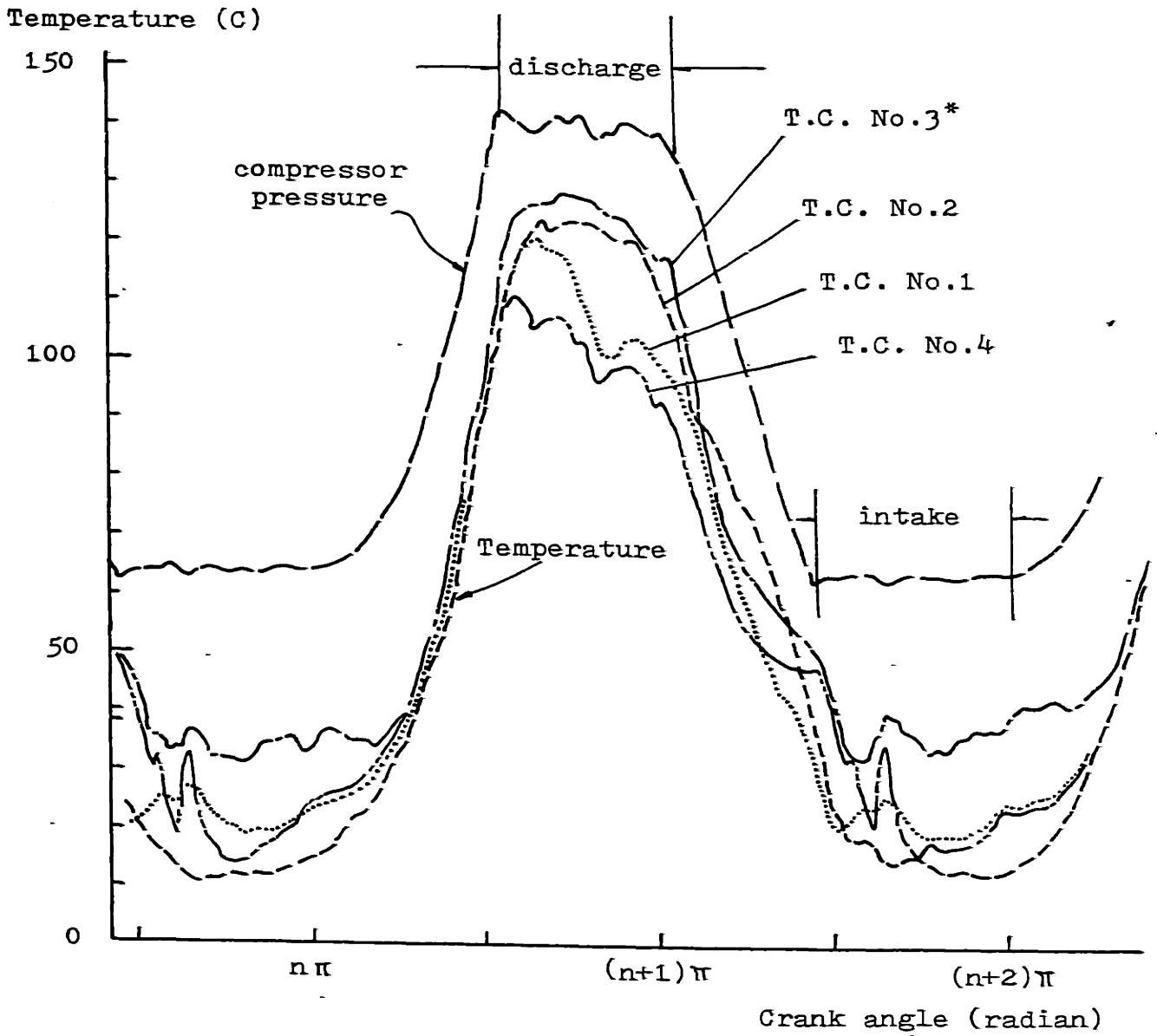
Fig. II-2   Temperature measurement at 4 locations inside
compressor before modification (Test #3)

* See Fig. II-1.

28

compressor cooling increased the overall indicated engine efficiency from 20.8% (Test #1) to 25.9%. The compressor adiabatic efficiency increased from 59% (Test #1) to 70% due to cooling, whereas, the expander adiabatic efficiency fell from 97% (Test #1) to 88%. The unusually high expander efficiency of test #1 was attributed to a favorable effect from the leakage into the expander. However, in Test #2, the temperature of the leaking gas dropped due to increased cooling of compressor which probably caused the drop in expander efficiency.

4)   Zero-piston-ring-leakage test (Test #3)

One of the observation from Test #2 was that the compressor efficiency increased by 11% as a result of cooling the wall even though piston-ring leakage was present. In subsequent tests, the piston-ring leakage was eliminated by the use of a rubber O-ring to study the heat-transfer phenomena inside the cylinder without uncertain leakage. One of the four grooves for the polymide rings was filled with fiber-glass-reinforced epoxy up to appropriate depth to accommodate a rubber O-ring. A felt O-ring soaked into O-ring lubricant was placed in the adjacent groove. After the installation, the piston seal was thoroughly checked for possible leakage by both static and dynamic test, and proved to be quite satisfactory. One problem with the O-ring was that the O-ring swept area had to be maintained relatively cool to prevent early failure; thus the

cylinder water jacket was extended closer to the expander section of the cylinder. The increased cooling of the expander limited the improvement so that the increase in expander efficiency for no leakage was moderate (88.1% to 90.5%). The compressor efficiency remained virtually the same (69.7% to 69.8%), and the overall efficiency increased from 25.9% to 27.7%. The slight changes in efficiency implies that once the compressor is cooled sufficiently, leakage was not an important parameter but the internal cyclic heat transfer was. This point will be treated in detail in a later section on cyclic heat transfer.

5) Modified compressor test (Test #4, #5, #6)

The results of the internal cyclic heat-transfer analysis (Fig.Ⅱ-7,Fig.Ⅱ-8) show that an increase in the efficiency requires a decrease in the magnitude of the cyclic heat transfer. The following modifications of the compressor were made to reduce the cyclic heat transfer (Fig.Ⅱ-1): (a) Removal of the piston-rod-seal assembly. Elimination of the annular space. Replacement of the six polyimide piston-rod seals with a rubber O-ring: (b) Removal of the separate clearance-volume adjusting cylinder which extended horizontally and replacement with a movable compressor head complete with cooling water circuits and a O ring piston rod seal; (c) Insulation of the bottom face of the piston with a 3 cm layer of phenolic Micarta. The piston bottom face had been

30

suspected as one of the hot spots inside the compressor; and
(d) Replacement of the low carbon steel compressor block with
a newly fabricated brass block which had water cooling near
the inner surface and valve ports(see Fig. II-3). Because of
the new arrangement, it was possible to insert transient
temperature probes well inside the compressor volume. Thus,
the thermocouples recorded temperatures close to the bulk gas
temperature. The compressor adiabatic efficiency increased
significantly from 69.8% to 82.9% (Test #6), and the clearance
volume of compressor for the 2:1 pressure ratio increased
from $2.950 \times 10^{-4} \ m^3$ to $4.542 \times 10^{-4} m^3$ which was quite close to
the $5.244 \times 10^{-4} m^3$ for isentropic compression. Expander
efficiency decreased somewhat (90.5% to 86.7%) which could be
attributed to the following: (a) Lower intake temperature and
(b) More heat loss to the cylinder jacket. The indicated engine
efficiency based on net heat input to the engine was 33.3% in
Test #6.

2. Mass Flow Rate and Energy Balance

     Referring back to section I.3, the apparent mass flow
rates through engine components were quite different from one
another. The apparent mass flow rates for the heat exchange
components were calculated from the estimated heat fluxes and
the temperature changes across the component. The energy bal-
ance for the entire engine showed that about 10% of the total
heat input was unaccountable. The consistency with which the

31
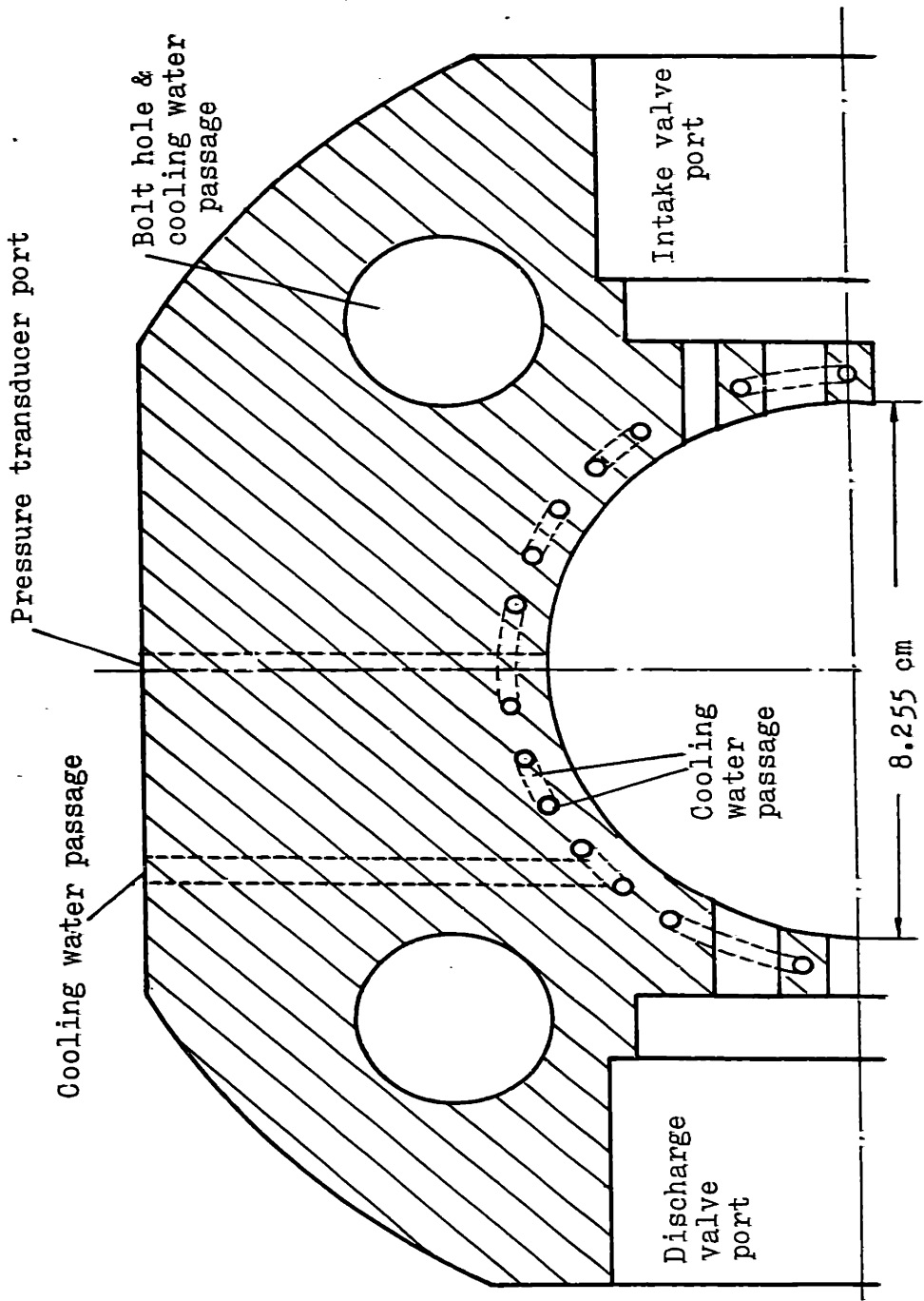
Fig. II-3 (a) New, effectively cooled compressor block (cross-sectional top view)

Intake valve port

Bolt hole & cooling water passage

Pressure transducer port

Cooling water passage

Cooling water passage

8.255 cm

Discharge valve port

32
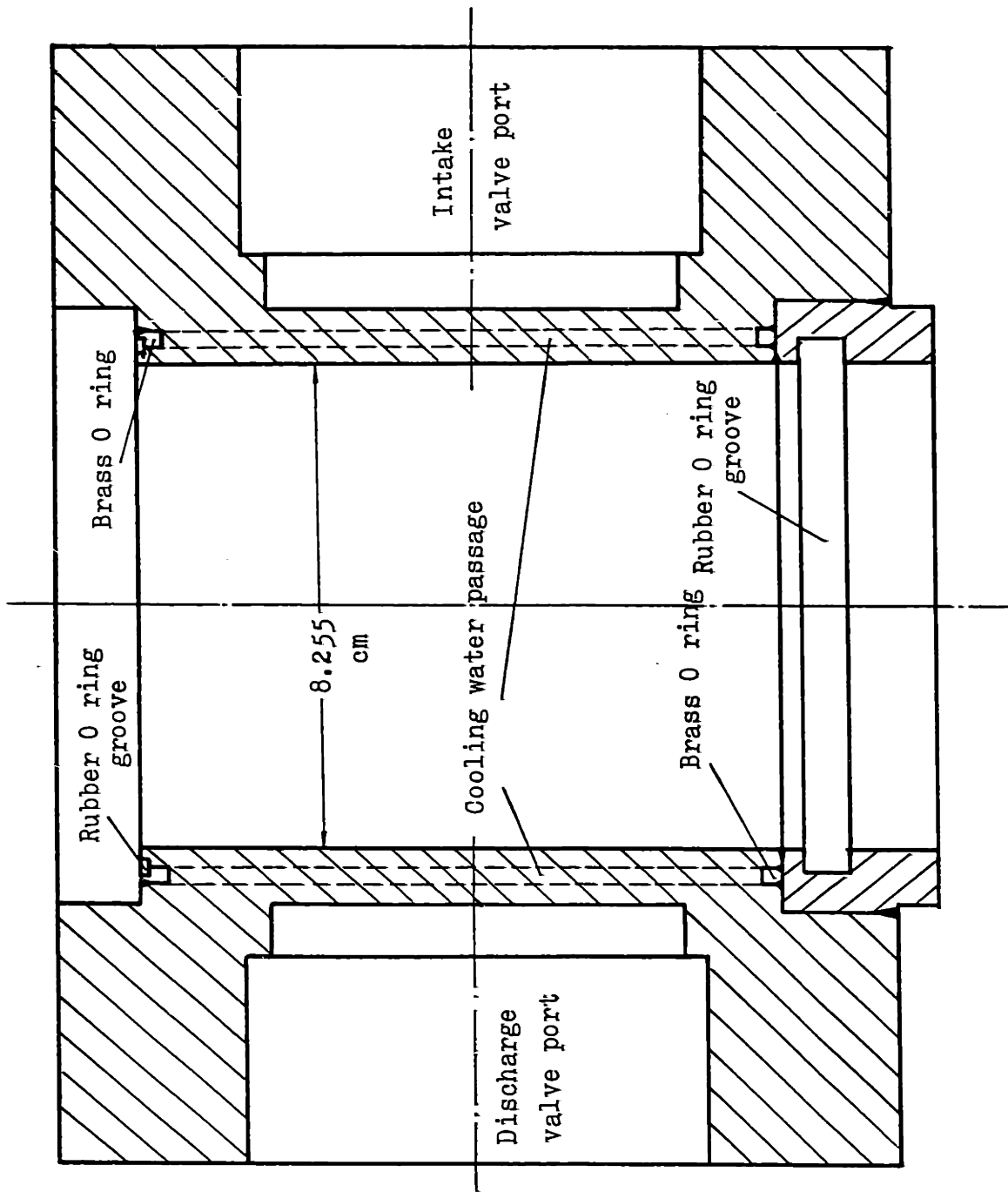
Fig. II-3(b) New, effectively cooled compressor block (cross-sectional sideview)

Intake valve port

Brass O ring

Rubber O ring groove

Rubber O ring groove

8.255 cm

Cooling water passage

Brass O ring

Brass O ring

Discharge valve port

33

apparent mass flow rate of the heater exceeded the apparent mass flow rate of the cooler indicated the heater heat leak into the environment was under-estimated. In addition, the temperature drop for the low-pressure stream of the regenerative heat exchanger always exceeded the temperature increase for the high-pressure stream. This was first attributed to an imbalance of the mass flow because of friction and leakage; however, the results did not change when the leakage was eliminated.

The other possibility was that the external heat leak for the regenerative heat exchanger had been underestimated. For Test #3, the gas temperatures indicated a 0.62 kW heat leak while conduction and convection calculations for the external insulation predicted only 0.15 kW. An error in estimating the external heat leak of both the heater and the regenerative heat exchanger also proved to be the cause of the error in the energy balance and the difference in calculated heater and cooler flow rates. This conclusion was proved by two tests, a heat-transfer flow test of the engine and a direct measurement of the mass flow rate.

1) Heat-transfer flow test*

In this test, the expander valves were blocked open so that the pressure inside the entire engine was nearly constant except for small flow-friction losses. The expander-inlet temperature was set at the average of the intake and discharge

* See Appendix A. 5 for detail.

temperature for normal operation, and the pressure was close
to normal low pressure. With the expander and compressor
powers essentially zero, the heat leaks of the engine could
be observed directly and the external heat leaks were verified,
0.35 kW for the regenerative heat exchanger and 0.88 kW for
the heater. However, a direct measurement was still needed
to confirm the actual engine flow rate.

2) Instantaneous mass flow measurement

Two square-edged orifices were installed, one before
and one after the compressor. The connecting tubes were
rearranged to provide adequate straight runs before and after
the orifices. Although orifices are not usually recommended
for pulsating flow, the actual gas flow through the orifice
was nearly quasistatic at any given time. The instantaneous
flow was accurately indicated because the natural frequency of
the differential-pressure transducer (6000 Hz) and of the trans-
ducer pressure taps (1400 Hz) were much higher than the flow
pulsating frequencies (10 Hz due to engine speed, 300 Hz due
to valve motion). The error due to pulsation was estimated
to be at most 1∿2%. The instantaneous mass flow rate was
calculated from the ΔP data of Test #5 and integrated in time
to yield 7.60×10^{-3} kg/sec for intake and 7.71×10^{-3} kg/sec
for discharge, while the cooler flow rate was 7.56×10^{-3}
kg/sec. Since the pulsating error is positive (6), the use
of the cooler-flow-rate calculation in preference to the heater-

flow-rate calculations is justified. For more detail on mass flow measurement, refer to section III.2.

3. Cyclic Heat Transfer Inside Cylinder

1) Evidences of cyclic heat transfer

The importance of internal heat transfer was well demonstrated by the marked changes in performance when the compressor block was first cooled (Test #2). The compressor adiabatic efficiency increased from 58.9% to 69.7%, and indicated engine efficiency increased from 20.8% to 25.9%.

The observed gas-temperature differences of up to 30 C (Fig.II-2) between different locations within the compressor indicate the reason for the continued low compressor efficiency. The lower temperature was in the annular space near the valves (Fig. II-2)   and the higher temperature was at the edge of the compressor swept volume. The high apparent mass flow of the compressor* compared to actual flow indicated an even higher gas temperature in the swept volume where thermocouples could not be located. The implication of the temperature gradient in the gas inside the compressor was that a significant internal heat transfer was taking place between the gas and the walls of the compressor. The nature of the heat transfer was cyclic in time: heating during reexpansion and intake, cooling during compression and discharge. The temperature data indicated a similar heat transfer in the expander with the incoming gas cooled by as much as 100 C during intake. However, the

* See Table I-1.

average discharge temperature recorded outside the expander
was very close to the reversible adiabatic temperature, indicating a significant reheating of the gas during expansion and
discharge.

2) Mechanism of cyclic heat transfer

The simplest explanation of the cyclic heat transfer is
that the inside walls of the compressor and expander are operating as a thermal regenerator, extracting heat from the gas in
the cylinder when the gas is hotter than the wall, storing
the heat in the wall, and returning the heat to the gas when
the gas is colder than the wall. The simplest analysis of this
action is to consider an infinitely thick plate in contact with
a fluid experiencing a periodic change of temperature.

The unsteady conduction equation is $\frac{\partial \Theta}{\partial \tau} = \alpha \frac{\partial^2 \Theta}{\partial x^2}$ and the
boundary condition at the surface is $k \left. \frac{\partial \Theta}{\partial x} \right]_0 = h \Delta \Theta \big]_0$. The heat
energy stored in half a cycle can be expressed as (7),

$$H = \frac{1}{\omega} \rho \, ck \, \Delta\Theta_{ma} \, Y, \qquad (\text{II} - 1)$$

where Θ_{ma} is the temperature amplitude of the medium, Θ is the
temperature above the average plate-surface temperature which
is assumed to be equal to the average of medium temperature, τ
is time, α is the thermal diffusivity, k is the thermal conductivity of plate, h is the heat-transfer coefficient, ω is the
angular speed   of the temperature pulsation, and ρc is the
thermal capacity of plate. The ratio of temperature amplitude
of the plate surface to that of the medium, Y, can be expressed

37

as

$$Y = (1 + 2a/b + 2(a/b)^2)^{-0.5} \; ;$$
$$a \equiv (\alpha/\omega)^{0.5} \; ; \quad b \equiv h/k.$$

For the actual processes, equation II-1 cannot be applied directly because the wall temperature at an instant of time is not uniform throughout and usually the local time-average wall temperature is not the same as the local average gas temperature. Furthermore, the gas flows by different parts of the cylinder so that the gas sees a certain wall temperature distribution along the flow path. Flow past a wall with a temperature distribution but with little change in local temperature (i.e. low Y) can create the effect in the gas of a wall of uniform temperature that has high surface-temperature amplitude (i.e. high Y) facing a quiescent gas undergoing temperature fluctuation. This means that the wall-temperature distribution can enhance or inhibit heat transfer.

The above argument and equation II-1 show how to design a compressor and expander to decrease the internal cyclic heat transfer: (a) Decrease heat-transfer surface area A, by decreasing the surface-to-volume ratio; (b) use a material with a low $\rho c k$ for the inside wall; (c) maintain proper wall temperature distribution; and (d) decrease the heat transfer coefficient h by reducing the turbulence level. This involves change in flow pattern, proper choice of the shape of the chamber, and location, direction and size of the valves.

3) Effective intake temperature, Effective discharge temperature

In both expander and compressor, inlet density or outlet density, measured external to the cylinder, can be combined with the volume changes during intake or discharge to calculate "apparent mass flow rates". Apparent mass flow rates thus calculated are significantly different from actual mass flow rate. In view of this, it was appropriate to introduce new temperatures which will better represent the conditions inside the cylinder during intake or discharge. The effective intake temperature T_{ei} is defined as the mean gas temperature which will give correct average mass flow rate during intake. The effective discharge temperature T_{ed} is defined similarly.

$$T_{ei} \equiv \frac{\overline{P}_i \, \Delta V_i}{m_f \, R} \qquad ; \qquad T_{ed} \equiv \frac{\overline{P}_d \, \Delta V_d}{m_f \, R} \qquad (\text{II-2})$$

where $\overline{P}_i$ is mean intake pressure ; $\overline{P}_d$ is mean discharge pressure ; ΔV_i is intake displacement ; ΔV_d is discharge displacement ; m_f is mass flow/cycle ; R is gas constant.

These new definitions are related to the effect of heat transfer on volumetric efficiency, n_v. Take the intake process for example :

$$n_v \equiv \frac{\text{actual mass drawn in}}{\text{displacement x inlet density}} = \frac{\Delta V_i}{\Delta V_D} \frac{\overline{P}_i}{P_i} \frac{T_i}{T_{ei}} \qquad (\text{III-3})$$

39

where T_i, P_i are inlet temperature, and inlet pressure respectively. The ratio $\Delta V_i/V_D$ is the effect of re-expansion. The ratio $\overline{P}_i/P_i$ is the effect of valve pressure drop and T_i/T_{ei} is the effect of heat transfer during intake. T_{ei} and T_{ed} for the engine tests are given in Table II-1 along with measured inlet temperature T_i, and discharge temperature T_d.

Table II-1 Effective Intake and Discharge Temperatures of
　　　　　Compressor

K	Test #1	Test #2	Test #3	Test #4	Test #5	Test #6
T_{ei}/T_i	412/296	402/297	400/293	317/288	314/287	302/280
T_{ed}/T_d	634/415	582/409	549/397	453/367	436/369	447/360

4) Cyclic heat-transfer estimate

Two methods will be used for estimating the amount of cyclic heat transfer for the compressor or expander, the equivalent isentropic method and the equivalent reversible polytropic method. The isentropic method is a very simple approach, requires minimum input data, but somewhat lacks the accuracy of the polytropic method which requires additional data on mass, pressure and volume.

(1) Equivalent isentropic method

This method models the observed heat-transfer effects

inside the cylinder by equivalent steadyflow processes. The compressor is modeled as a preheater, an isentropic steady-flow compressor and an aftercooler. The expander is modeled as a precooler, an isentropic expander, and an afterheater. Fig.II-4 and Fig.II-5 show the states and the model for the engine.

The cyclic heat transfer is calculated from measured values of P_h/P_L, T_1, T_2 and the actual indicated compressor power $\dot{W}_c$, where the states refer to Fig.II-4. The inlet temperature T_{1i} for the equivalent isentropic compression is adjusted so that the steady-flow isentropic compressor power $\dot{W}_{1i-2i} = \dot{W}_c$. The magnitude of cyclic heat transfer $\overline{Q}_{cyclic}$ is the average of the magnitude of heat transfer in preheater $|\dot{Q}_+|$ and the magnitude of heat transfer in the aftercooler $|\dot{Q}_-|$. Table II-2 lists the values of $\overline{Q}_{cyclic}$ for the compressor and the expander in non-dimensional form $X = \overline{Q}_{cyclic}/\Delta H$, where total-enthalpy change $\Delta H = H_2 - H_1$ for compressor, and $\Delta H = H_4 - H_5$ for expander. For examples of calculation using Equivalent Isentropic method, see Appendix C.

Table II-2 Magnitude of Cyclic Heat Transfer

(Equivalent Isentropic Method)

	Test #1	Test #2	Test #3	Test #4	Test #5	Test #6
X_c	2.01	1.31	1.69	1.46	0.97	0.93
X_e	0.12	0.37	0.27	0.22	0.46	0.41
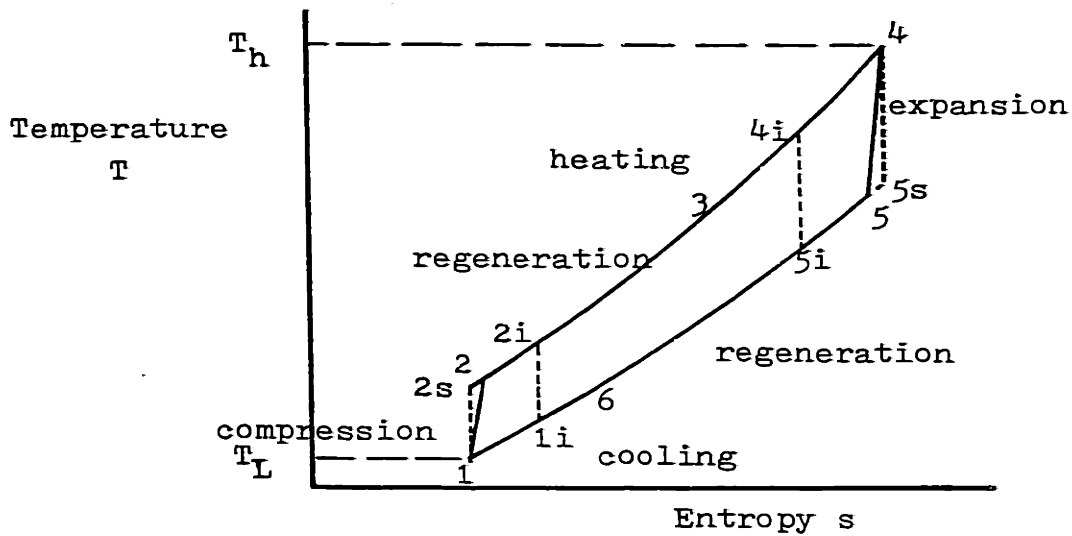
Fig. II-4   T-s diagram of VHGE for equivalent isentropic method
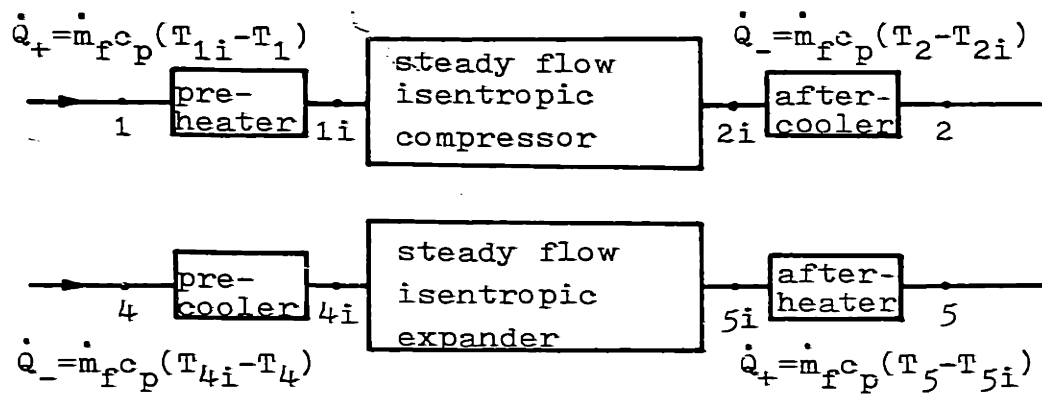
Fig. II-5   Equivalent isentropic approximation

(2) Equivalent reversible polytropic method

This method requires indicated P-V data, mass flow rate $\dot{m}_f$, and inlet and outlet temperatures. This matches the measured indicated power with reversible-polytropic compression and reexpansion processes, and constant-pressure intake and discharge process. Fig. II-6 shows the flow diagram for the model of the processes of the compressor. $\dot{W}_{pm}$ and $\dot{Q}_{pm}$ in Fig. II-6 denote power and heat-transfer rate during the process p for mass portion m where p = i, c, d, r, denoting intake, compression, discharge and reexpansion respectively; and, m = f, c, t, denoting flow mass, clearance mass, and total mass respectively.

The sum of the powers $\sum_{m,p} \dot{W}_{pm}$ is equated to the measured indicated power $\dot{W}_c$. Heat-transfer rate into the gas inside the compressor $\dot{Q}_+$, and out of the gas $\dot{Q}_-$ are given as

$$\dot{Q}_+ \equiv \dot{Q}_{if} + \dot{Q}_{ic} + \dot{Q}_{rc}$$
$$\dot{Q}_- \equiv \dot{Q}_{df} + \dot{Q}_{dc} + \dot{Q}_{ct}$$

(II-4)

The heat-transfer rates $\dot{Q}_+$ and $\dot{Q}_-$ are expressed in terms of the effective intake temperature T_{ei}, and the effective discharge temperature T_{ed}.

$$\dot{Q}_+ = \dot{m}_f c_p (T_{ei} - T_{in}) + \dot{Q}_{rc}$$
$$\dot{Q}_- = \dot{m}_f c_p (T_{out} - T_{ed}) + \dot{Q}_{ct}$$

(II-5)

As before, the non-dimensional magnitude of cyclic heat transfor of compressor X_c is as follows.
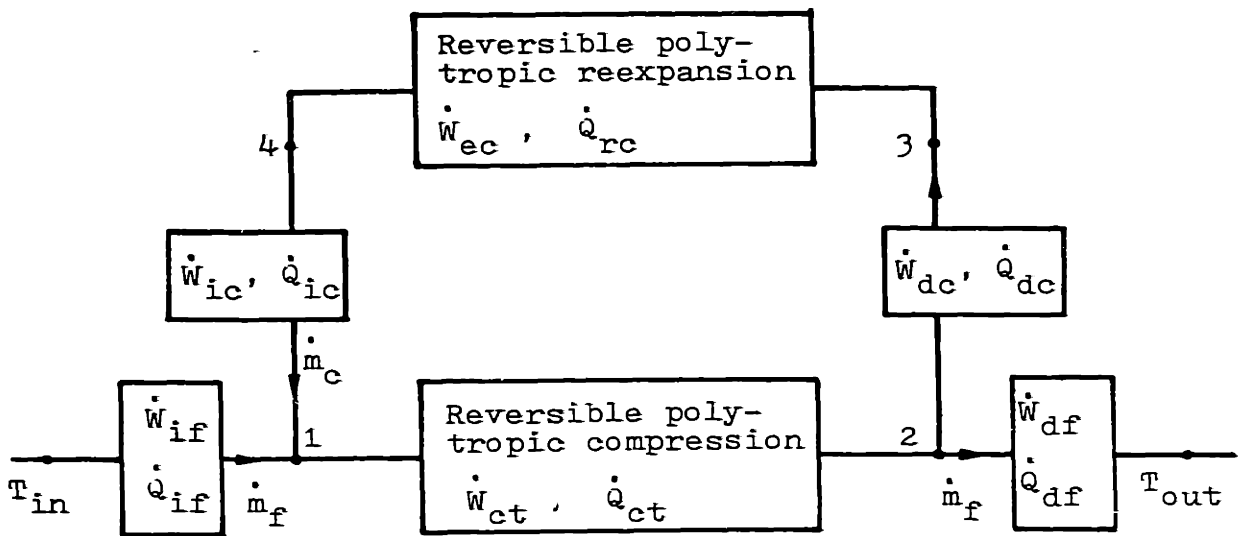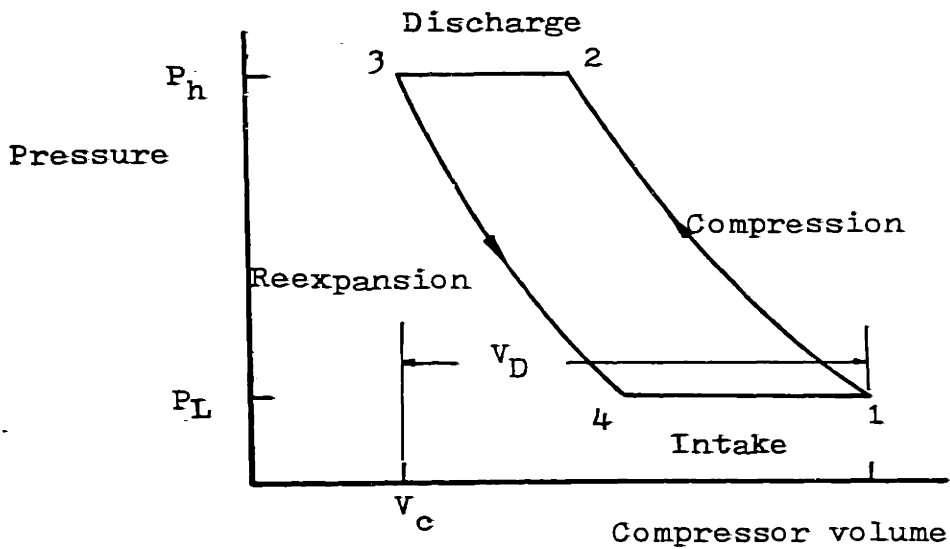
Fig. II-6 Equivalent reversible polytropic
approximation for compressor

$$X_c = (|\dot{Q}_+| + |\dot{Q}_-|) / (2 \times \Delta H), \qquad (\text{II-6})$$

where $\Delta H = \dot{m}_f c_p (T_{out} - T_{in})$. Table II-3 lists X_c for engine tests using Equivalent Reversible Polytropic method. Appendix C shows the examples of calculation.

Table II-3   Magnitude of Cyclic Heat Transfer (Equivalent
Reversible Polytropic Method)

	Test #1	Test #2	Test #3	Test #4	Test #5	Test #6
X_c	1.71	1.45	1.69	1.47	0.99	0.99

The accuracy of equivalent-reversible-polytropic method was confirmed by a first-law integral analysis to be described in detail in section III.3. This analysis uses instantaneous mass flow rate data together with instantaneous pressure and volume data to calculate the instantaneous mixed mean temperature of the gas in the cylinder. The heat transfer is calculated by numerical integration of the first law. For the compressor data of Test #5, the difference between the reversible polytropic method and the first-law integral analysis was less than 1%. The data of Table II-2 and II-3 show that the much simpler Equivalent Isentropic method gives almost as accurate a result as the Equivalent Reversible Polytropic method, except for Test #1 and #2 with piston ring leakage.

4. Influence of Cyclic Heat Transfer on VHGE Performance .

1) Adiabatic efficiency vs. polytropic efficiency

Conventionally, compressors are modeled as adiabatic
or at least overall-adiabatic. Thus, adiabatic efficiency
η_c is usually defined as

$$\eta_c = \frac{\dot{W}_{sc} \ (\text{Isentropic compressor power})}{\dot{W}_c \ (\text{Actual compressor power})} \ , \qquad \text{(II-7)}$$

where $\dot{W}_{sc}$ and $\dot{W}_c$ are for the same mass flow rate, inlet state,
discharge pressure referring to Fig. II-4. For an ideal gas
with constant specific heats,

$$\eta_c = \frac{h_{2s} - h_1}{h_2 - h_1} = \frac{T_{2s} - T_1}{T_2 - T_1} \ , \qquad \text{(II-8)}$$

where h is specific enthalpy and s denotes isentropic process.
However, when the compressor has net heat transfer, $\dot{Q}_c$, equation
II-8 must be modified to include $\dot{Q}_c$.

$$\eta_c = \frac{h_{2s} - h_1}{(h_2 - h_1) - \dot{Q}_c/\dot{m}_f} \qquad \text{(II-9)}$$

Therefore, in a non-adiabatic case for given initial state
and compression pressure ratio, η_c can give the value of $\dot{W}_c$,
but $\dot{Q}_c$ is also required to fix the discharge state.

46

The polytropic efficiency of a compressor η_{nc}, and the polytropic coefficient η_c are introduced to describe the non-adiabatic compressor.

The adiabatic efficiency of a compressor may be separated into two parts,

$$\eta_c = \frac{\dot{W}_{sc}}{\dot{W}_c} = \frac{\dot{W}_{sc}}{\dot{W}_{nc}} \cdot \frac{\dot{W}_{nc}}{\dot{W}_c} = \frac{(1-P_r^{C_1})}{\xi_c(1-P_r^{C_0})} \cdot \eta_{nc} \qquad \text{(II-10)}$$

where $\xi_c \equiv$ polytropic coefficient of compressor $= \dfrac{\gamma-1}{\gamma} \dfrac{\log P_r}{\log T_{rc}}$,

$\eta_{nc} \equiv$ polytropic efficiency of compressor $= (\dot{W}_{nc} / \dot{W}_c)$,

$\dot{W}_{nc} \equiv$ reversible polytropic compressor power

$\qquad = \xi_c \dot{m}_f c_p T_L (1-P_r^{C_1})$,

$P_r \equiv P_h / P_L \qquad ; \qquad T_{rc} \equiv T_2 / T_L$

$C_0 \equiv (\gamma-1)/\gamma \qquad ; \qquad C_1 \equiv C_0 / \xi_c.$

The first term, $\dot{W}_{sc} / \dot{W}_{nc}$, reflects the effect of reversible net heat transfer following the path 1-2 in Fig. II-4. The second term, $\dot{W}_{nc} / \dot{W}_c = \eta_{nc}$ reflects the effect of irreversible cyclic heat transfer. The net heat transfer rate $\dot{Q}_c$ is given in terms of ξ_c and η_{nc} as,

$$\dot{Q}_c = (\xi_c / \eta_{nc} - 1) \dot{m}_f c_p T_1 (1-P_r^{C_1}). \qquad \text{(II-11)}$$

When $\dot{Q}_c = 0$, i.e. at least overall adiabatic, ξ_c is equal to the polytropic efficiency η_{nc}. In fact, ξ_c is called the polytropic efficiency in adiabatic turbines or compressors (8). In non-adiabatic case, the newly defined η_{nc}, not ξ_c, is more appropriate to be called polytropic efficiency. Thus, prescribing ξ_c and η_{nc} gives both $\dot{W}_c$ and the end state for a given initial state and pressure ratio.

Polytropic efficiency of expander η_{ne} and polytropic coefficient of expander ξ_e are similarly defined:

$$\eta_e = \frac{\dot{W}_e}{\dot{W}_{se}} = \frac{\dot{W}_{ne}}{\dot{W}_{se}} \cdot \frac{\dot{W}_e}{\dot{W}_{ne}} = \frac{\xi_e (1 - P_r^{C_2})}{(1 - P_r^{C_0})} \cdot \eta_{ne} \qquad \text{(II-12)}$$

where $\xi_e = \dfrac{\gamma - 1}{\gamma} \cdot \dfrac{\log P_r}{\log T_{re}}$; $T_{re} = T_h / T_5$,

$$\eta_{ne} = \dot{W}_e / \dot{W}_{ne} \qquad ; \qquad C_2 = C_0 / \xi_e,$$

$\dot{W}_{ne}$ = reversible polytropic expander power
$$= \xi_e \dot{m}_f c_p T_h (1 - P_r^{C_2}).$$

The net heat transfer of expander can be given in terms of ξ_e and η_{ne} as,

$$\dot{Q}_e = (\xi_e \eta_{ne} - 1) \dot{m}_f c_p T_4 (1 - P_r^{C_2}). \qquad \text{(II-13)}$$

2) Simple Cycle Analysis of VHGE

Fig.II-4 shows the thermodynamic processes inside the engine as the working gas circulates through the components of the engine. Indicated engine efficiency, η_i is defined as $\eta_i \equiv \dfrac{\text{net indicated power of engine}}{\text{net heat input rate of engine}}$. Net indicated power of the engine is the sum of compressor indicated power $\dot{W}_c$ and expander indicated power $\dot{W}_e$.

From definitions of ξ_c, ξ_e, η_{nc}, η_{ne}, $\dot{W}_c$ and $\dot{W}_e$,

$$\dot{W}_c = \dot{W}_{nc}/\eta_{nc} = (\xi_c/\eta_{nc}) \, \dot{m}_f c_p T_L \, (1-P_r^{C_1})$$

$$\dot{W}_e = \dot{W}_{ne} \cdot \eta_{ne} = (\xi_e \eta_{ne}) \, \dot{m}_f c_p T_h \, (1-P_r^{C_2}) \qquad \text{(II-14)}$$

Net heat input rate, $\dot{Q}_{net} = \dot{m}_f c_p \, (T_h - T_3)$. After some algebraic manipulations,

$$\dot{Q}_{net} = \dot{m}_f c_p \, (T_h - T_L P_r^{C_1} + \eta_R (T_L P_r^{C_1} - T_h P_r^{C_2})). \qquad \text{(II-15)}$$

The indicated efficiency η_i is,

$$\eta_i = \frac{(\xi_c/\eta_{nc}) \, (1-P_r^{C_1}) + \xi_e \eta_{ne} T_r \, (1-P_r^{C_2})}{T_r - P_r^{C_1} + \eta_R \, (P_r^{C_1} - T_r P_r^{C_2})} \qquad \text{(II-16)}$$

where $T_r \equiv T_h/T_L$; $\eta_R \equiv$ regenerative heat exchanger effectiveness.

3) Engine performance vs. cyclic heat transfer

Table II-4 lists the polytropic coefficient of the compressor ξ_c and of the expander ξ_e, the polytropic efficiency of the compressor η_c, of the expander η_e, and indicated engine efficiency η_i based on net input power to the engine for Tests #1 through #6.

Table II-4   Polytropic Coefficients (ξ_c, ξ_e), Polytropic Efficiencies (η_{nc}, η_{ne}), and Indicated Engine Efficiency η_i for Engine Tests

	Test #1	Test #2	Test #3	Test #4	Test #5	Test #6
ξ_c	0.924	0.925	0.999	1.120	1.140	1.178
ξ_e	1.041	0.906	0.933	0.926	0.938	0.956
η_{nc}	0.597	0.706	0.698	0.740	0.804	0.811
η_{ne}	0.963	0.887	0.914	0.932	0.860	0.873
η_i	20.8	25.9	27.7	33.1	29.8	33.3

From Table II-2, II-3, and II-4, polytropic efficiencies η_c and η_e can be plotted with respect to the non-dimensional magnitude of the cyclic heat transfer of the compressor X_c and of the expander X_e as shown in Fig. II-7 . By definition, η_{nc} and η_{ne} become 100% when cyclic heat transfer goes to zero. In the expander case, polytropic efficiency η_{ne} is related to

Polytropic
efficiency
η_{nc}, η_{ne}
(%)

⊙ Compressor (Equivalent isentropic method)

⊡ Compressor (Equivalent reversible polytropic method)

▲ Expander (Equivalent isentropic method)

$\eta_{nc} = 1-0.177\ X_c$

Compressor

$\eta_{ne} = 1-0.310\ X_e$

Expander

Test #1

X_c, X_e Non-Dimensional Cyclic Heat Transfer
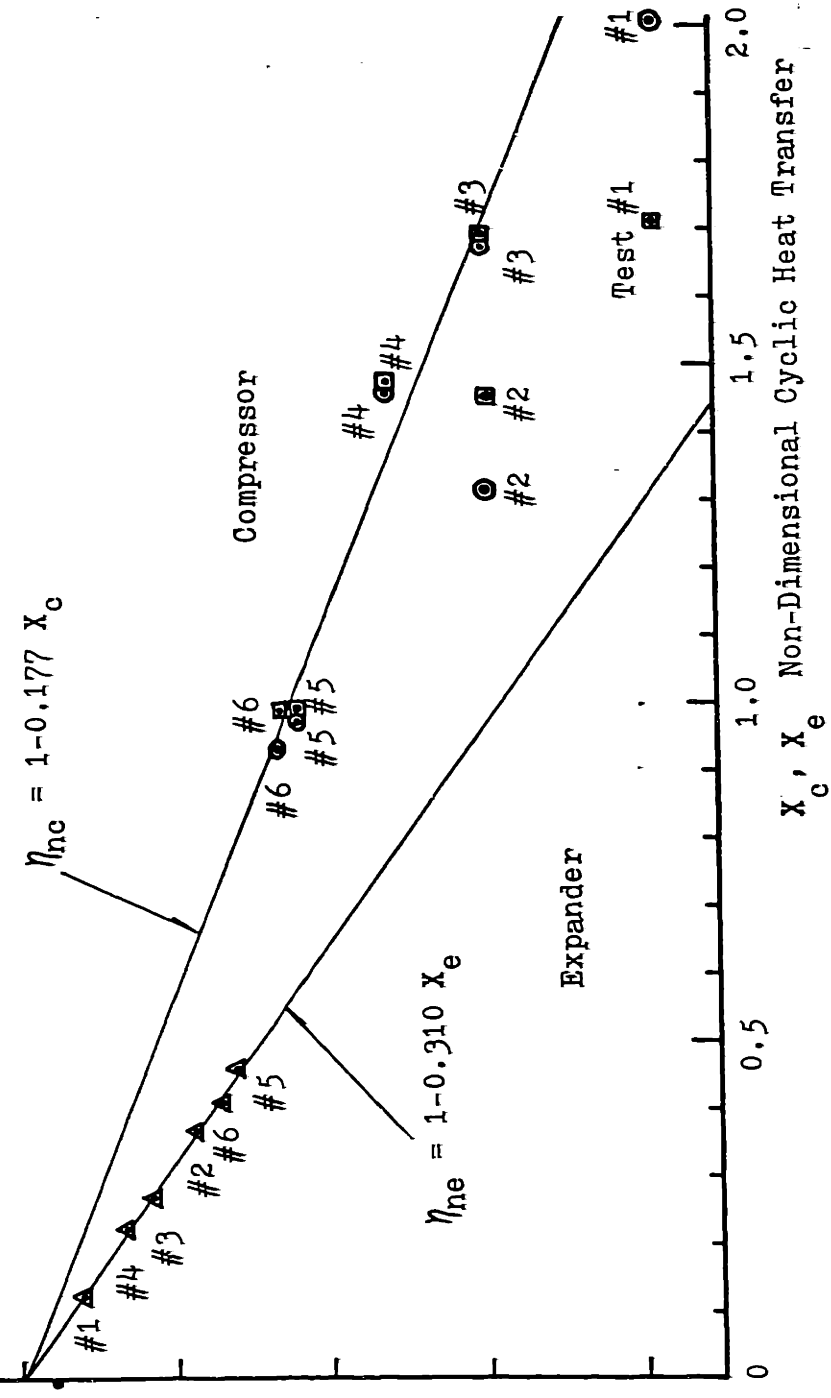
Fig. II-7 Polytropic efficiencies of compressor and expander
vs. Cyclic heat transfer

51

the non-dimensional magnitude of cyclic heat transfer X_e by the linear-regression relation

$$\eta_{ne} = 1 - 0.310 \, X_e. \qquad\qquad \text{(II-17)}$$

In the compressor case, polytropic efficinecy η_{nc} is related to the non-dimensional magnitude of cyclic heat transfer X_c by the linear regression relation

$$\eta_{nc} = 1 - 0.177 \, X_c. \qquad\qquad \text{(II-18)}$$

The significant deviation of Test #1 and Test #2 from the linear-regression relations is believed to be due to the effect of piston-ring leakage on compressor performance. The serious effect of cyclic heat transfer on compressor and expander efficiencies is clear in Fig. II-7.

The influence of cyclic heat transfer on the indicated engine efficiency η_i is shown in Fig. II-8, which was plotted from equation II-16, with the aid of the linear-regression relations of equations II-17, and II-18.

52

$\xi_c = 1.15$

$\xi_e = 0.95$

$p_h/p_L = 2.0$, $T_h/T_L = 3.5$
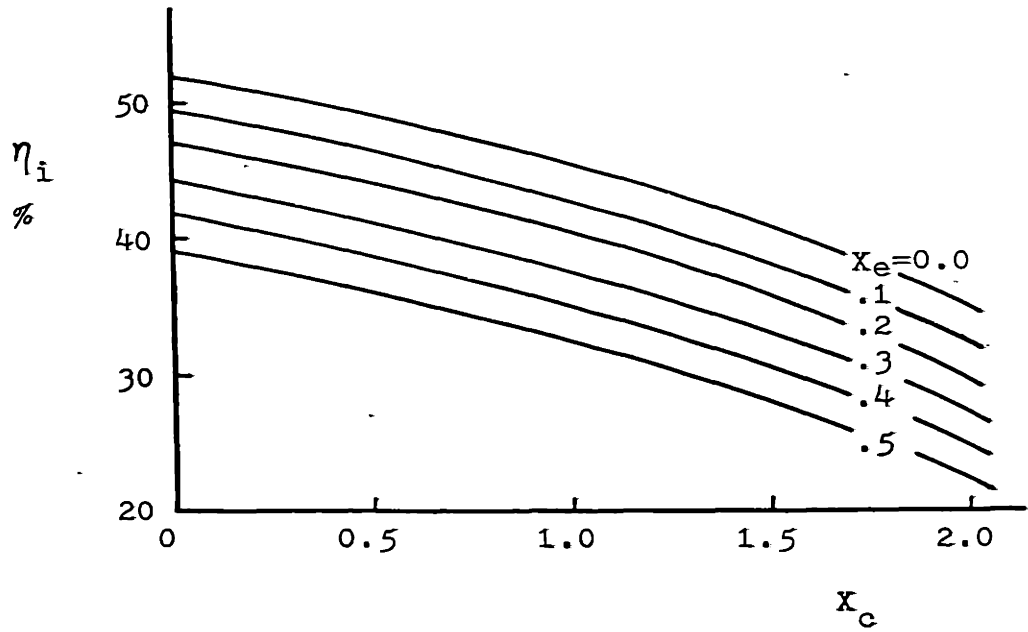
Fig. II-8 Indicated engine efficiency vs. cyclic heat transfer

53

Chapter III   DETAILED STUDY AND MEASUREMENT OF INTERNAL
               STATES INSIDE COMPRESSOR

The need for more information on internal states arose
when we could not determine the cause of low efficiency from
indicated P-V diagram and average temperatures measured out-
side the cylinder. For complete specification of the thermo-
dynamic state of cylinder at a given time, temperature and
mass of cylinder gas were also needed. Transient gas temper-
ature was measured by fast-response thermocouples inserted
into the cylinder. Although the information thus obtained
was very useful in understanding internal states changes, there
was a question as to how closely the local temperatures read
by thermocouples approximate the mixed mean temperature of
the gas inside cylinder. Most of the time, the spatial vari-
ation of gas temperature inside cylinder makes it difficult
to accept the thermocouple readings even after corrctions for
errors, unless there are enough of them distributed throughout
the cylinder space. Since this is not practical for a recipro-
cating engine due to sweeping motion of the piston, an indirect
method utilizing instantaneous mass flow rate was used.
The measurement of instantaneous mass flow rate serves two
purposes : (a) confirmation of cooler flow rate as the engine
flow rate, (b) calculation of the mixed mean temperature of
cylinder gas.

1. Transient Gas Temperature Measurement

1) Thermocouple-probe design

To measure the temperature fluctuation during each cycle inside the cylinder, it is necessary to design a special thermocouple probe which can withstand up to 3.8 MPa, 800 K, and maximum gas velocity of 50m/sec. Chromel-alumel wire was chosen since it has suitable temperature-emf characteristics and durability in such an environment. Since the characteristic thermal response time τ of a thermocouple decreases as the diameter of the wire gets smaller, 25.4 μm O.D. wire was used for the hot end of the thermocouple junction. Lead wire of 254μm O.D. was welded to the junction wire. The two wires were separated by a two-hole alumina insulation tube which was inserted into 4.76 mm O.D. Inconel 600 protection tube. At the hot end of the thermocouple, high-temperature cement was used to support the thermocouple junction. To prevent the working gas from leaking through the thermocouple probe, a compression fitting with a Teflon seal was soldered to the external end of the protection tube and cooled to protect the Teflon seal from being overheated. The final assembly of the probe is shown in Fig.Ⅲ-1

There are four kinds of error to be considered in thermocouple design: velocity, conduction, radiation, and transient error. If the environmental effects are small enough so that one effect has little influence on others, i.e. if they are

55

3.02 cm

Teflon Seal

Epoxy

Silver Soldered

Hot Junction

Water Jacket

Follower Soldered
to Protection Tube

0.05cm

76.2 μm

25.4 μm

High Temperature Cement

0.318 O.D. Alumina Insulator
cm

0.476 O.D. Inconel 600
cm Protection Tube

254 μm Lead Wire
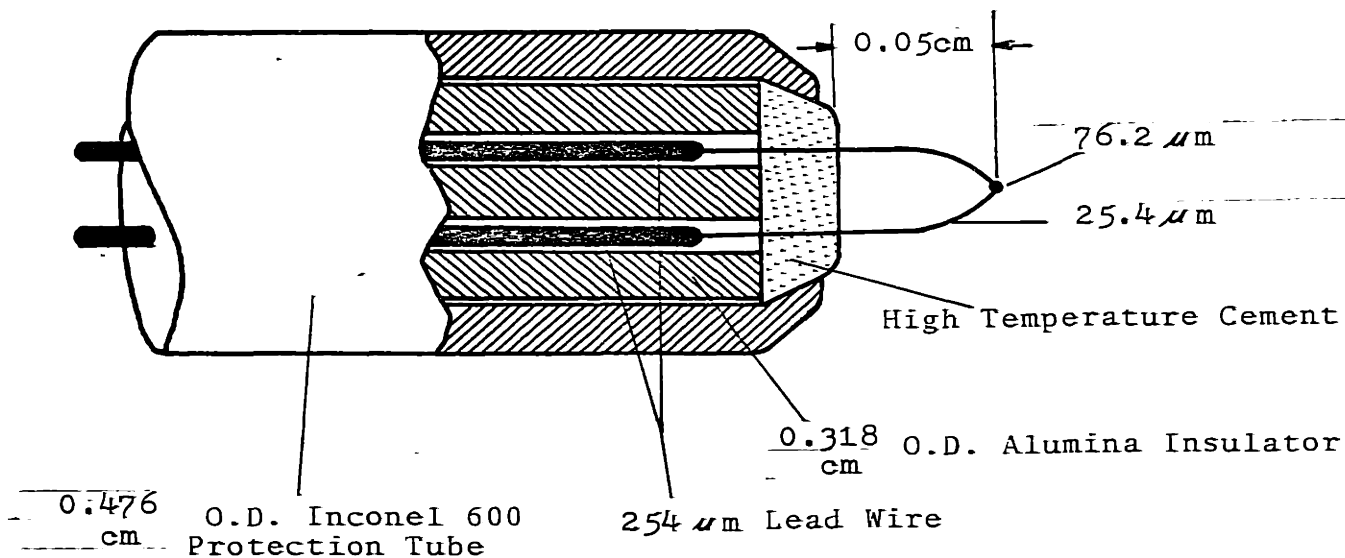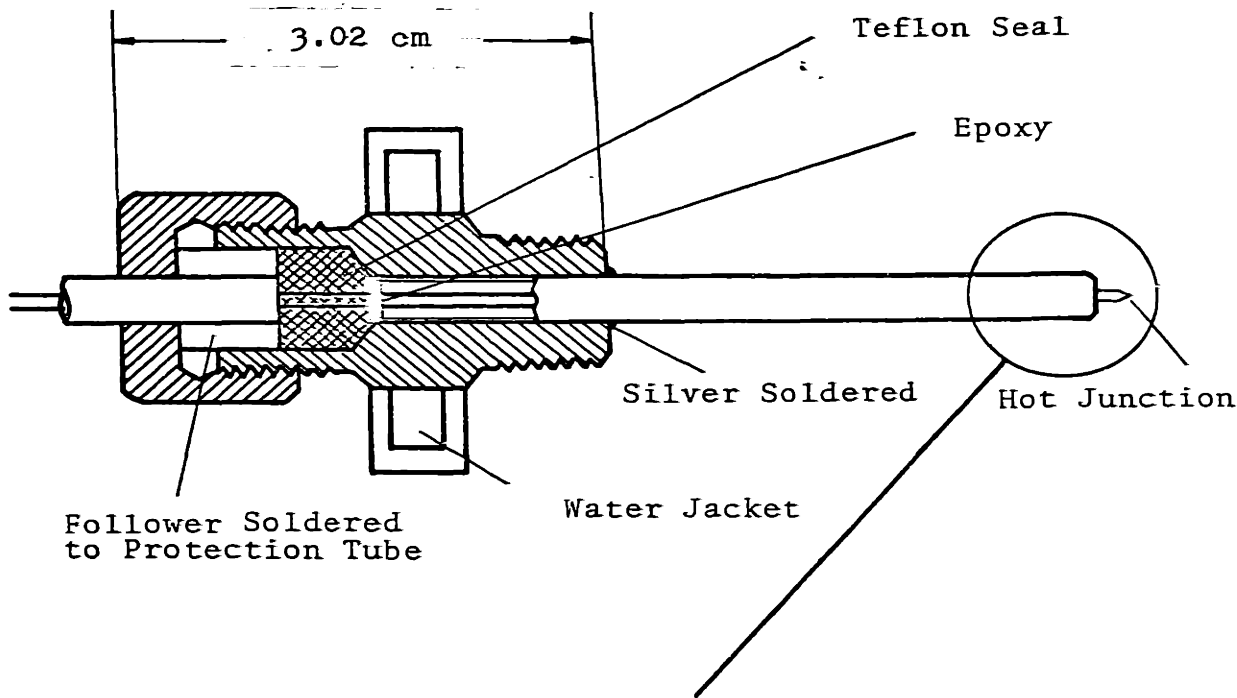
Fig. III-1 Thermocouple probe assembly
Drawing not to Scale

linear to a first-order approximation, we can estimate the errors separately and add them together (9). The velocity error is given by

$$\Delta T_v = T_g \; (1-\alpha) \; (\gamma-1)M^2 / \; (2+ \; (\gamma-1)M^2), \qquad (\text{III-1})$$

where $\alpha \equiv$ recovery factor and $\gamma \equiv c_p/c_v$, $M \equiv$ Mach number. For a given α, as long as M is low, ΔT_v remains small. The conduction error is given by

$$\Delta T_c = (T_g - T_m) \; / \; \cosh \; (2(L/d) \; (hd/k_s)^{.5}), \qquad (\text{III-2})$$

where L = length of the wire exposed to gas stream, d = wire diameter, k_s = average thermal conductivity of the two wires, which means, ΔT_c will decrease as L/d and (hd/k_s) increases. As will be shown later, L/d is limited by the stiffness of the wire. Convection-heat-transfer coefficient h is given by (10):

$$Nu \equiv (hd/k_g) = (Pr_g)^{0.3} \; (0.35 + 0.56 \; (Re_d)^{0.52})$$

$$(\text{III-3})$$

where subscript g denotes the gas. The radiation error is given by

$$\Delta T_r = (F\sigma/h) \; (T_j^4 - T_w^4) \qquad (\text{III-4})$$

where the radiation view factor F is, in this case, the emissivity ε of the thermocouple junction, T_j is the junction temperature, and T_w is the temperature of the surrounding walls.

The only practical method of reducing the radiation error is
to choose a wire of the smallest possible diameter, which gives
a high value of h. Transient error is given by

$$\Delta T_t = \tau_c (dT_j/dt) \qquad (\text{III-5})$$

For a junction with a bead of diameter D,

$$\tau_c = (D/d)^{0.375} \tau_0 \qquad (\text{III-6})$$

where $\tau_0 = (\rho c v/hA) = (\rho c d/4h)$ (for a butt-welded junction).

The drag force exerted by the gas on the thermocouple is
given by

$$F_d = C_d A_d \rho_g V^2 / 2g_c \qquad (\text{III-7})$$

where $A_d = (\pi D^2/4)$ for a sphere (bead), $A_d = d \times L$ for a wire,
C_d = drag coefficient, which is a function of Reynolds number
R_{ed} and the shape of the object, ρ_g is the density of the gas.
Maximum bending stress occurs at the foot of the thermocouple
wire and is given by

$$\sigma_{max} = M_{max} \, d/ \, (2I) \qquad (\text{III-8})$$

where maximum bending moment $M_{max} = (F_{bead} + 0.5F_{wire}) L$,
L = length of the thermocouple exposed to the gas stream,
d = diameter of the wire, I = moment of inertia of the cross
section at the foot of the wire. Maximum shear stress also

58

occurs at the foot of the thermocouple and is given by

$$\tau_{max} = (4/3A_w)\ (F_{d\ wire} + F_{d\ bead}) \qquad\qquad (\text{III}-9)$$

where A_w is the cross section area of the wire.

Since the gas velocity and the temperature at the expander inlet valve are the highest among the four thermocouple location, we use the condition at that point. Given the average mass flow rate of 7.56×10^{-3} kg/sec, flow area $4.55 \times 10^{-4} m^2$, the speed 10 rev/sec, temperature 900 C, and pressure 3.79MPa, the velocity, and radiation errors are negligible. Conduction error also becomes negligble when L/d is about 20. In this case, the maximum bending stress, σ_{max}, is about 0.6 MPa, and the maximum shear stress τ_{max} is about 0.14 MPa. According to Mises yield criterion (11), these stress levels are low enough for the thermocouple to withstand the drag force exerted by the gas stream at moderate temperatures. Later in the tests, expander-inlet-side thermocouples were bent over when the inlet temperature exceeded 950 K. The characteristic time was calculated to be about 1 m-sec at the expander inlet valve side when the valve was wide open, which is short enough for our purpose.

Drilling holes to insert the thermocouple probes into the engine required a special care because there was a possibility of dropping the chips into the cylinder. For the expander intake valve port, a Plexiglass plug was inserted through the

valve-access port. The Plexiglass plug was pressed against the wall, and a hole was drilled through the engine wall into the plug, leaving the chips inside the plug. For the expander discharge side, a hole was drilled through the closure plug of the discharge-valve access port.

Before the modification of compressor, thermocouple ports into the compression chamber were provided by drilling axially along the wall of the cylinder used for controlling the clearance volume. Plexiglass plugs were again used to prevent chips from entering the cylinder. The thermocouples are located right down stream of the inlet valves and right up stream of the discharge valves. The results are given in App. A for Tests #1 through #6. The result from Test #5 will be later compared to the mixed mean temperature obtained indirectly by measuring instantaneous mass flow rate (see section III.3).

2. Instantaneous-Mass-Flow-Rate Measurement

1) Flow-meter design

Two square-edged orifice plates were made of S.S.300. The diameters of them were properly sized[*] so that at maximum-flow condition, the ΔP across the orifice would not exceed 0.1 MPa. Two ±0.1 MPa differential-pressure transducers (un-bonded-strain-gauge type) were used to record the differential pressure across the orifice. Special adapters for the transducers were made of S.S.300 as shown in Fig. III-2 . The tubings before and after the orifices were arranged to ensure enough straight runs satisfying the requirement prescribed in ref. 6 (see Fig. III-3, and III-4).

As mentioned in section II. 2.2), accurate measurement of gas flow using orifice meter requires that the flow be quasi-steady. According to reference 6 , when the flow pulsating frequency is less than one fifth that of the flow-metering device, the pulsation is slow enough to be considered quasisteady.

Fig. III-5 and III-6 shows ΔP from intake orifice and discharge orifice with respect to crank angle in Test #5. The high-frequency noise at about 1400 Hz is thought to be due to resonance of the adapter system. The flow pulsation around 300 Hz is thought to be due to the movement of compresser valves. Flow-pulsation frequency due to engine speed is 10 Hz. Considering the natural frequency of the pressure transducer

* See Appendix D.
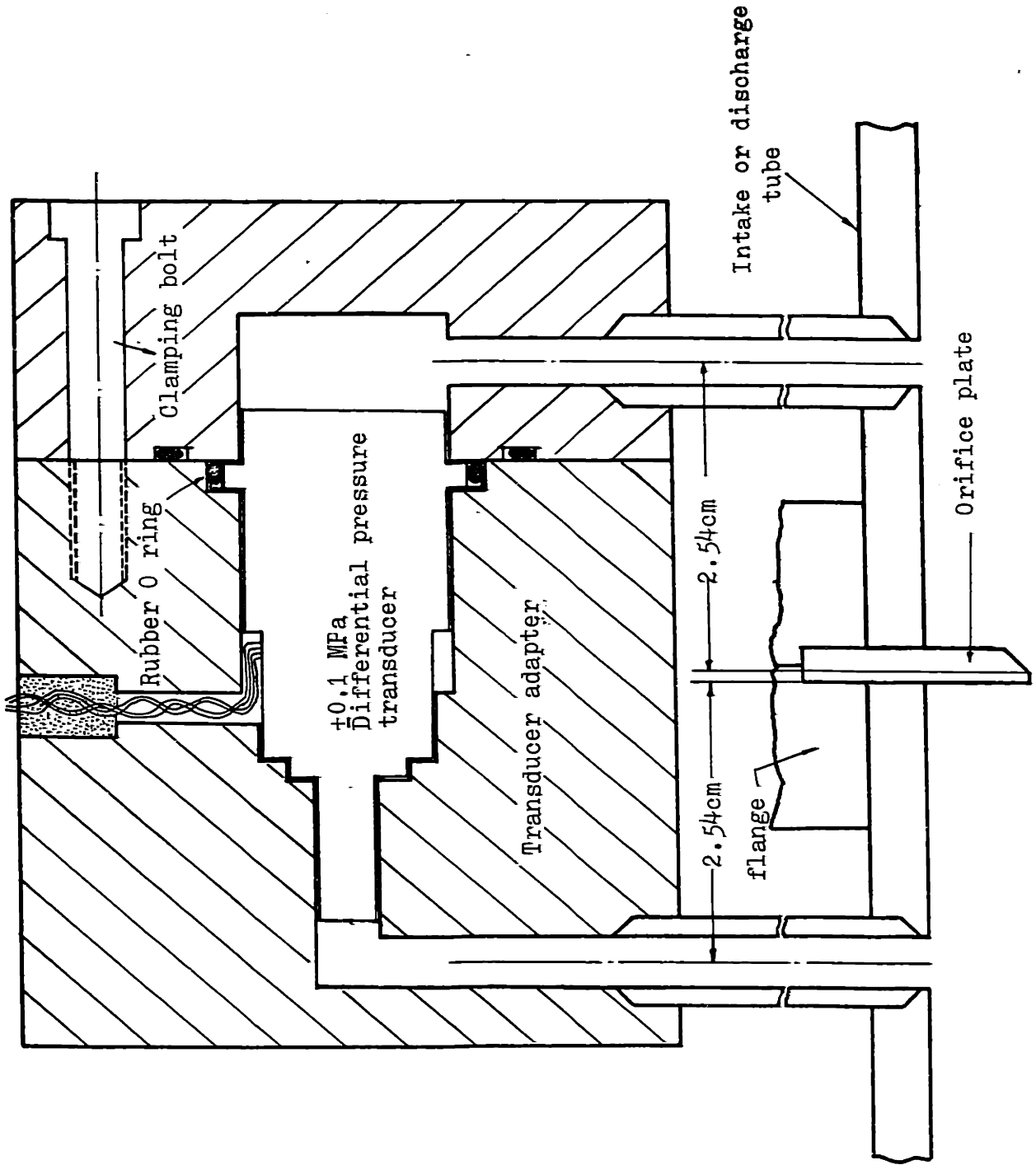
Fig. III-2 Differential-pressure transducer and its adapter for orifice metering (schematic)

Intake or discharge tube

Orifice plate

Clamping bolt

Rubber O ring

±0.1 MPa Differential pressure transducer

Transducer adapter

2.54cm

2.54cm

flange

Front view

Pressure gauge & gas supply

Differential pressure transducer & adapter

Stainless steel flanges & orifice plate

Gas reservoir

Compressor inlet valve flange

Flexible joint

Cooler

Top view

Nipples

75 cm

50 cm

3.175 cm I.D.

Compressor block

Fig. III-3 Gas line arrangement for the orifice meter (intake side)

63

Differential pressure transducer and adapter

Stainless steel flanges & orifice plate

Regenerative heat exchanger

Compressor block

Discharge valve flange

Side View

To pressure gauge and supply

Nipple

To reservoir

Top View

Reservoir

Reservoir

100 cm

18 cm
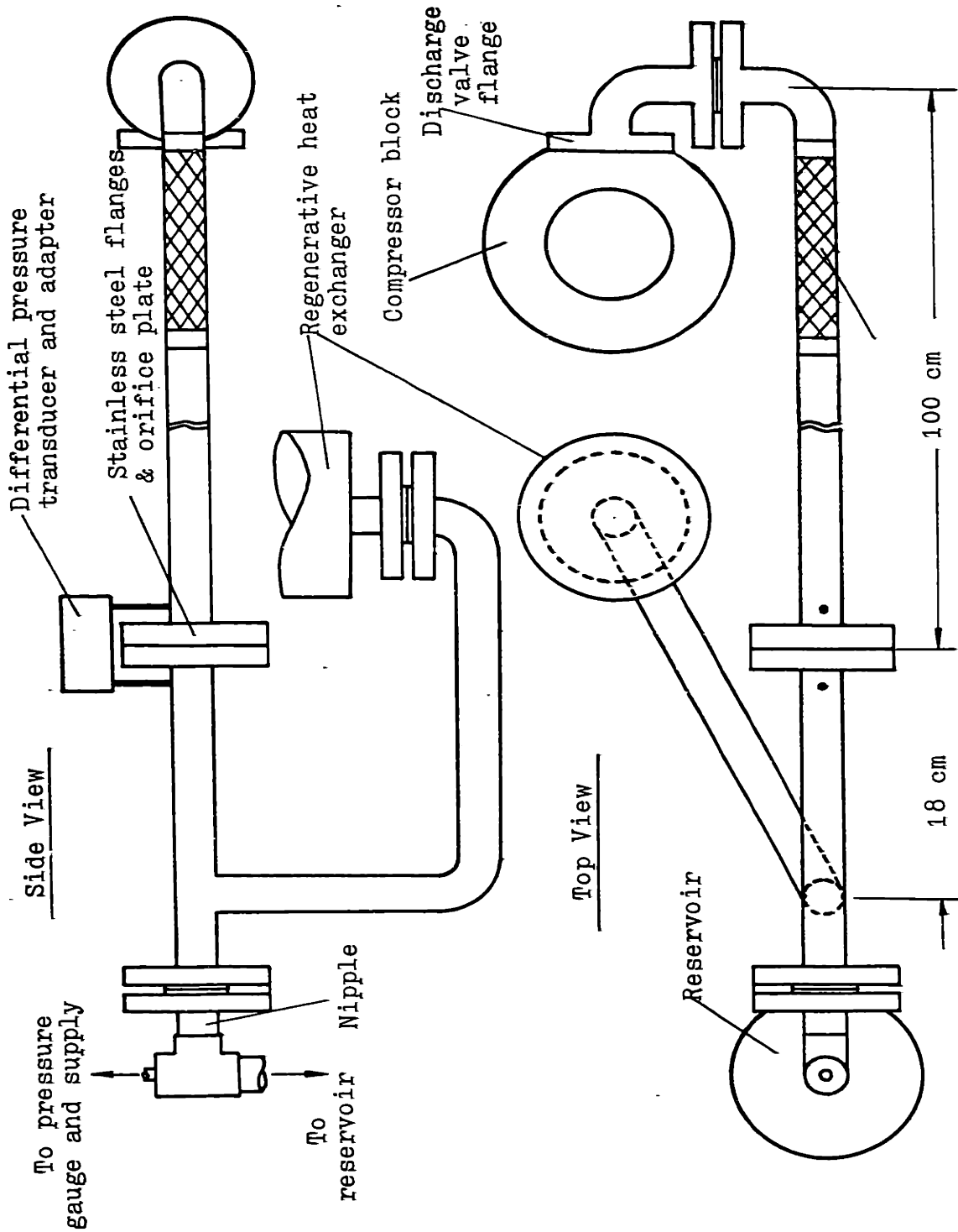
Fig. III-4 Gas line arrangement for the orifice meter (discharge side)
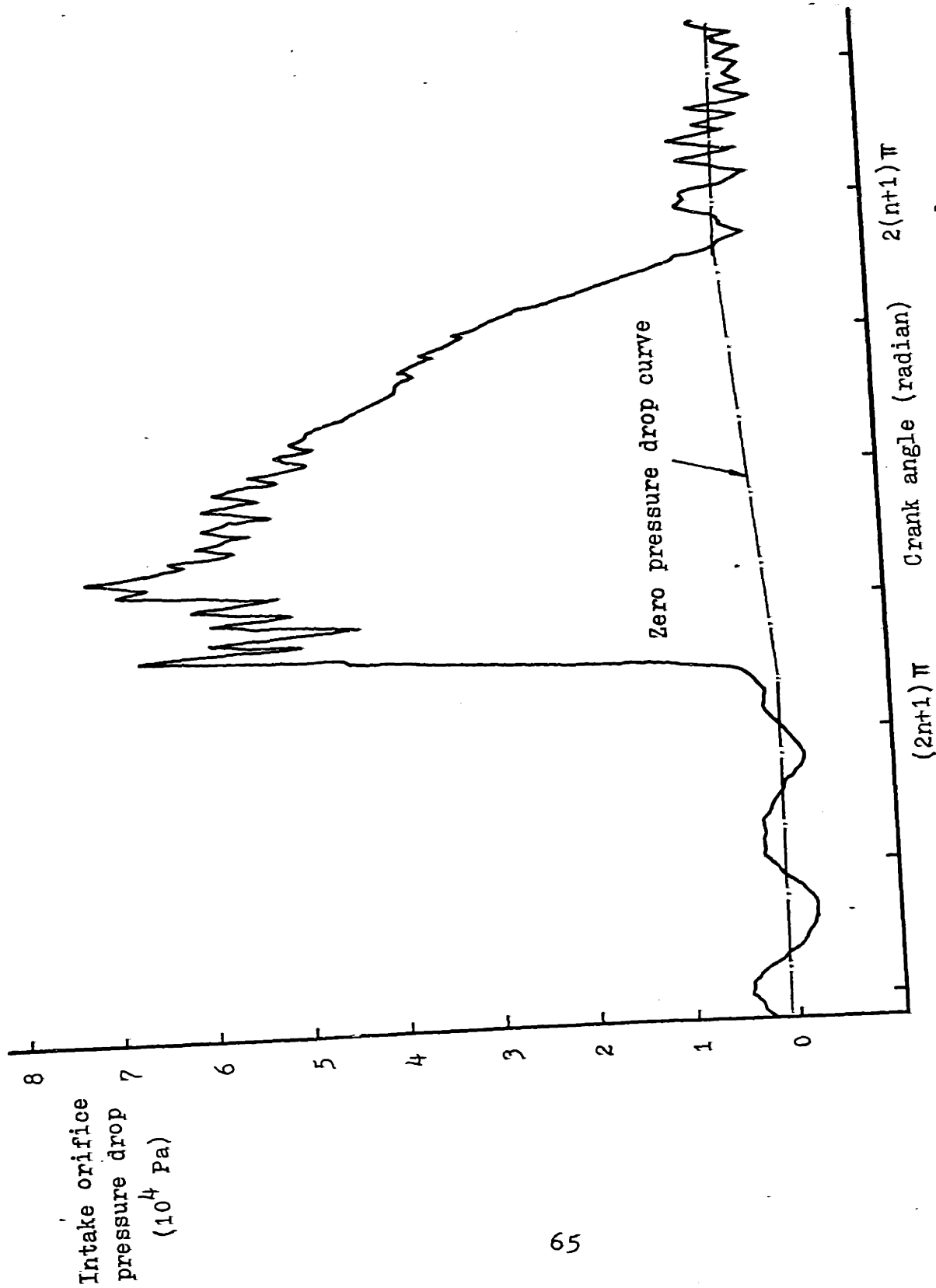
Fig. III-5 Pressure drop across intake orifice vs. crank angle
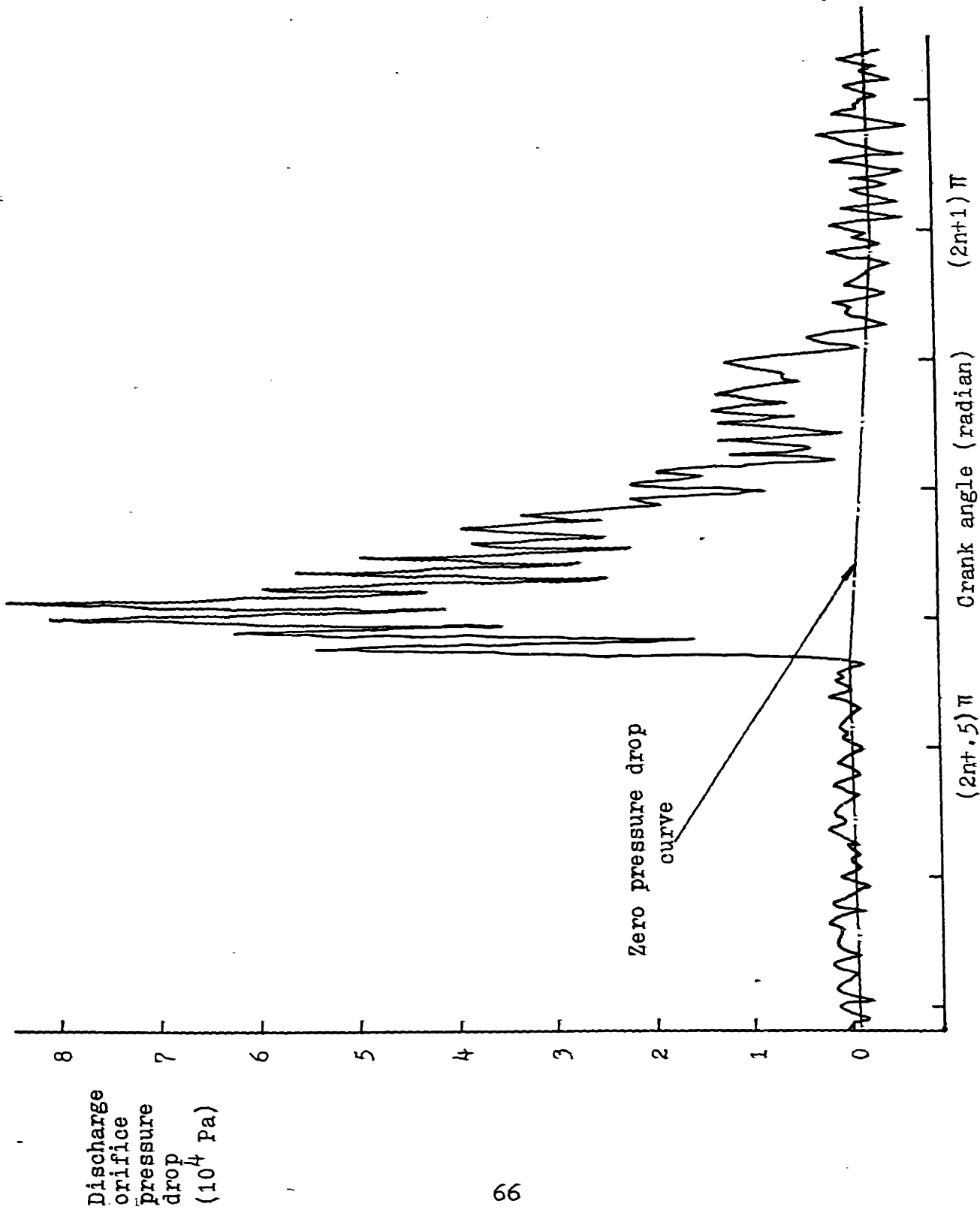
Fig. III-6 Pressure drop across discharge orifice vs. crank angle

66

was 6000 Hz, the flow condition can be assumed quasisteady. The error due to pulsation is estimated to be at most 1~2% (see Appendix D).

One difficulty with the orifice-ΔP data was the zero shift during the measurement as shown in Fig.III-5 and Fig.III-6. The zero shift of this kind in much larger scale had been previously observed during compression-expansion test[*] of the expander without any gas flow through the valves.

Assuming that when the compressor valves are closed, the gas flow across the orifice is almost negligible, or at least the net flow is negligible, the zero reference for the orifice-pressure-drop data was drawn using line segments as shown in Fig.III-5 and Fig. III-6 . Orifice-ΔP data thus obtained were used in the computer program to calculate instantaneous mass flow rate and mixed mean gas temperature of the compresser in section III. 3.

2) Results

The mass flow rate was first calculated using the orifice-ΔP data as it was (Fig.III-5, III-6), and then recalculated using the data after smoothing out 1400 Hz noise (due to adapter resonance) numerically (Fig. E-4 , Fig. E-5). Both methods gave almost the same mass flow rate of 7.60×10^{-3} kg/sec during the intake process, and 7.71×10^{-3} kg/sec during the discharge process.

* See Appendix A.

Considering the error caused by pulsation and temperature change across the orifice, the intake-side flow rate is more accurate than the discharge-side flow rate to be regarded as engine flow rate. The calculated cooler flow rate had been regarded as engine flow rate from energy-balance considerations. It turned out to be very close to the measured engine flow rate (99.5% of intake orifice measurement).

3. First-Law Integral Analysis

1) Formulation

Ignoring changes in kinetic energy and potential energy associated with mass fluxes, the First Law of thermocynamics for control volume (compressor space) is

$$\left. \frac{\partial E}{\partial t} \right)_{c.v.} = \dot{Q}_{c.v.} - \dot{W}_{c.v.} + \sum_{in} \dot{m}h - \sum_{out} \dot{m}h, \qquad (\text{III}-10)$$

where $\dot{Q}_{c.v.}$, $\dot{W}_{c.v.}$, $\left. \frac{\partial E}{\partial t} \right)_{c.v.}$ are the rate of heat transfer, work transfer, and change in internal energy of the control volume respectively ; $\sum_{in} \dot{m}h$, $\sum_{out} \dot{m}h$ are enthalpy-flux terms due to mass in-flow and out-flow respectively. It is assumed that mass inside the tube spaces between the compressor and orifices remain constant with respect to time. Thus, with appropriate phase lag adjustment, the mass flow rates through the compressor valves and orifices are the same.

In finite difference form between time t_i and t_{i+1}, the above equation becomes as follows :

68

$$E_{i+1} - E_i = Q_{i+1,i} - W_{i+1,i} + (\Delta H_{i+1,i})_{in} - (\Delta H_{i+1,i})_{out}$$

where $\Delta H_{i+1,i} = \int_{t_i}^{t_{i+1}} \dot{m}\, h\, dt; \quad W_{i+1,i} \approx \dfrac{(P_i + P_{i+1})(V_{i+1} - V_i)}{2}$

$$\text{(III-11)}$$

If the working gas (helium) is assumed to be an ideal gas with constant specific heats,

$$E_{i+1} - E_i = m_{i+1}\, c_v\, T_{i+1} - m_i\, c_v\, T_i \ ,$$

$$\text{(III-12)}$$

$$\Delta H_{i+1,i} = \int_{t_i}^{t_i} \dot{m}\, c_p\, T\, dt \ ,$$

where temperatures (T, T_i, T_{i+1}) are mixed mean temperatures. During the intake process, assuming intake temperature is constant T_{in},

$$\Delta H_{i+1,i})_{in} = (m_{i+1} - m_i)\, c_p\, T_{in}$$

$$\text{(III-13)}$$

$$\Delta H_{i+1,i})_{out} = 0.$$

During the discharge process, assuming discharge temperature is equal to the mixed mean temperature,

$$\Delta H_{i+1,i})_{in} = 0$$

$$\text{(III-14)}$$

$$\Delta H_{i+1,i})_{out} = (m_{i+1} - m_i)\, c_p\, (T_{i+1} + T_i) /2$$

III

During the compression and reexpansion processes,

$$\Delta H_{i+1,i})_{in} = 0,$$

(III-15)

$$\Delta H_{i+1,i})_{out} = 0.$$

The equation of state for ideal gas PV = mRT is used to relate P, V, and mixed mean temperature T of compressor gas. Specific entropy of the gas is approximated by

$$s = s_{ref.} + c_p \log (T/T_{ref.}) - R \log (P/P_{ref.})$$ (III-16)

where ref. means reference state.

2) Implementation

Pressure and volume in equation III-11 are given from the pressure, volume - crank angle data (Fig. A-8) recorded by oscillograph. The instantaneous mass flow rates measured by orifice meters give the changes in cylinder mass $m_{i+1} - m_i$ during intake and discharge processes.

From the equation of state and equation III-11, knowing P_i, P_{i+1}, V_i, V_{i+1}, $m_{i+1} - m_i$, T_{in} and T_{out}, the heat transfer $Q_{i+1,i}$ can be calculated. In order to calculate the mixed mean temperature also, one more information is needed either on m_i or T_i at any time t_i. Specifying either one would fix m_i and T_i for the entire cycle, because $m_i T_i$ is equal to $P_i V_i/R$, which

70

is given by pressure volume data.

It was decided to use one data point from the transient gas temperature measurement. The temperature at the start of compression (end of intake) was chosen from Fig. A-14 as the mixed mean gas temperature at that instant. It was thought that spatial temperature variation inside the compressor would be minimum at this instant being preceded by a mixing period during intake process.

The resulting mixed mean temperature is shown in Fig. E-6, (curve A). Fig. E-10 shows the heat-transfer rate (kW) vs. crank angle calculated from equation using the mixed mean temperature of curve A in Fig. E-6.

In Fig. E-10, the sudden change in heat-transfer direction during discharge and intake of curve A is artificially caused by the mismatch between the slope of input-pressure data and the mass flow rate. The First Law during intake and discharge (Equation III-17 and III-18) shows that the heat-transfer rate depends on the slope of pressure and temperature.

$$\dot{Q}^{*}_{discharge} = -V\frac{\partial P}{\partial \theta} + m\ c_p\frac{\partial T}{\partial \theta} \qquad (III-17)$$

$$\dot{Q}_{intake} = -V\frac{\partial P}{\partial \theta} + \frac{\partial}{\partial \theta}\ (\ m\ c_p\ (T - T_{in})\ ) \qquad (III-18)$$

The specific entropy s of the gas from equation III-16 will be used to reduce the mismatch mentioned above. Fig. E-9 shows the specific entropy s vs. crank angle before and after the

* assume $T_{discharge}$ = mixed mean temperature

numerical curve smoothing. Using the specific entropy s of the
smoothed curve, the new mixed mean temperature can be calculated
from equation III-16 which is shown in Fig. E-6 (curve B) along
with the thermocouple recordings without any corrections for
errors. Taking into account the transient error due to finite
response time (minimum 1 m sec during intake, section III.1),
the agreement between the measured local temperatures and the
calculated mixed mean temperature seems to reasonable. The new
mixed mean temperature decreases the degree of mismatch between
P,V and T data, and resulting heat transfer (curve B,Fig. E-10)
bears this out. The flow chart in Fig. E-1 is the summary of
the procedures in this section.

3) Results

Data from Test #5 were used in the computer program listed
in Appendix E. Some of the results are discussed here.
a) The engine mass flow rate from the orifice-meter measure-
ment (7,60 x 10^{-3}kg/sec) confirmed the accuracy of the calcu-
lated cooler flow rate (7.56 x 10^{-3} kg/sec) as the engine flow
rate. This is very important for energy balance of the engine
(Appendix B) and gives more reliability to cyclic heat-transfer
estimates from both the compressor and the expander.
b) Step-by-step integration of the First Law for the Compressor
gives cyclic heat-transfer rate of 3.24 kW which is very close
to 3.23 kW from Equivalent Reversible Polytropic method.
c) The following is observed from heat-transfer rate vs. crank
angle plot (Fig. E-10). The fact that the heat transfer is

72

out of the gas into the wall throughout the compression process
is quite unusual considering the fact that the wall temperature
is supposed to be higher than the mixed mean gas temperature
in the beginning of compression. This fact can be explained
as follows. At the end of intake, the gas layer near the wall
is in thermal equilibrium with the wall. So, as soon as com-
pression starts, the temperature of the gas layer starts in-
creasing above the wall temperature. This causes heat transfer
from the gas layer into the wall, even though the mixed mean
gas temperature at that moment is lower than wall temperature.

During reexpansion (about $100°$ crank angle duration), it
takes a while (about $20°$ crank angle, 5.5 msec) for the tem-
perature of the gas layer near the wall to decrease below wall
temperature due to expansion causing heat transfer into the
gas. The 5.5 m sec delay indicated that at the end of discharge
the gas layer near the wall was not in thermal equilibrium
with the wall.

From above observations, we can say that the mixed mean
temperature is not a good representative gas temperature in cal-
culating the instantaneous heat transfer inside cylinder when
there is a significant spatial temperature variation, especially
in the radial direction.

CONCLUSIONS

The low performance of the VHGE has been primarily the result of irreversible cyclic heat transfer between the gas and the cylinder walls inside the expander and compressor. This heat transfer has a large effect on the mass per cycle and a small effect on the indicated P-V diagram and the indicated work per cycle.

The observed loss $(1-\eta)$ in the expander and the compressor are linearly related to the observed magnitude of the cyclic heat transfer. The cyclic heat transfer in the VHGE compressor was significantly reduced by changes in the wall-temperature distribution and by changes in the internal geometric configuration of the compressor and valves.

The cyclic heat transfer in a reciprocating expander or compressor can be calculated from observation of inlet temperature, discharge temperature, the mass per cycle and the indicated P-V diagram.

Further improvement in the performance of the VHGE will require additional reduction in the cyclic heat transfer in both the compressor and the expander. A reduction to about one half the present level will be required to achieve the performance levels originally projected (about 47% indicated efficiency).

REFERENCES

1. B.C. Fryer, "Design, Construction, and Testing of a New Valved Hot-Gas Engine", Sc.D. Thesis, M.I.T., Camb., MA., Feb. 1973.

2. R. Stein, "A Progress Report on the Development of the Valved, Hot-Gas Engine", S.M. Thesis, M.I.T., Camb.,MA., Jan. 1974.

3. T.R. Hankard, "Instrumentation and Testing of a Closed Reciprocating Brayton Cycle Engine", M.S. and M.E. Thesis, M.I.T., Camb., MA., May, 1973.

4. K.A. Yu, "Development of the Valved Hot-Gas Engine", S.M. Thesis, M.I.T., Camb., MA., May 1975

5. B.C. Fryer and J.L. Smith, Jr., "Design Construction and Testing of a New Valved Hot-Gas Engine", Proc. of 8th Intersociety Energy Conversion Engineering Conference, AIAA, Aug.1973.

6. H.S. Bean, "Fluid Meters, Their Theory and Application", Report of ASME Research Committee on Fluid Meters, 6th ed.,1971.

7. Max Jacob, "Heat Transfer", Vol. I, John Wiley & Sons, Inc., 1950

8. W.J. Hesse and N.V.S. Mumford. Jr., "Jet Propulsion for Aerospace Applications", 2nd ed., Pitman Publishing Corp., 1964.

9. P.K. Stein, Measurement Engineering, Vol. 1, Stein Engineering Services, Inc., Phoenix, 1964

10. W.M. Rohsenow and H.Y. Choi, "Heat, Mass and Momentum

Transfer, Prentice-Hall, Inc., Englewood Cliffs, N.J., 1961

11.   S.H. Crandall, N.C. Dahl, and T.J. Lardner, "An Introduc-
tion to the Mechanics of Solids", 2nd ed., McGraw-Hill Book
Company, 1972.

12.   L.E. Kinsler and A.R. Frey, "Fundamentals of Acoustics",
2nd ed., John Wiley & Sons, Inc., 1962.

Appendix A   ENGINE TEST DATA

The engine tests are identified as follows :

Test #1.   Brent Fryer's Test (ref.1, 1972)

Test #2.   First Cooled Compressor Head Test (1975)

Test #3.   First Rubber O Ring Test (1976)

Test #4.   After Compressor Modification (1977)

Test #5.   After Compressor Modification (1977)

Test #6.   After Compressor Modification (1978)

1. Pressure and Volume Data

Cylinder pressures are measured by two unbonded strain gauge type pressure transducers, and recorded on oscilloscope pictures and/or oscillograph recording paper.

Silicon rubber was coated (about 1 mm) on the diaphragm of pressure transducers to decrease excessive zero shift due to temperature.   In the expander case, the pressure transducer was water-cooled. The volume was measured by a displacement transducer whose plunger was in contact with a cam that was mounted on dynamometer axis and was shaped to convert the crank angle into the piston displacement.*

Fig. A-1, 2, 3, 4, 5 show indicated P-v diagrams of the compressor and the expander for Tests #2, #3, #4, #5, #6 respectively. Fig. A-6, 7, 8, 9 show pressure-crank angle plot of the compressor and expander for Tests #3, #4, #5, #6 respectively.

* See reference 3.

Compressor Volume (10^{-4} m^3)

8.741   2.950

3.55   3.55

Expander   Compressor
Pressure   Pressure
(MPa)   (MPa)

1.70   1.70

0.876   6.992

Expander Volume (10^{-4} m^3)

Expander
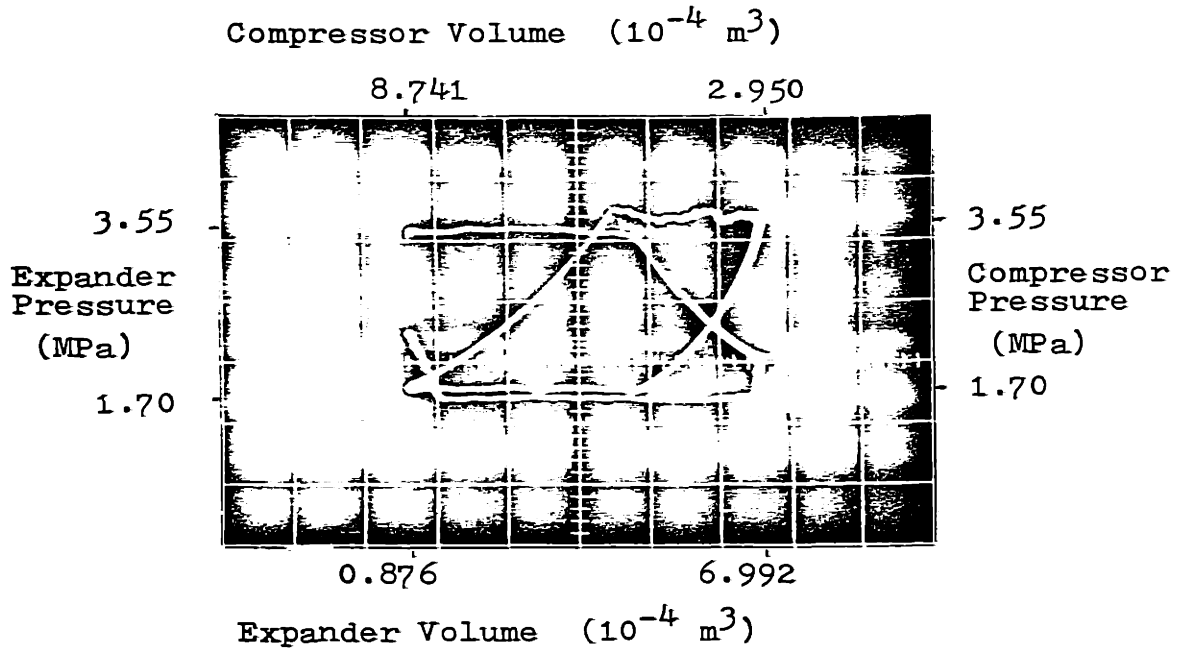
Compressor

Fig. A-1   Indicated P-V diagrams (Test #2)

Compressor Volume (10^{-4} m^3)

8.741   2.950

3.83 –

Pressure
(MPa)

1.79 –

0.876   6.992

Expander Volume (10^{-4} m^3)
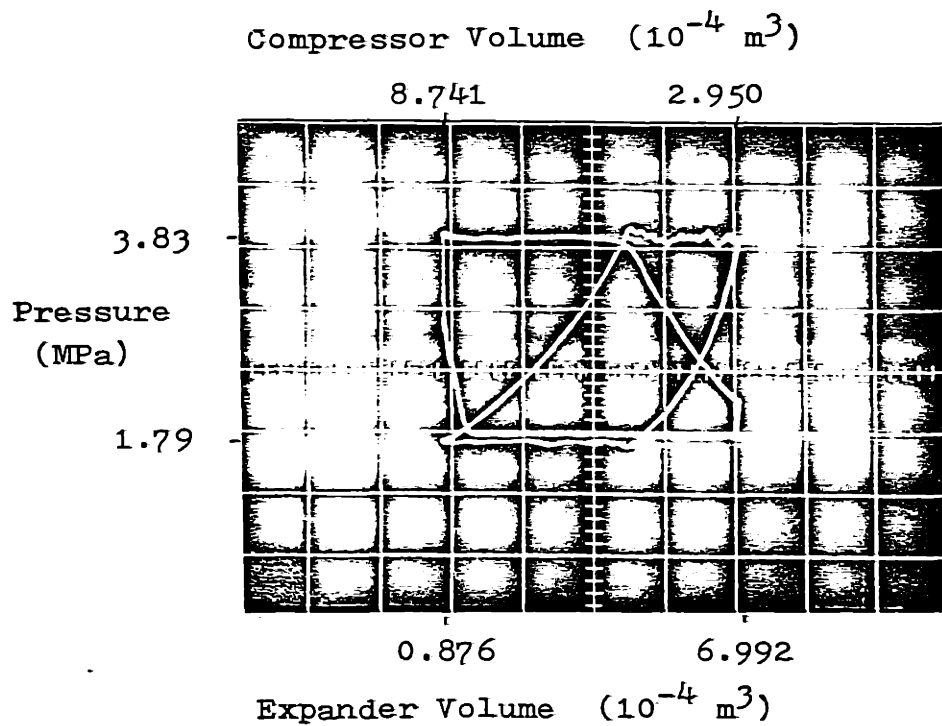
Fig. A-2 Indicated P-V diagrams (Test #3)

Compressor Volume ($10^{-4}m^3$)

10.216   4.425

3.24

Pressure
(MPa)

1.56

0.876   6.992

Expander Volume ($10^{-4}m^3$)
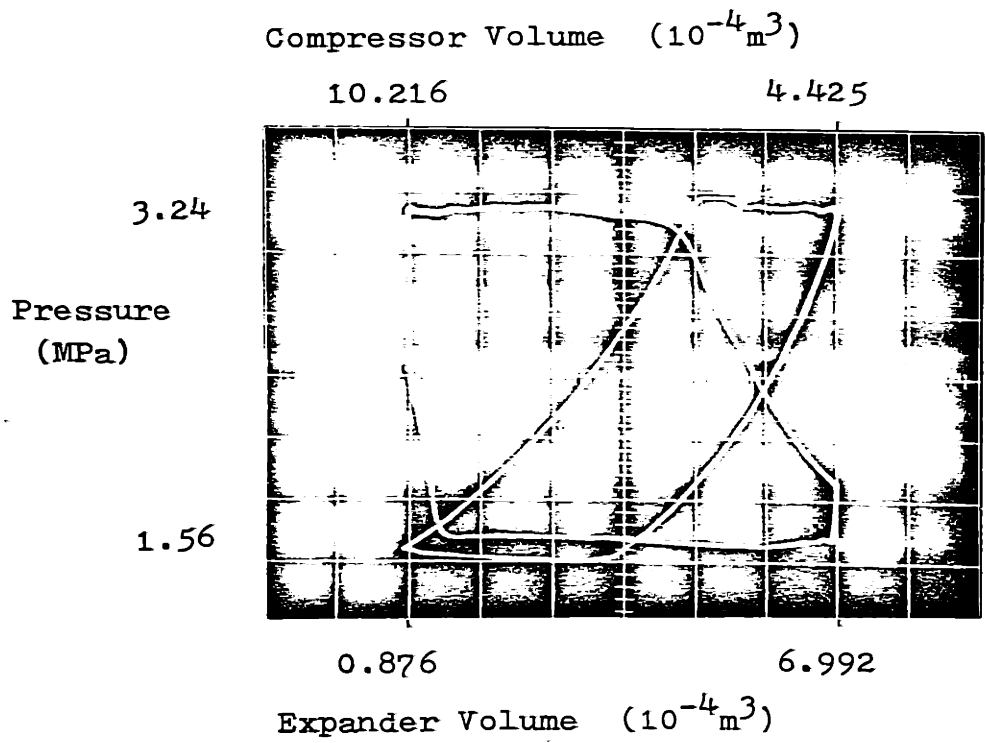
Fig. A-3   Indicated P-V diagrams (Test #4)

80

Compressor Volume (10^{-4} m^3)

10.333   4.542

Pressure
(MPa)

3.43

1.66

0.876   0.6992

Expander Volume (10^{-4} m^3)
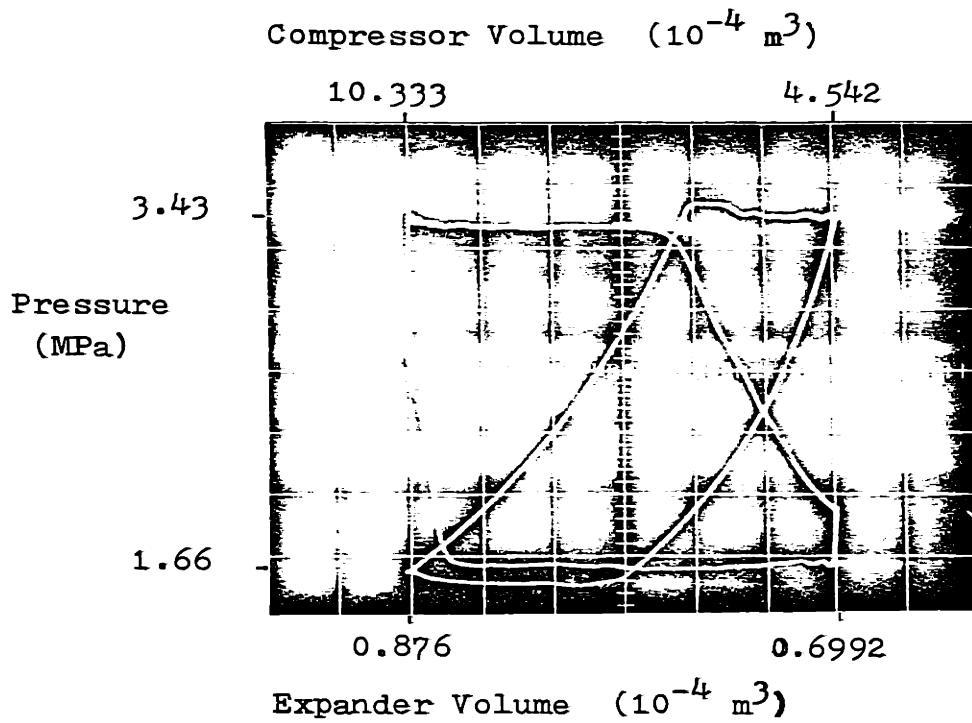
Fig. A-4   Indicated P-V diagrams (Test #5)

Compressor Volume $(10^{-4}\ m^3)$

10.333   4.542

Pressure
(MPa)

3.45

1.64

0.876   0.6992

Expander Volume $(10^{-4}\ m^3)$
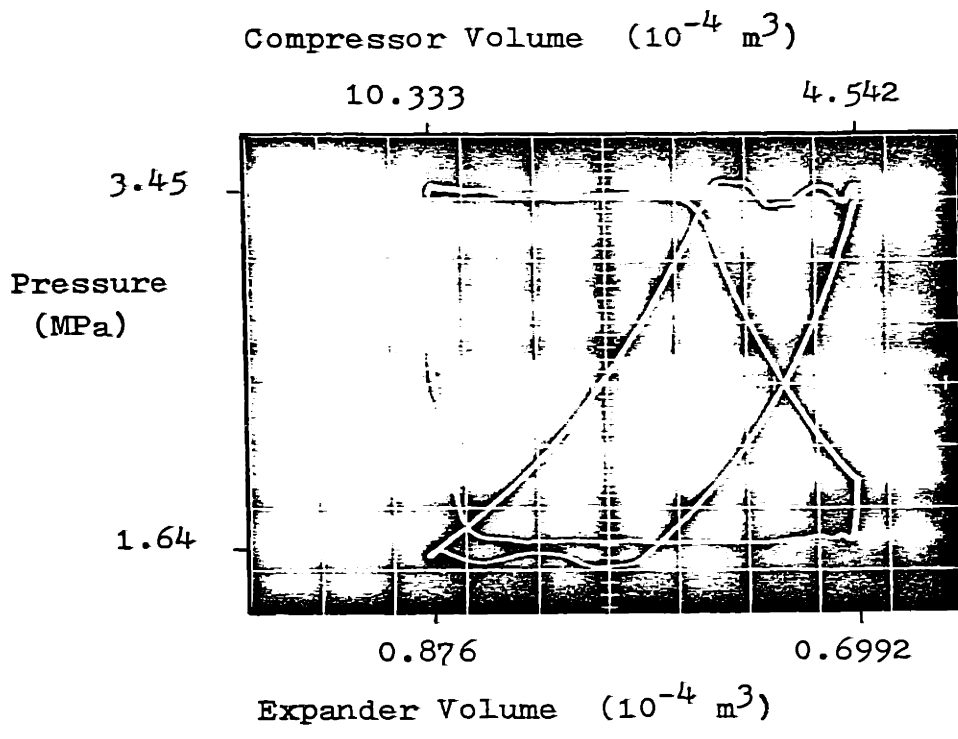
Fig. A-5 Indicated P-V diagrams (Test #6)
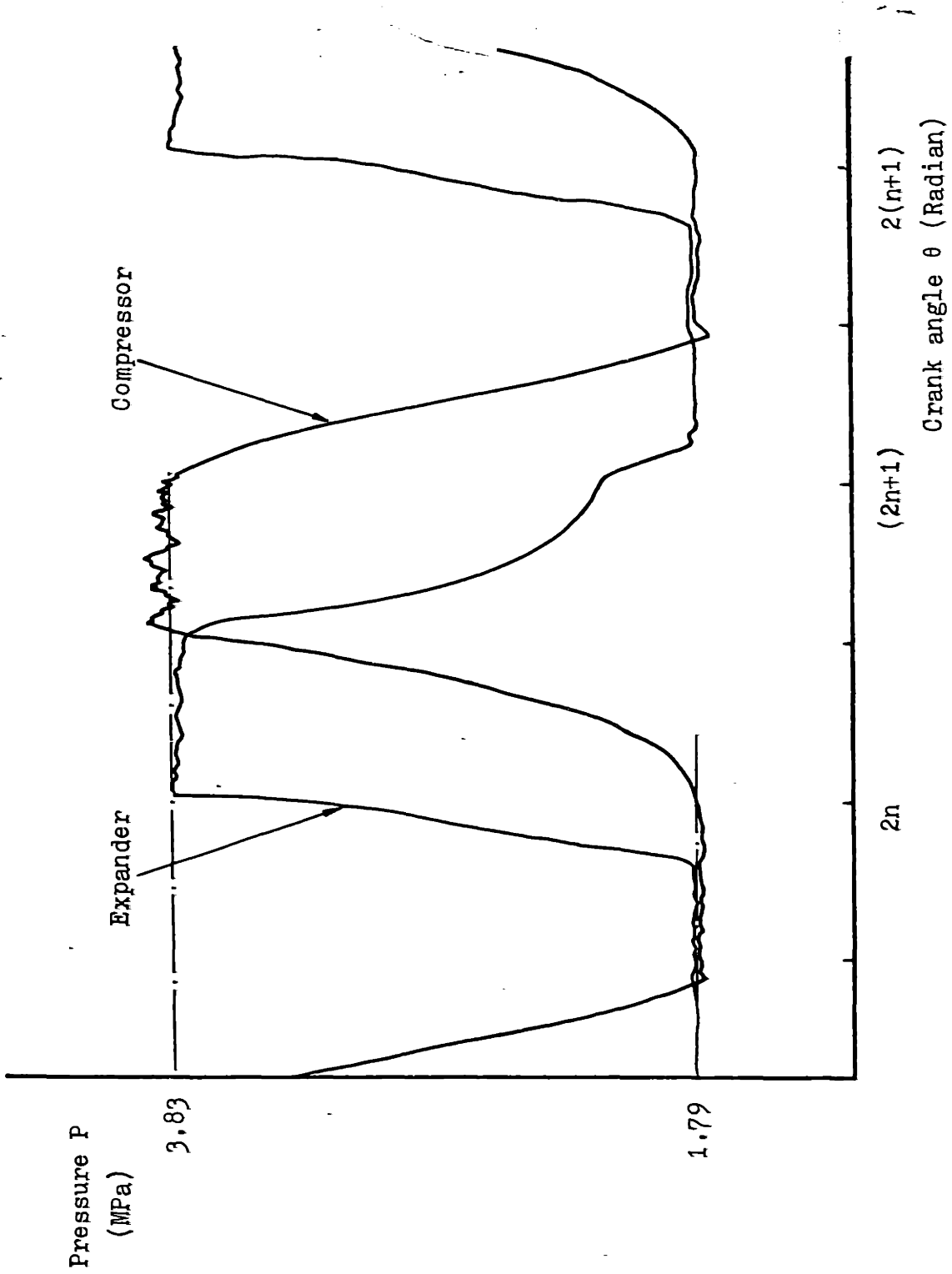
Fig. A-6 P-θ diagram for expander and compressor – Test #3

83
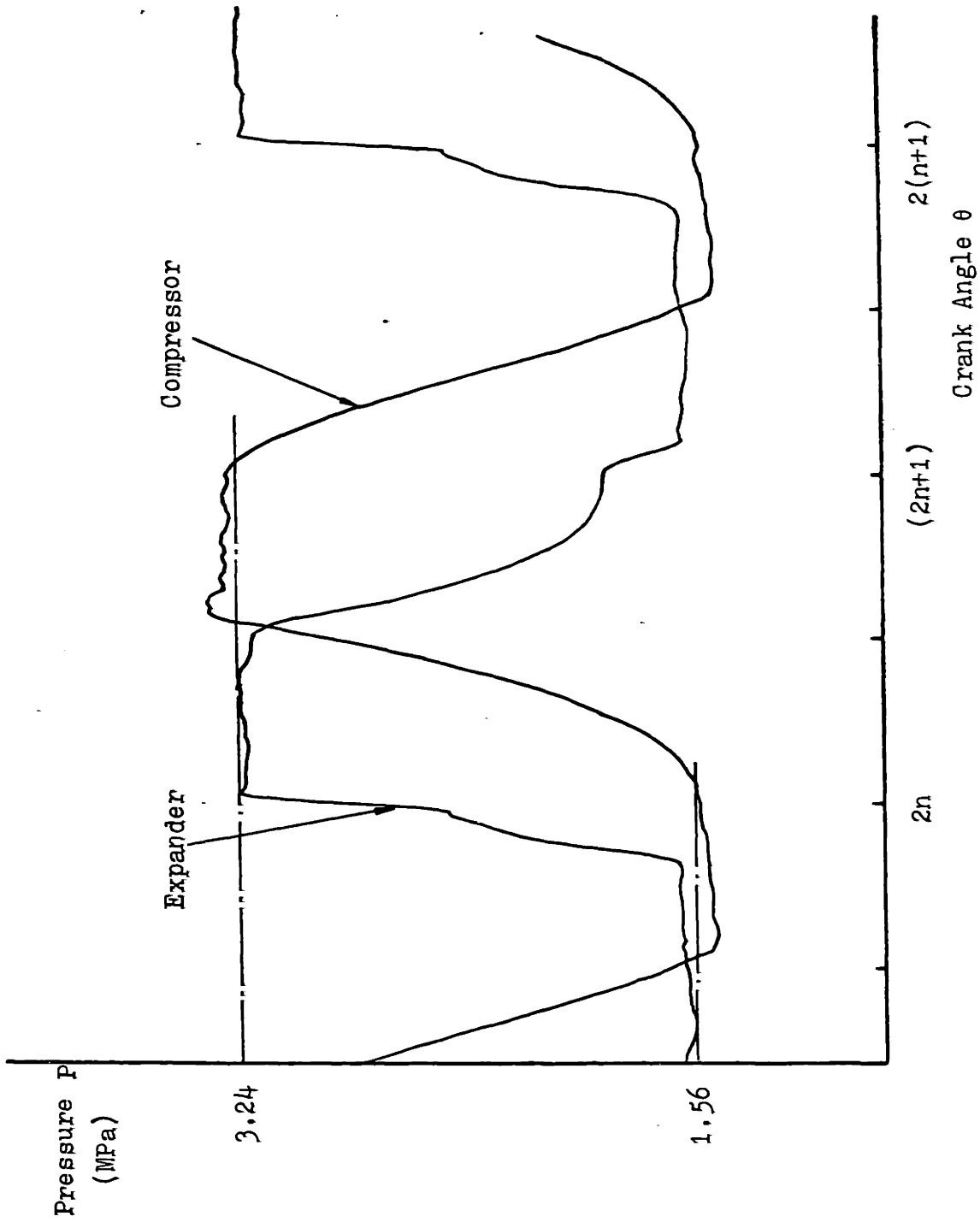
Fig. A-7 P-θ diagram for expander and compressor - Test #4

84
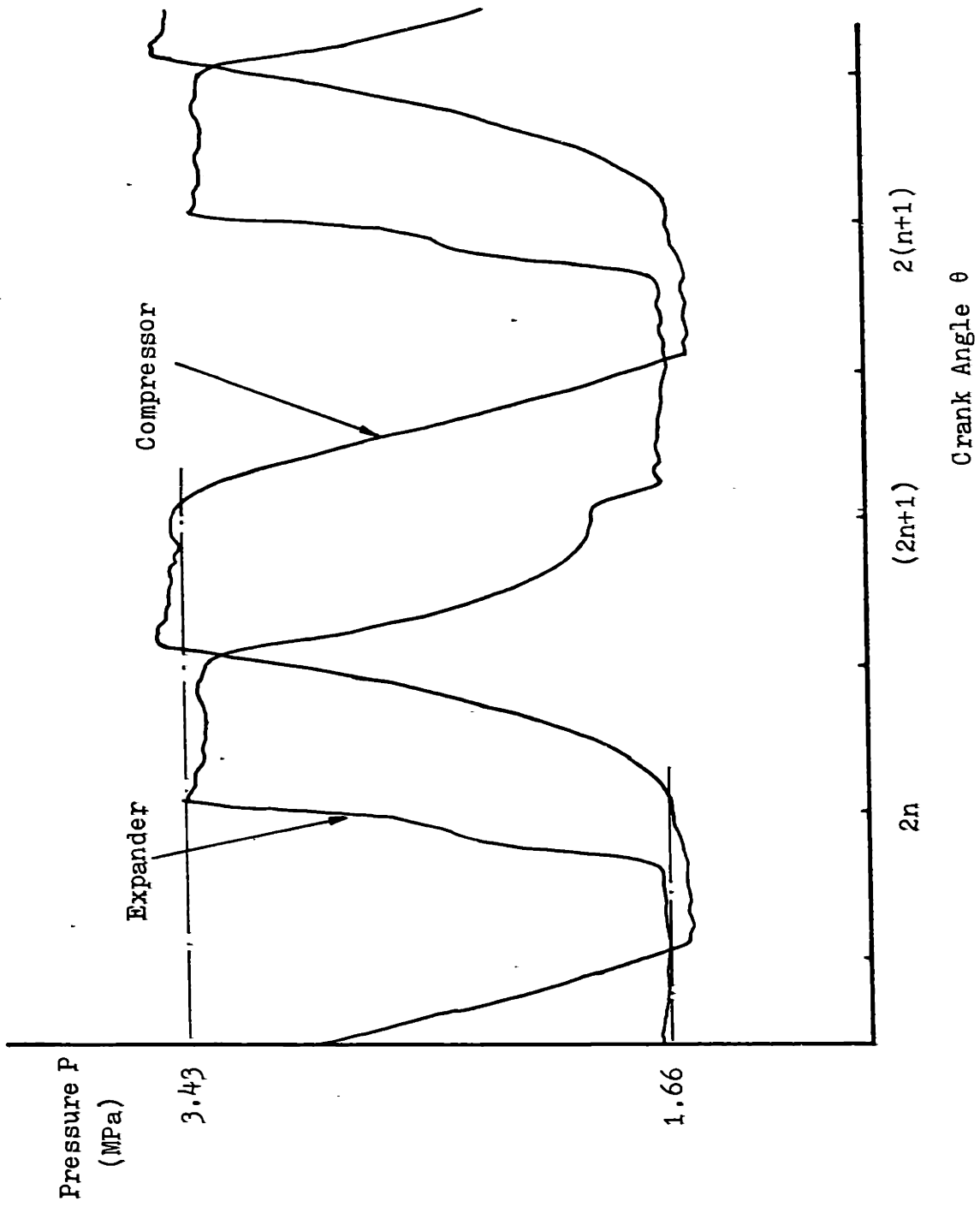
Fig. A-8 P-θ diagram for expander and compressor - Test #5

85
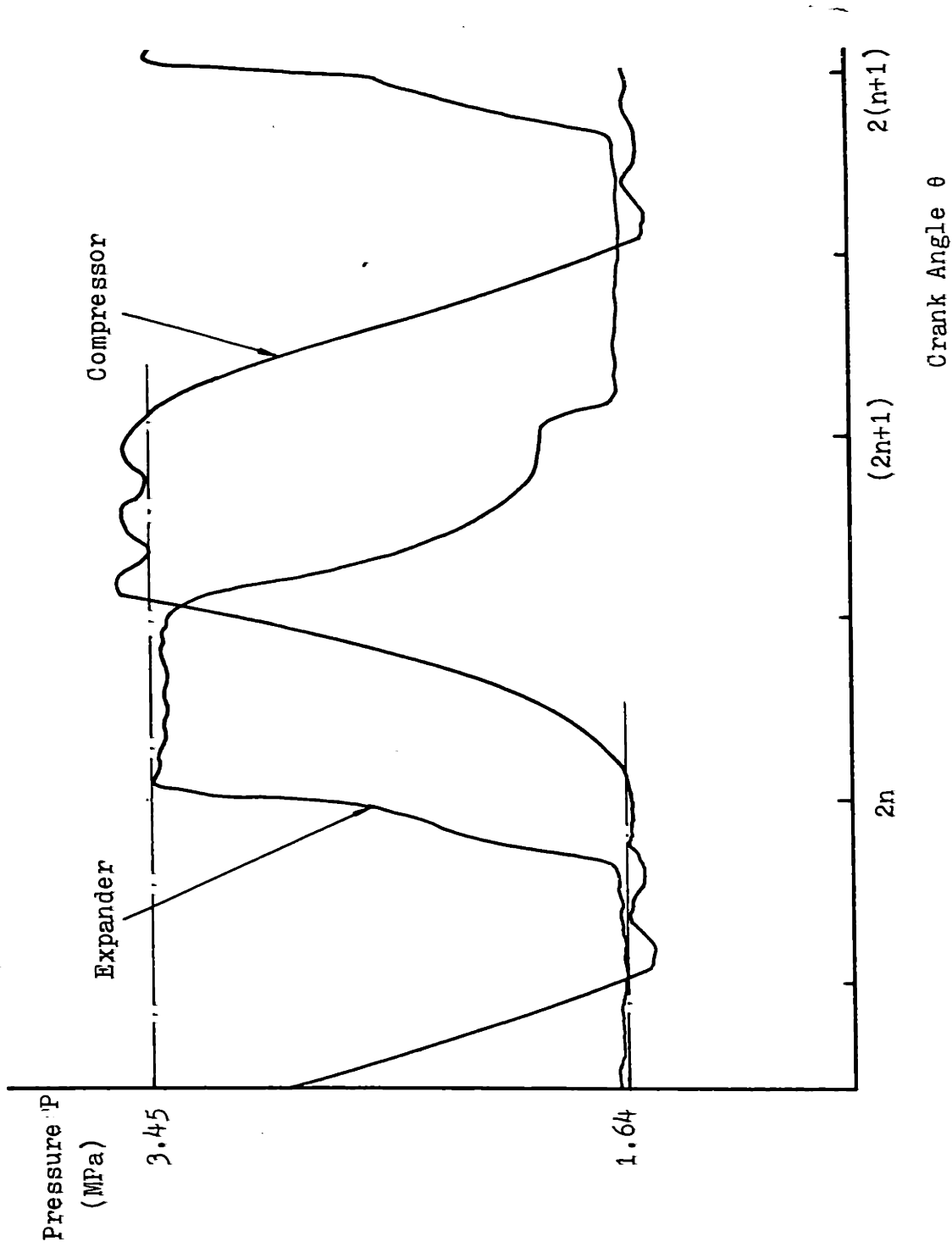
Fig. A-9 P-θ diagram for expander and compressor -Test #6

86

2. Temperature Data

1) Average temperatures

Multi-channel recorders were used to record average gas temperatures outside the cylinder and average surface temperatures of engine components. Fig. A-10 shows the locations of thermocouples recorded by multi-channel recorders. Table A-1 lists the recorded temperatures from Test #2 to #6.

2) Transient temperature data

The Chromel-Alumel thermocouples were used for the compressor and Platinum-Rhodium thermocouples were used inside expander. Of the two thermocouples inside the expander, the one in the intake port was bent over during Test #3. However, it gave us valuable information about heat transfer during the intake process. Fig. A-11 is the temperature volume plot of Test #2. Fig. A-12, 13, 14, 15 show the temperature fluctuation inside the compressor with respect to crank angle for Tests #3, 4, 5, 6 respectively. Fig. A-16 shows the significant temperature difference between the readings from the intake side and the discharge side thermocouple of the expander before the intake side thermocouple failed in Test #3. Fig. A-17, 18, 19, 20 show the expander temperature fluctuation with respect to crank angle measured by discharge side thermocouple for Tests #3, 4, 5, 6 respectively.

87
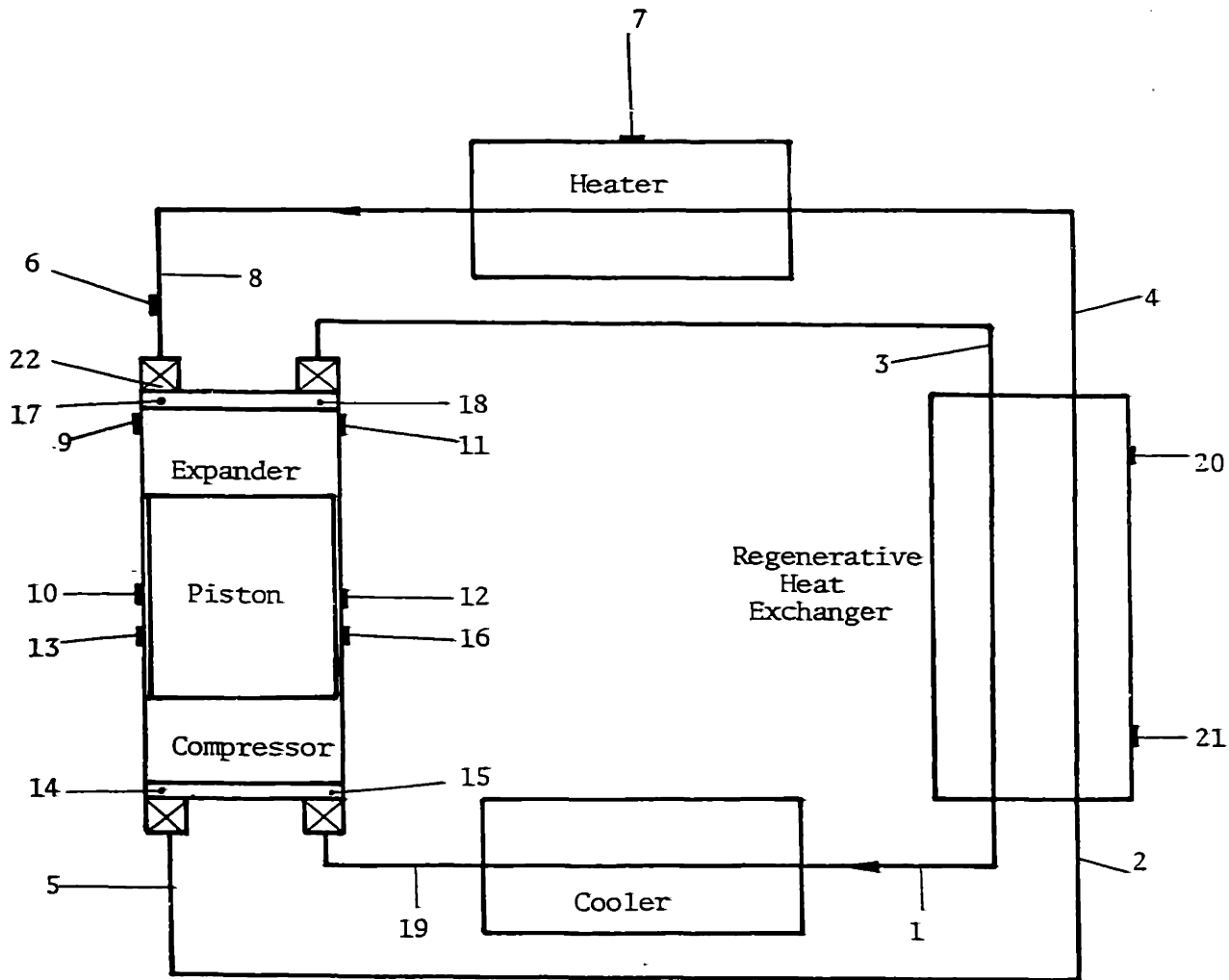
Fig. A-10 Locations of thermocouples
          connected to multirecorder

163 — Discharge Temperature (°C)

21 —

153 — Intake Temperature (°C)

31 —

8.741   2.950

Volume (10^{-4} m^3)

(a) Compressor Discharge and Intake

Temperature (°C)

702 —

465 —

0.876   6.992

Volume (10^{-4} m^3)
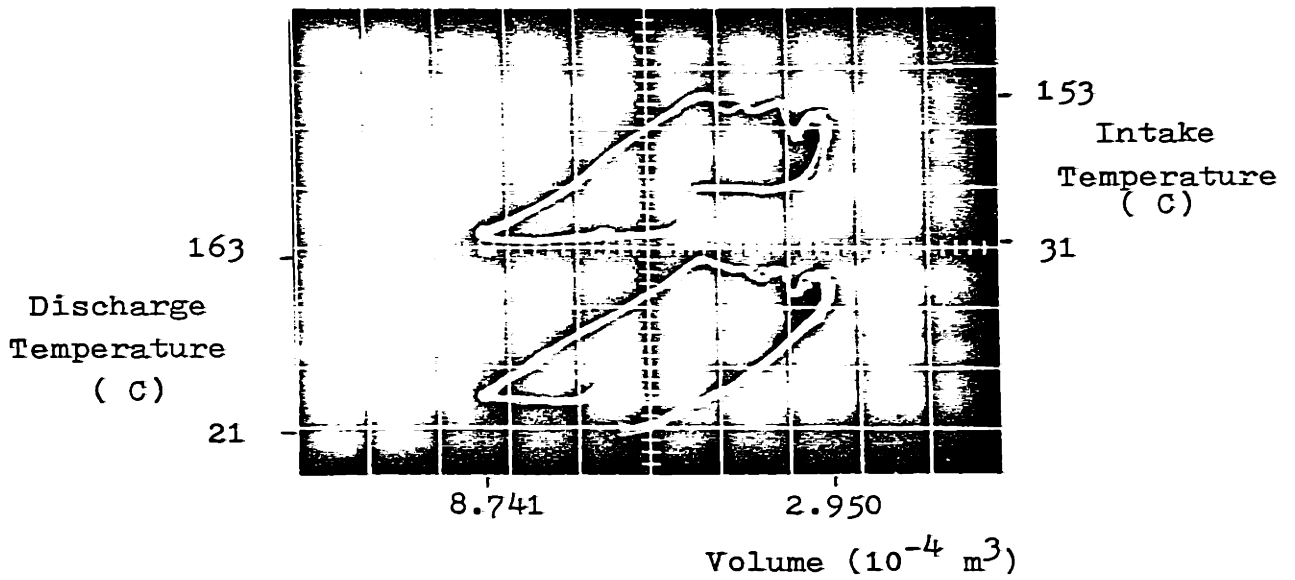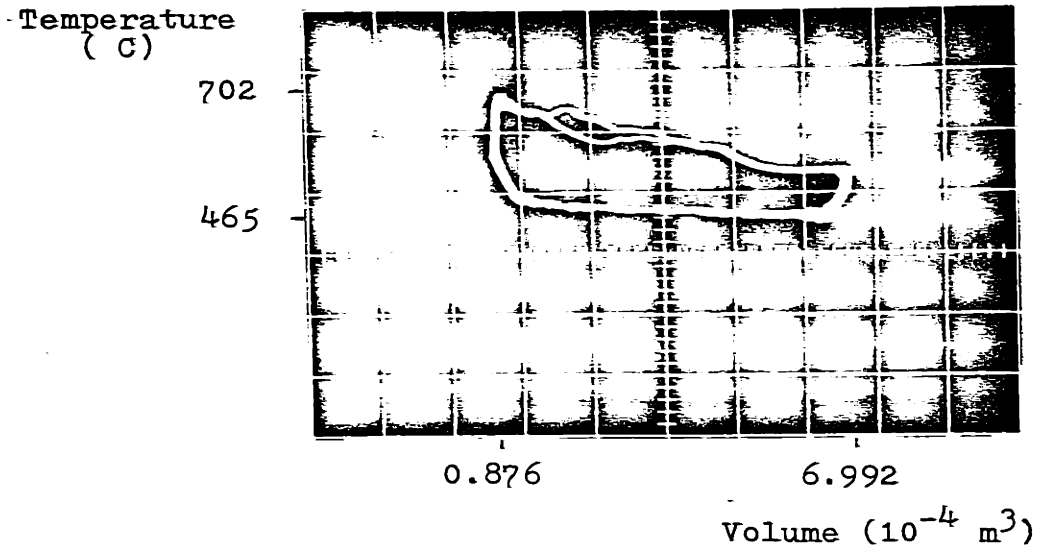
(b) Expander Discharge

Fig. A-11   Transient gas temperatures (Test #2)

89
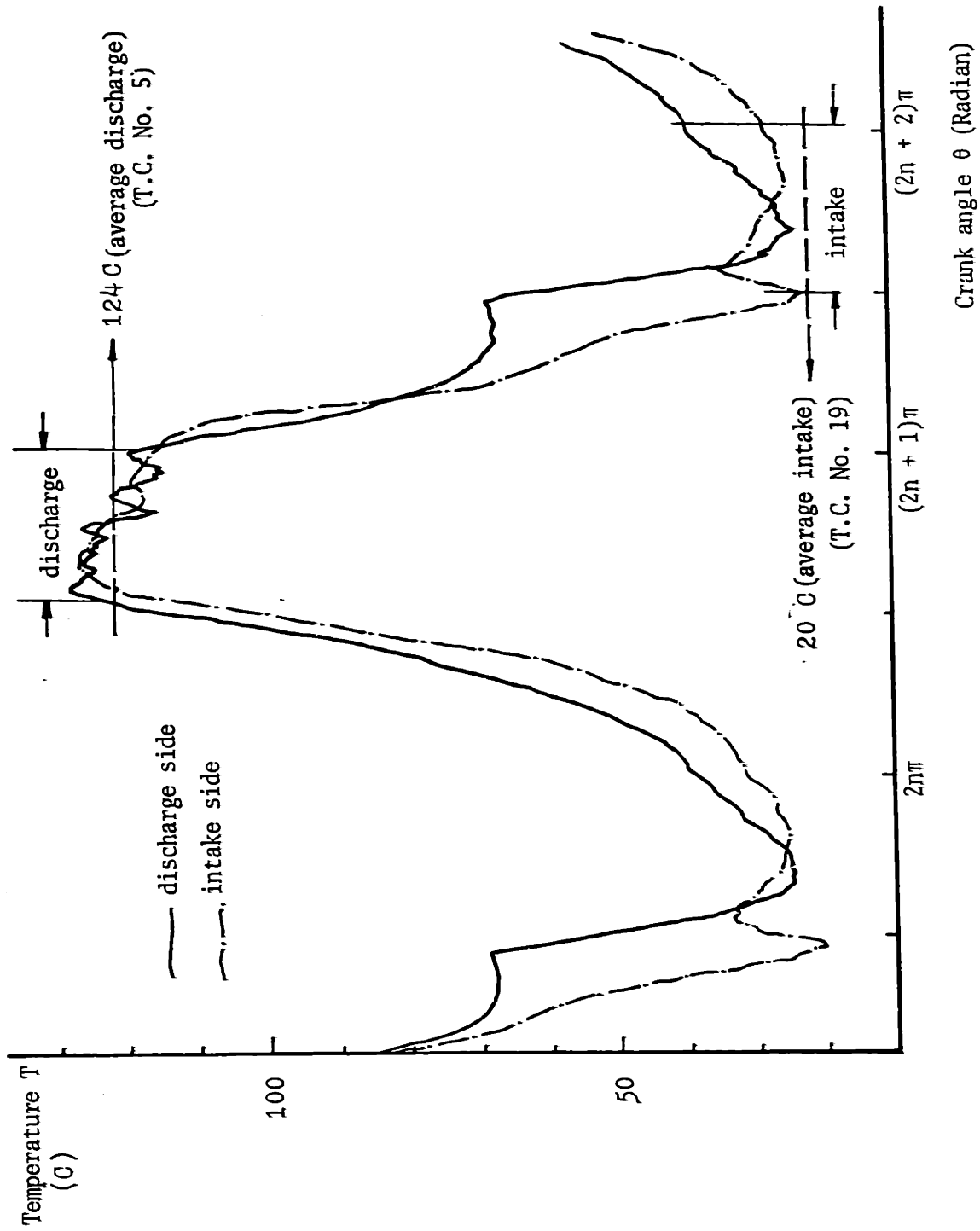
Fig. A-12 Compressor gas temperature vs. crank angle
(Test #3)

90
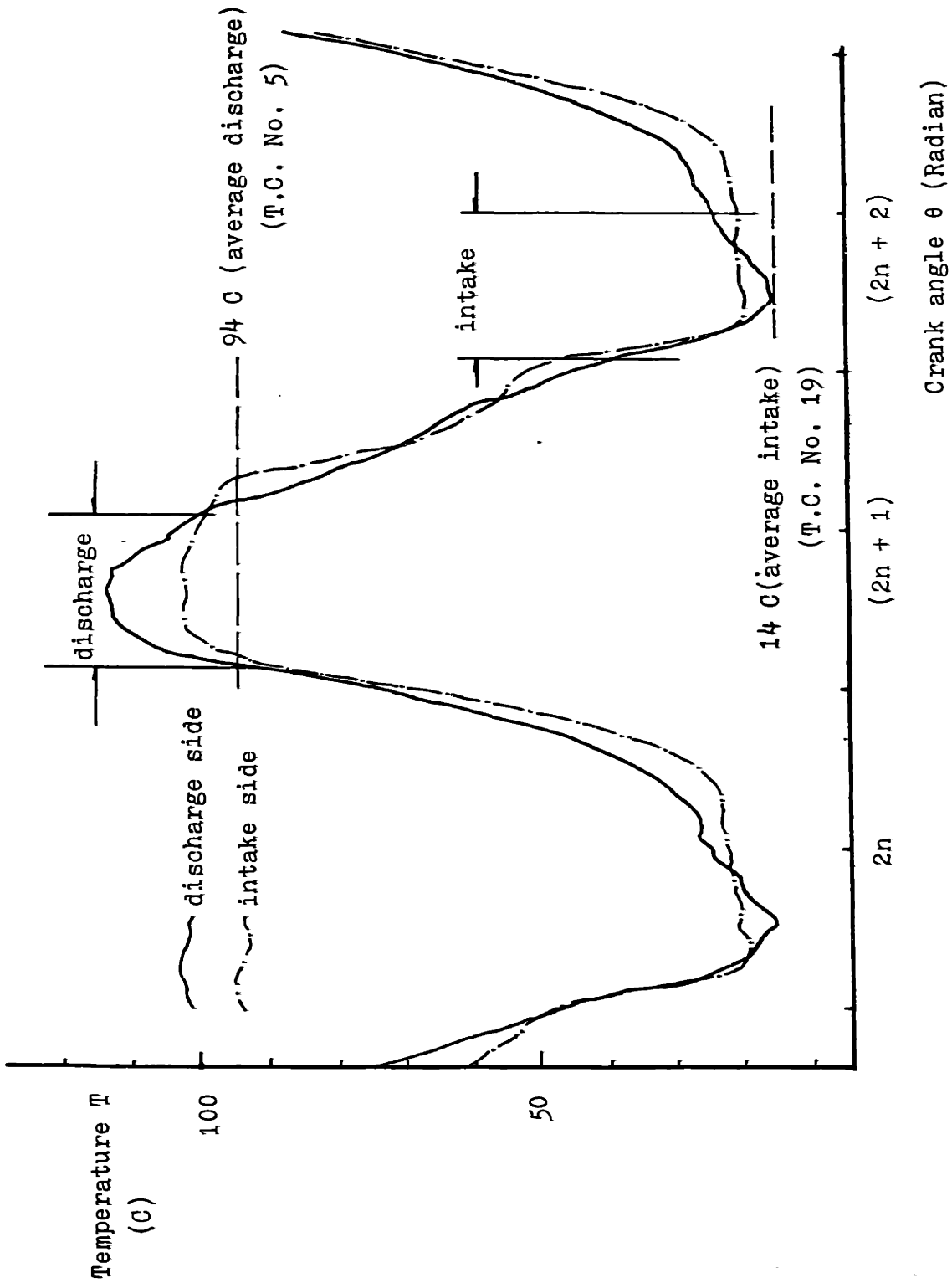
Fig. A-13 Compressor gas temperature vs. crank angle
(Test #4)
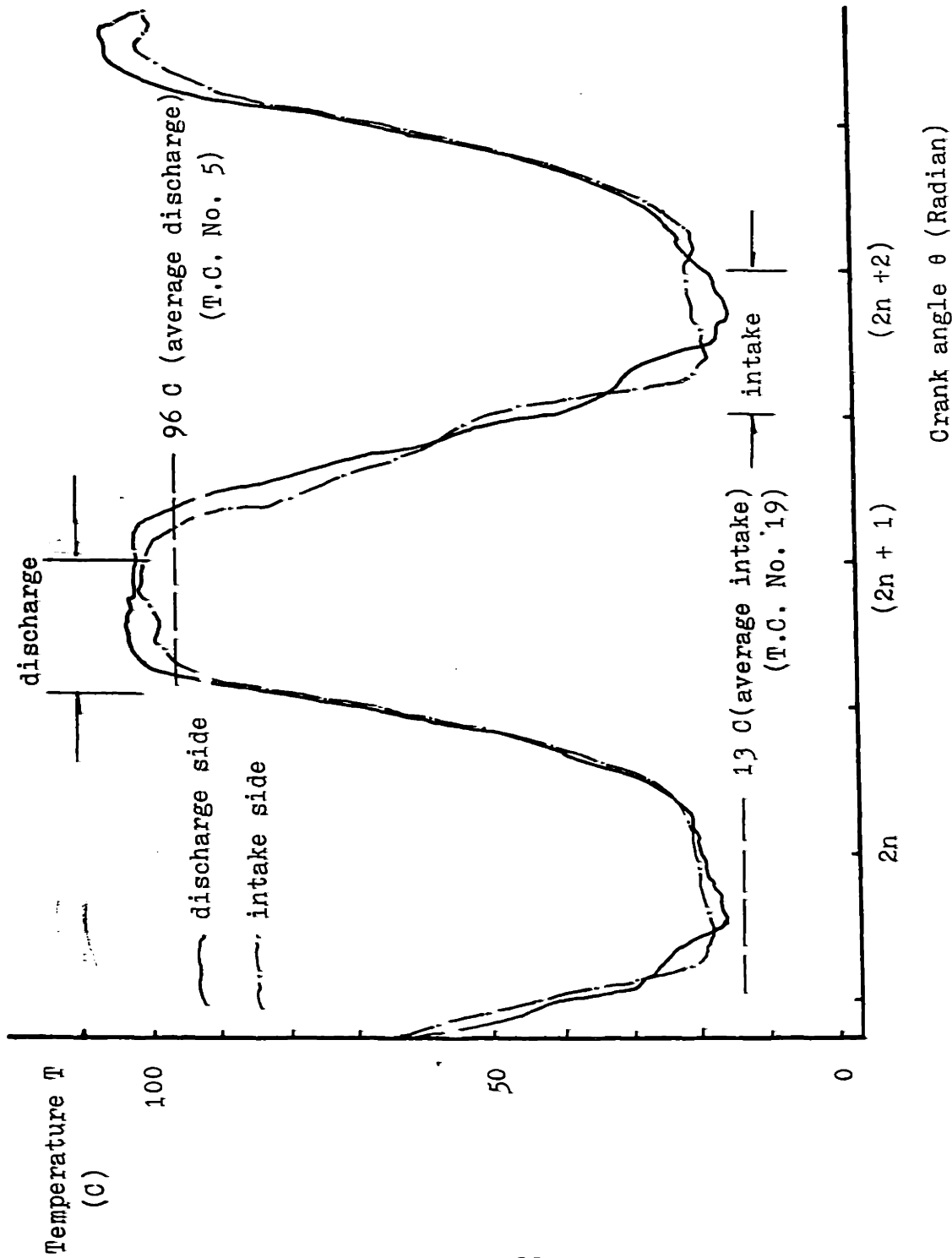
Fig. A-14 Compressor gas temperature vs. crank angle
(Test #5)

92
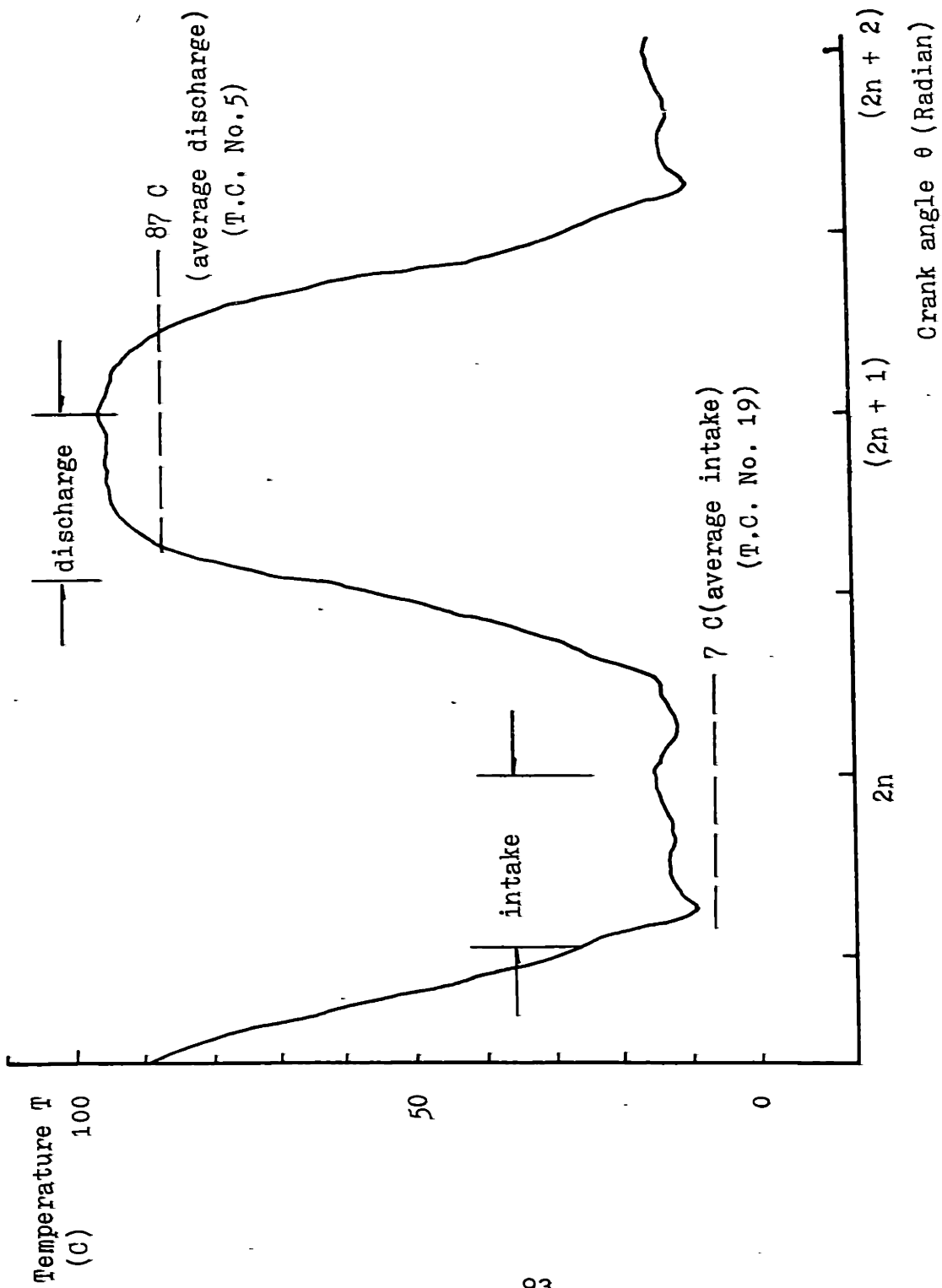
Fig. A-15 Compressor gas temperature vs. crank angle
(Test #6)

93
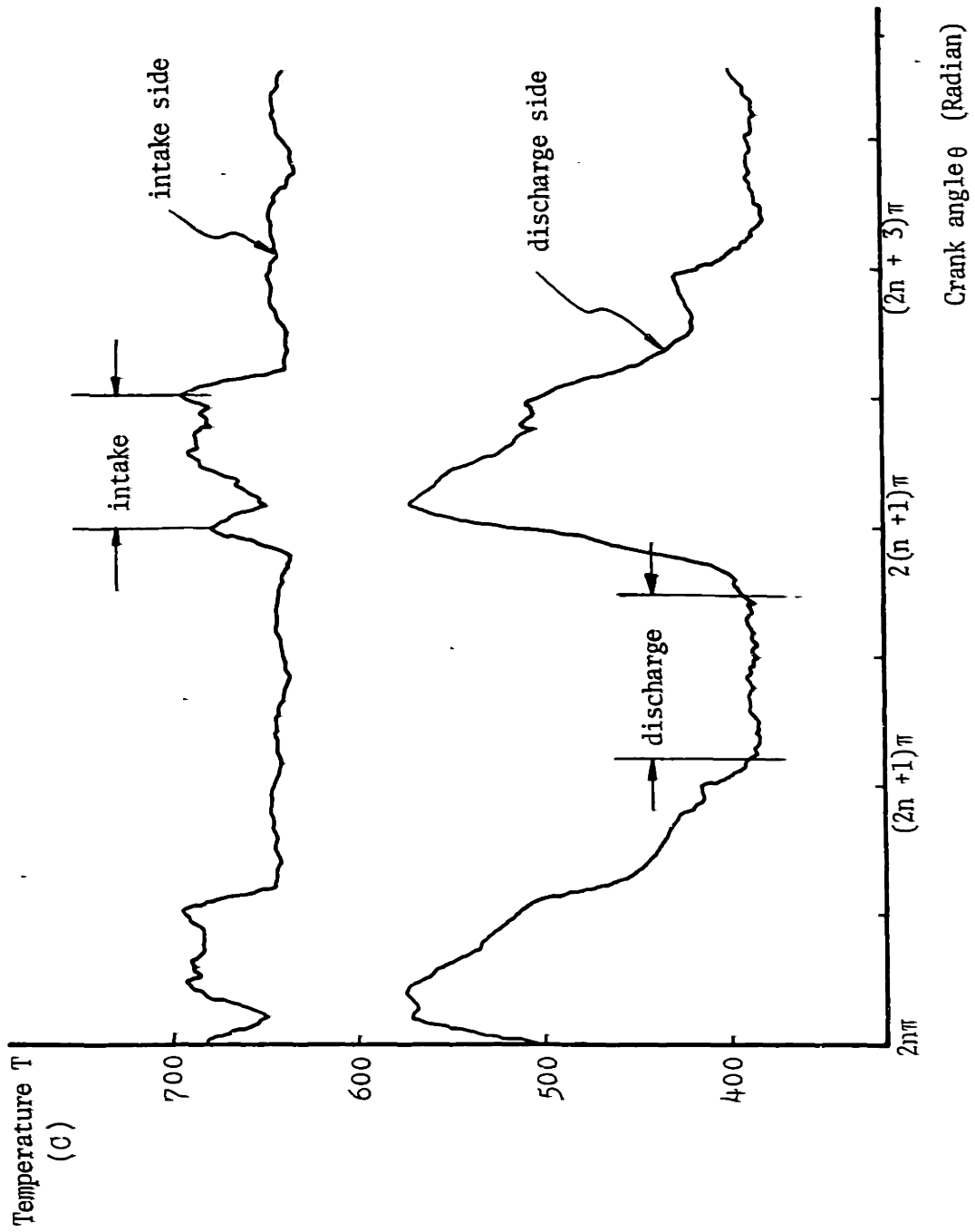
Fig. A-16   Comparison of the temperature readings from expander
            intake side and discharge side thermocouple   (Test #3)
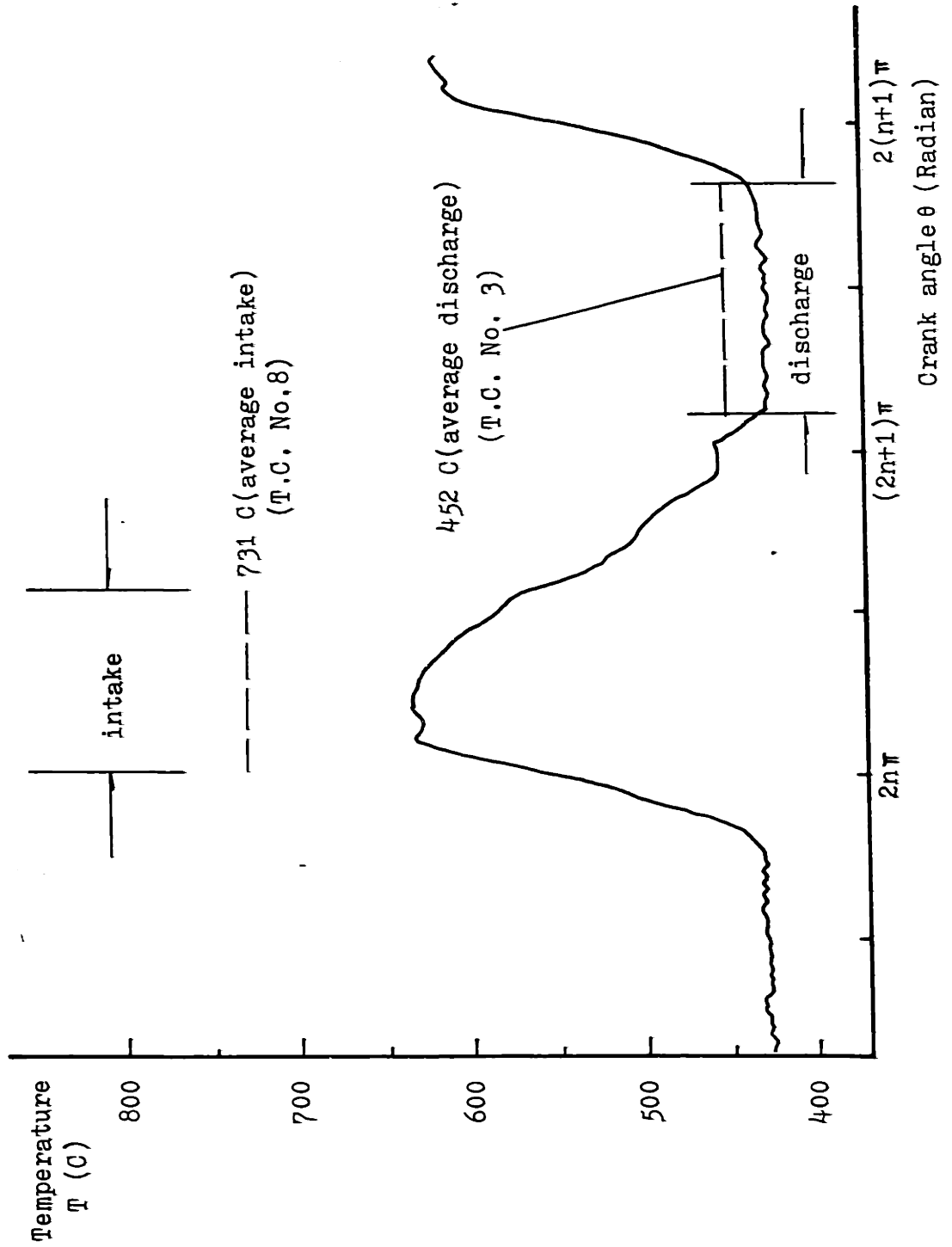
Fig. A-17 Expander gas temperature vs. crank angle
(Test #3)
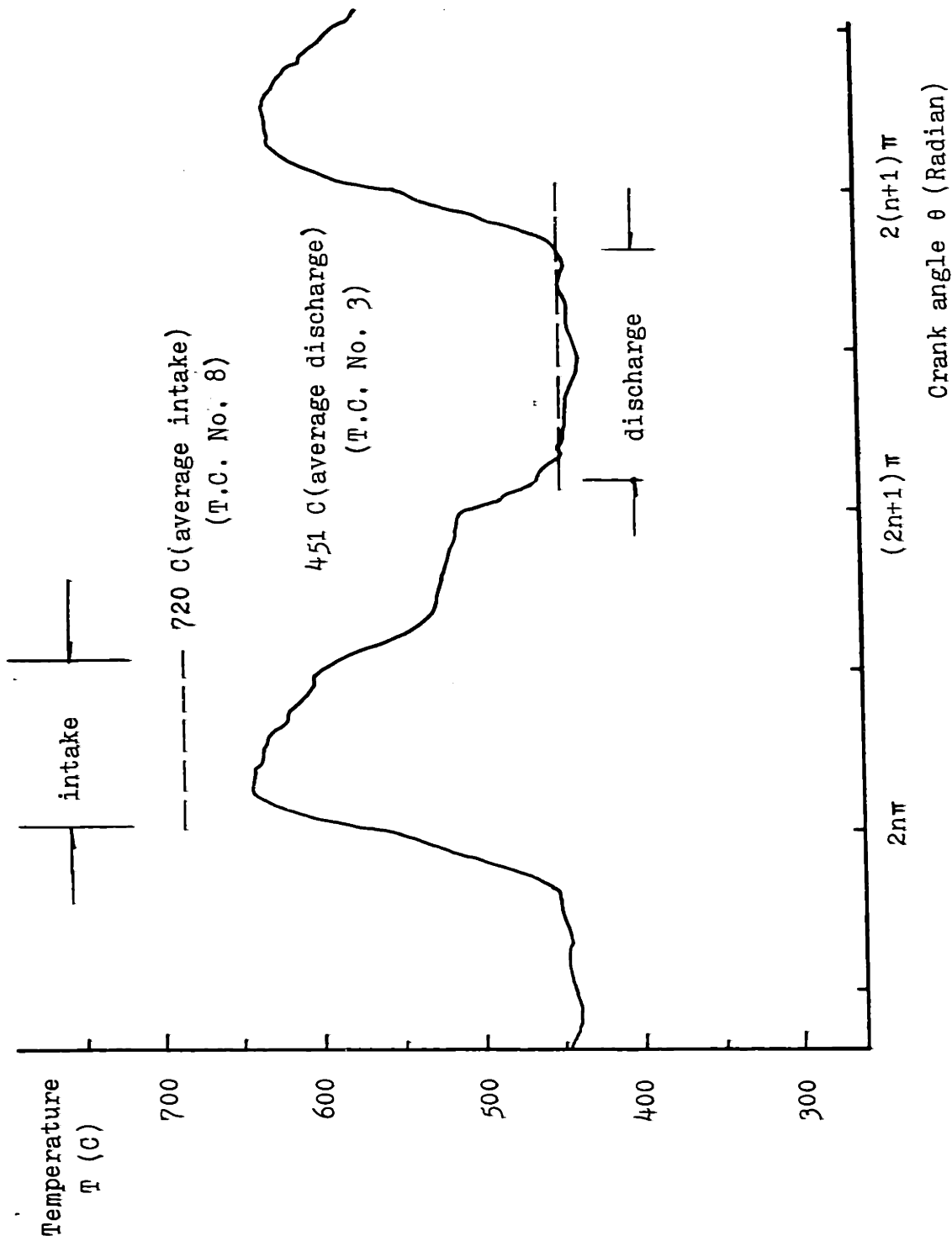
Fig. A-18 Expander gas temperature vs. crank angle (Test #4)

96
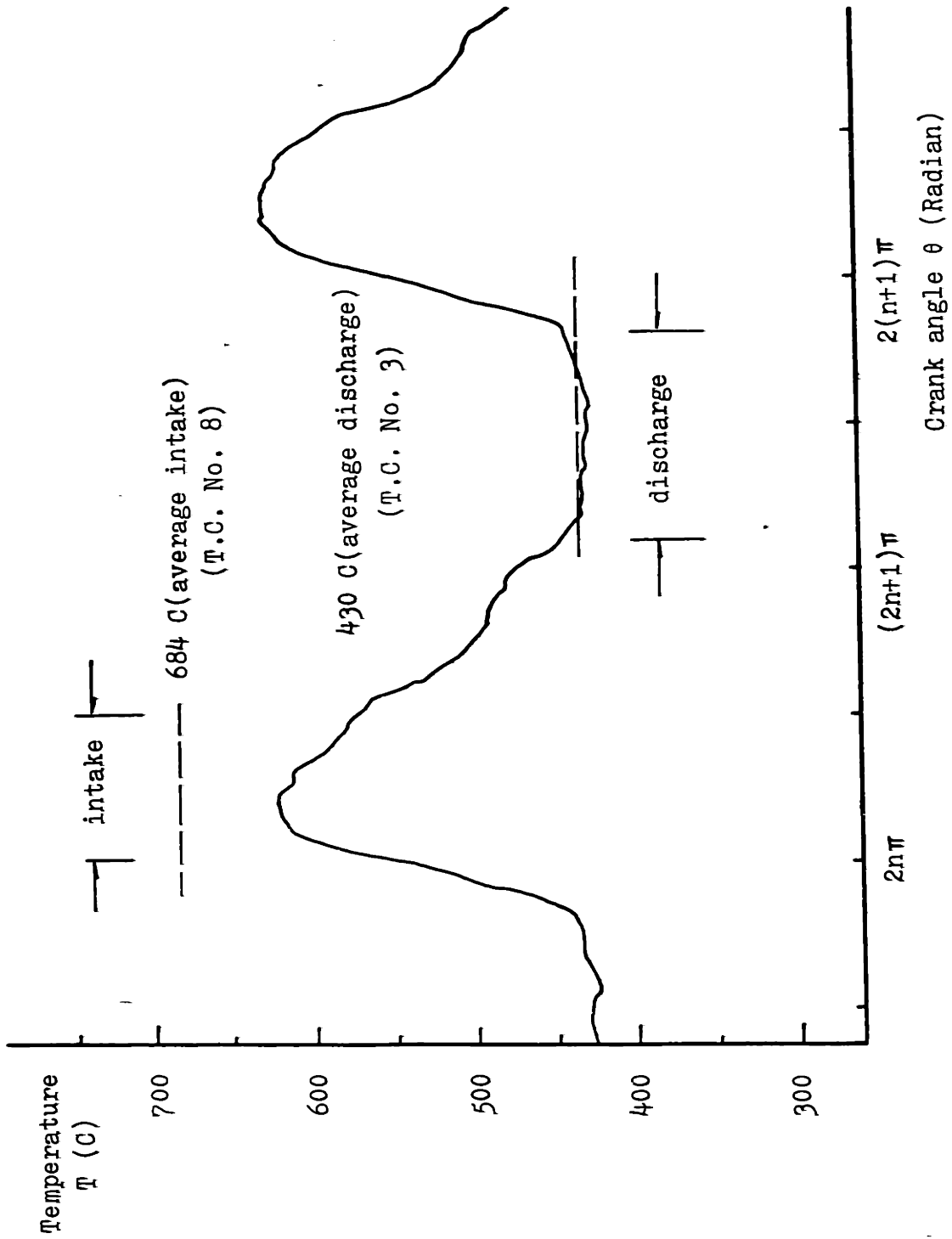
Fig. A-19 Expander gas temperature vs. crank angle
(Test #5)

97

Temperature T (C)

700 — 600 — 500 — 400 — 300

intake

699 C(average intake)
(T.C. No. 8)

439 C(average discharge)
(T.c. 3)

discharge

2nπ   (2n+1)π   2(n+1)π

Crank angle θ (Radian)
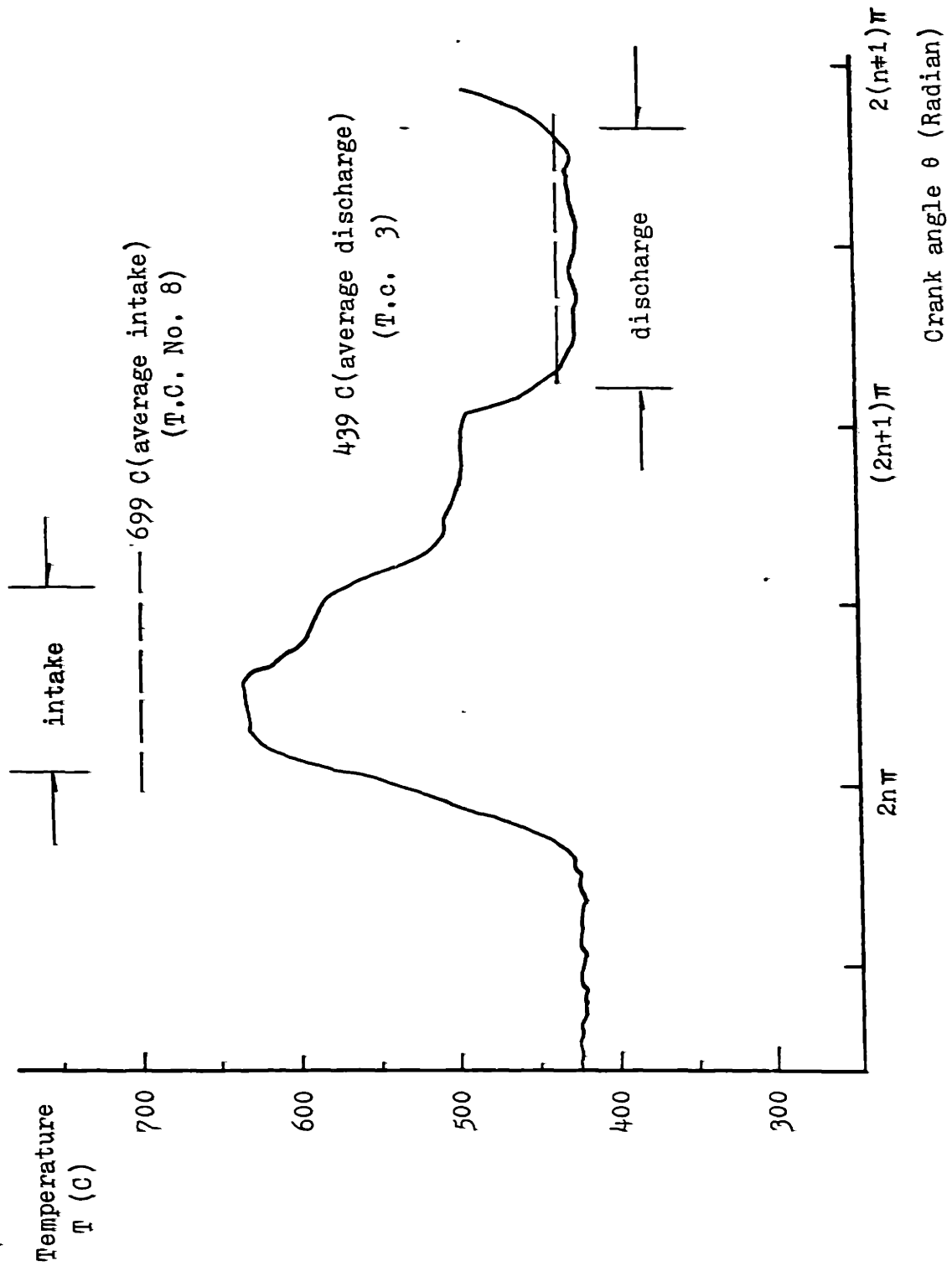
Fig. A-20 Expander gas temperature vs. crank angle
(Test #6)

98

Table A-1 Average Temperatures (C) from Multi-channel Recorders

T.C.No	Test #2	Test #3	Test #4	Test #5	Test #6
1	150	137	116	120	112
2	124	112	86	89	81
3	459	452	451	430	439
4	422	411	408	389	398
5	136	124	94	96	87
6	655	685	687	651	668
7	686	687	698	653	675
8	724	731	720	684	699
9	613	602	604	574	586
10	463	433	433	416	416
11	552	532	522	505	516
12	446	379	351	356	363
13	155	153	149	–	–
14	72	68	27	38	31
15	38	42	18	18	12
16	136	127	–	–	–
17	618	649	639	616	627
18	531	462	464	439	451
19	24	20	14	13	7
20	422	407	411	392	402
21	150	141	120	123	116

3. Cooling Water Data

Up to Test #2, thermometers of low resolution (maximum resolution error 0.5 C when water temperature drop in the cooler was about 5 C) were used. From Test #3, high resolution thermometers (maximum resolution error 0.05 C) were used. In order to increase the reliability of the water temperature measurement further, special receptacles (Fig. A-21), which will provide enough immersion depth, were fabricated and used in the measurements to minimize the thermometer error due to conduction through the thermometer stem.

Table A-2, 3 list the cooling water heat removal rates in Test #2, #3 respectively. Table A-4 lists the cooling water heat removal rates for Tests #4, #5, and #6.

Table A-2 Cooling Water Heat Removal Rates (kW)- Test #2

Cooler	4.63
Piston Rod Seal & Cyl. Jacket	1.86
Compressor Block (Jacket)	0.71
Expander Head	0.33
Heater	0.09
Total	7.62
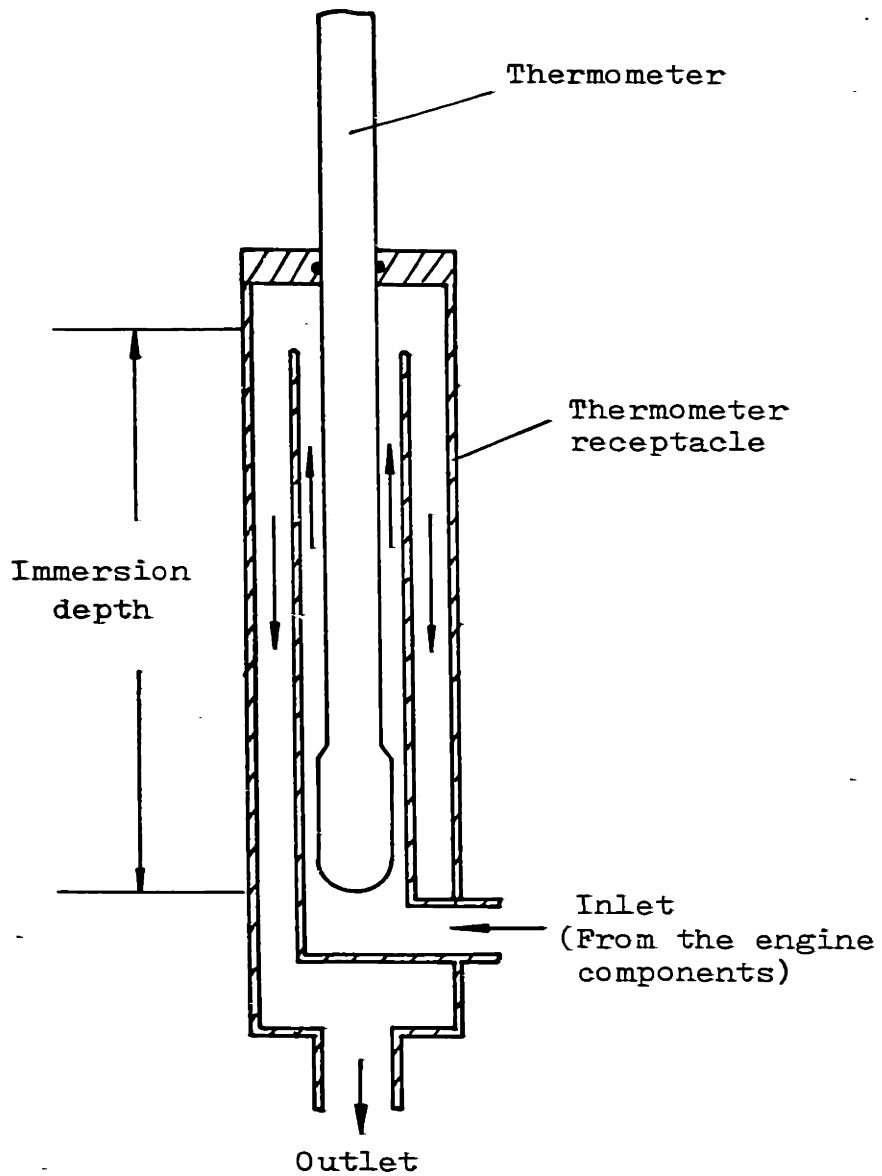
Fig. A-21 Receptacle for a thermometer (schematic)

Table A-3 Cooling Water Heat Removal Rates (kW) – Test #3

Cooler	4.37
Cylinder Jacket	1.42
Comperssor Block	0.92
Piston Rod Seal	1.07
Expander Head	0.43
Heater	0.05
Total	8.26

Table A-4 Cooling Water Heat Removal Rates (kW)-Test #4,5,6

	Test #4	Test #5	Test #6
Cooler	3.14	4.19	4.12
Cylinder Jacket	1.85	2.08	2.15
Compressor Block(Bolt holes)	0.37	0.40	0.49
Compressor Block (inner wall & valve ports)	0.65	0.76	0.75
Piston Rod Seal	0.16	0.19	0.22
Expander Head	0.36	0.37	0.44
Heater	0.09	0.09	0.13
Total	6.62	8.08	8.30

4. Power Measurement

1) Heater input

Electrical power input to the heater is calculated from

$$\dot{Q} \text{ (kW)} = \text{Voltage across heater (V)} \times \frac{100 \text{ (Amp)}}{50 \text{ (mV)}} \times \frac{\text{shunt Voltage(mV)}}{1000}$$

Table A-5 lists data for Tests #2 through #6.

Table A-5 Heater Electrical Input Data

	Test #2	#3	#4	#5	#6
Voltage across heater(V)	245	257	242	257	258
Shunt Voltage (mV)	24.02	25.04	23.20	24.60	24.95
Input Power (kW)	11.77	12.87	11.23	12.64	12.87

2) Brake power

The brake power is measured by a dynamometer, load cell, and manometer set up. It is calculated from the following equation.

$$\dot{W}_{brake} \text{(kW)} = 0.3491 \times \text{manometer reading above zero(m)}$$
$$\times \text{ rotational frequency } (\text{sec}^{-1})$$

Table A-6 lists data for Tests #2 through #6.

Table A-6 Brake Power Data

	Test #2	#3	#4	#5	#6
Manometer reading(m)	0.557	0.406	0.617	0.605	0.668
Rot. frequency (sec^{-1})	9.07	9.02	9.00	10.00	9.97
$\dot{W}_{brake}$ (kW)	1.76	1.28	1.94	2.11	2.32

3) Compressor indicated power $\dot{W}_c$, and expander indicated power $\dot{W}_e$

The areas of the P-V diagram (Fig. A-1 to 5) were measured by a planimeter and then multiplied by proper calibration factors to yield indicated powers :

$$\dot{W} \text{ (kW)} = \text{area of P-V diagram } (m^2) \times \text{vertical calibration } (\frac{kPa}{m})$$
$$\times \text{ horizontal calibration } (\frac{m^3}{m}) \times \text{ rotational frequency } (sec^{-1})$$

Table A-7 lists the compressor data and Table A-8 lists the expander data.

Table A-7 Indicated Power Data - Compressor

	Test #2	#3	#4	#5	#6
Area of P-V diagram($10^{-4} m^2$)	6.23	5.86	12.62	13.18	12.66
Vertical Calibration(kPa/m)	73020	68330	33380	33330	34240
Horizontal Calibration (10^{-2} m^3/m)	1.30	1.55	1.05	1.05	1.06
$-\dot{W}_c$ (kW)	5.37	5.58	3.98	4.61	4.57

Table A-8 Indicated Power Data - Expander

	Test #2	#3	#4	#5	#6
Area of P-V diagram($10^{-4}m^2$)	9.42	8.85	21.51	21.77	22.26
Vertical Calibration(kPa/m)	73020	68330	33380	33330	34240
Horizontal Calibration ($10^{-2}\ m^3/m$)	1.38	1.63	1.11	1.11	1.12
$\dot{W}_e$ (kW)	8.25	8.90	7.17	8.04	8.49

5. Miscellaneous Tests

In addition to the regular tests runs of the engine, the following tests were conducted : Expander compression-expansion test, heat transfer flow test, and a motoring test.

1) Expander compression-expansion test

(1) Purpose and procedure

The purpose of the test was to see the effect of heat transfer inside expander during expansion or compression with a fixed mass of gas. Both the intake and the discharge valves were closed. The intake valve was clamped in closed position using a bolt through the expander head plate and intake valve access port. This arrangement was necessary because there was a considerable amount of leakage past the intake valve when the high pressure of the intake tube was used to keep the intake valve closed. The leakage would have made it impossible to maintain a fixed amount of gas inside the expander. Gas was supplied through the thermocouple port. A throttle valve

and a pressure gauge was fitted to the gas supply line near the expander.

As shown in Fig. A-22, the P-V diagram does not open up, indicating that the process is nearly reversible. However, the fact that there is little loss in this test does not guarantee that the same is true with the actual running, in which case there are considerable T between the gas and wall temperature, and more turbulence.

(2) Pressure transducer zero shift

An important by-product of this test was the discovery of the unexpected pressure transducer behavior. At first, it seemed that the compression ratio was too small (about 3:1), which was far below the isothermal compression ratio (8:1) and the isentropic compression ratio (32:1). The compression ratio was based on the information in the specification sheet that the pressure transducer zero shift was negligible in the temperature range of 55 C to 120 C. also, we had anticipated that the gas temperature near the pressure transducer diaphragm would be within this range.

The following method was used to detect a considerable zero shift. After expander went through a number of cycles to warm up, the engine was stopped and expander was vented immediately to read atmospheric pressure. It was observed that the pressure transducer output was still well above the original zero point even after the expander was vented. The output voltage dropped slowly for about 30 seconds until it

Pressure
(MPa)

2.24 ─

0.1 ─

Zero shift

0.876   6.992

Expander volume (10^{-4} m^3)

Expander pressure

───── Intake tube pressure
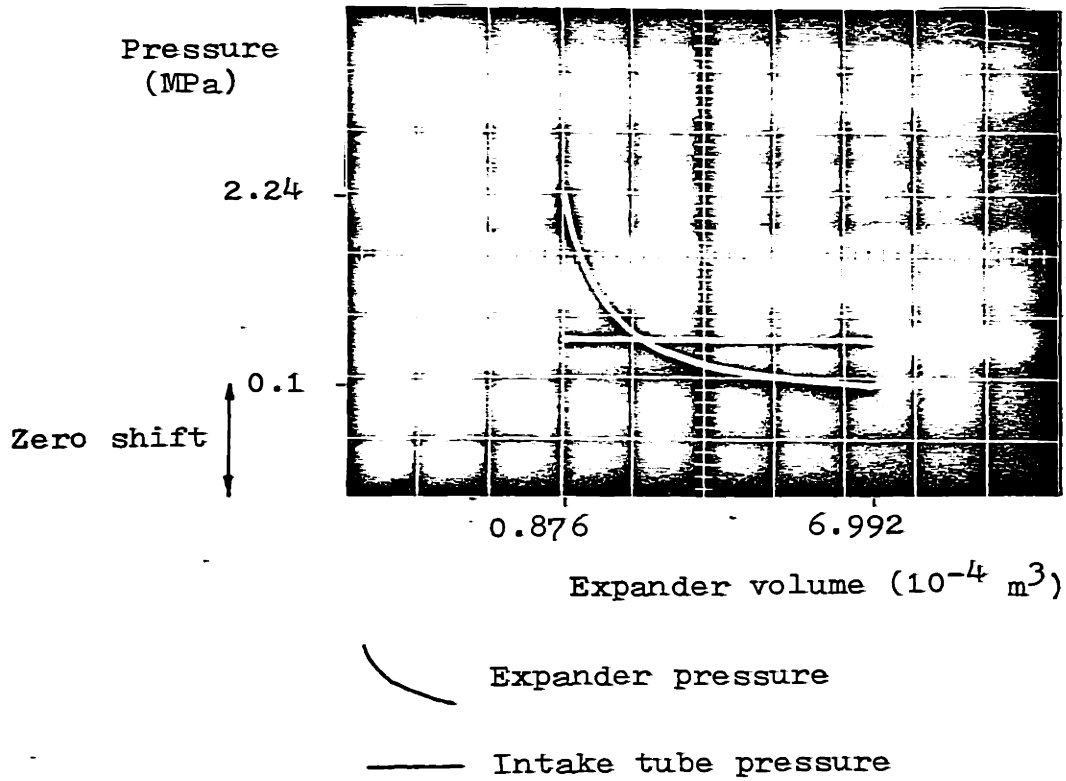
Fig. A-22   P-V diagram of compression-
            expansion test of expander

reached the original zero point. It was decided that the gas near the pressure transducer diaphragm reached a high temperature outside the compensated range. Taking into account the zero shift, the actual compression ratio 22:1 was reasonable.

As a cure to this problem, the transducer diaphragm was coated with RTV Silicon rubber to prevent the direct exposure to high temperature gas. The result was that the zero shift became significantly smaller, although it persisted. Therefore, it was decided to use the readings from two pressure gauges located outside the cylinder to decide the maximum and the minimum pressure during a cycle.

It was recommended that the gas near the pressure transducer be cooled more effectively in order to decrease the zero shift.

(3) Dynamic piston ring leakage

During the expander compression-expansion test, the compressor pressure was monitored to see if there was any leakage past the piston seal. Even when the peak pressure of the expander went up to 6.90 MPa, there was no sign of pressure increase in the compressor, which indicated the 0 ring was sealing perfectly.

2) Heat transfer flow test

The purpose of this test was to back up the assumptions concerning energy balance of the engine (section II.2 & Appendix B). The assumptions were as follows : a) Calculated cooler gas flow rate is the gas flow rate of the engine. b) Heat leak from the heater and the regenerative heat exchanger is much more than from natural convection.

As briefly explained in section II.2.1), the working gas was circulated through the engine components with both of the expander valves wide open. The pressure difference along the path was only due to flow friction and compressor check valve springs, which was very small compared to mean pressure of 1.38 MPa, making the expander and compressor power negligible. Table A-9 lists the test data on heater input power, shaft power, pressure, and cooling water. Table A-10 gives the average temperatures from the multi-channel recorder.

3) Motoring test

The purpose of the test was to determine the friction loss due to seals by measuring the torque required to turn the engine with dc powered dynamometer. Cooling water flow rates and temperatures were measured to calculate how much heat was generated due to friction.

Table A-11 lists the data from the motoring test. Of the measured motoring power 1.77 kW, about 0.44 kW is the linkage

109

Table A-9   Heat Transfer Flow Test Data

(Power, pressure, and cooling water)

Heater input power

Voltage across heater (V)	170
Shunt voltage (mV)	16.25
Heater electrical input (kW)	5.53

Shaft power due to friction

Manometer reading (m Hg)	0.72
Rotational frequency (sec^{-1})	9.17
$\dot{W}_{shaft}$ (kW)	-2.07

Mean pressure (MPa)

1.38

Cooling water heat removal rate (kW)

Cooler	3.42
Cylinder jacket	1.66
Compressor block	0.23
Piston rod	0.30
Expander head	0.45
Heater	0.08
Total	6.14

Table A-10   Average Temperatures Measured by the
             Multi-channel Recorder(Heat Transfer Flow Test)

T.C. No.[*]	Location of Thermocouple	Temp (C)
1	Cooler Inlet (from R.H. Ex.)	62
2	R.H. Ex. Inlet (from Comp. Disch.)	13
3	R.H. Ex. Inlet (from Exp. Disch.)	500
4	R.H. Ex. Outlet (to Heater)	443
5	Comp. Discharge	13
6	Exp. Inlet Wall	489
7	Heater Wall	508
8	Exp. Inlet (Tube T.C.)	520
9	Cylinder Wall	503
10	Cylinder Wall	391
11	Cylinder Wall	479
12	Cylinder Wall	343
13	Cylinder Wall	134
14	Comp. Block (Discharge Side)	13
15	Comp. Block (Inlet Side)	6
16	Cylinder Wall	110
17	Exp. Head (Inlet Side)	509
18	Exp. Head (Discharge Side)	485
19	Comp. Inlet	8
20	R.H. Ex. Wall (Upper part)	456
21	R.H. Ex. Wall (Lower part)	62

* See Fig. A-10

loss due to crankcase friction (3). The remaining 1.33 kW
is composed of the total of cooling water heat removal rates
1.20 kW and unmeasured heat leak from the engine components
to the environment.

Table A-11   Motoring Test Data

<u>Motoring power (kW)</u>   1.77

<u>Cooling water heat removal rates (kW)</u>

Cooler	0.20
Cylinder jacket	0.70
Compressor block	0.12
Piston rod seal	0.12
Expander head	0.05
Heater	0.01
Total	1.20

Appendix B   ENERGY BALANCE CALCULATION

The First law for control volume (equation III-10) will be used for control volumes drawn around engine components, and around the entire engine as shown in Fig. B-1. For temperatures, average temperature data from the multichannel recorders (Table A-1) will be used. For pressures, average pressures measured by pressure gauges (Appendix A.1) will be used. Apparent mass flow rate of cooler, which was confirmed to be very close to the actual engine flow rate by orifice metering (section III.2.2)) will be used as the mass flow rate.

Assuming steady operation, $\frac{\partial E}{\partial t}$ will be identical to zero for each control volume.

(a)   Control volume 1 (Entire engine)

Knowing the electrical heat input to the heater $\dot{Q}_{heater}$, cooling water heat removal rates $\dot{Q}_{cooler}$, $\dot{Q}_{other\ sinks}$, brake engine power $\dot{W}_{brake}$, linkage power loss $\dot{W}_{linkage}$, the energy balance for the control volume 1 gives the rate of heat loss to the environment from the engine components $\dot{Q}_{environ,1}$. Table B-1 summarizes the energy balance calculations for the first zero piston ring leakage test (Test #3), the after compressor modification test (Test #5), and the heat transfer flow test (H.T.F. Test).

control volume 1   control volume 3

Heater

Expander

control volume 4

control
volume 5

Piston

Regenerative
Heat
Exchanger

control volume 2

Compressor   cooler
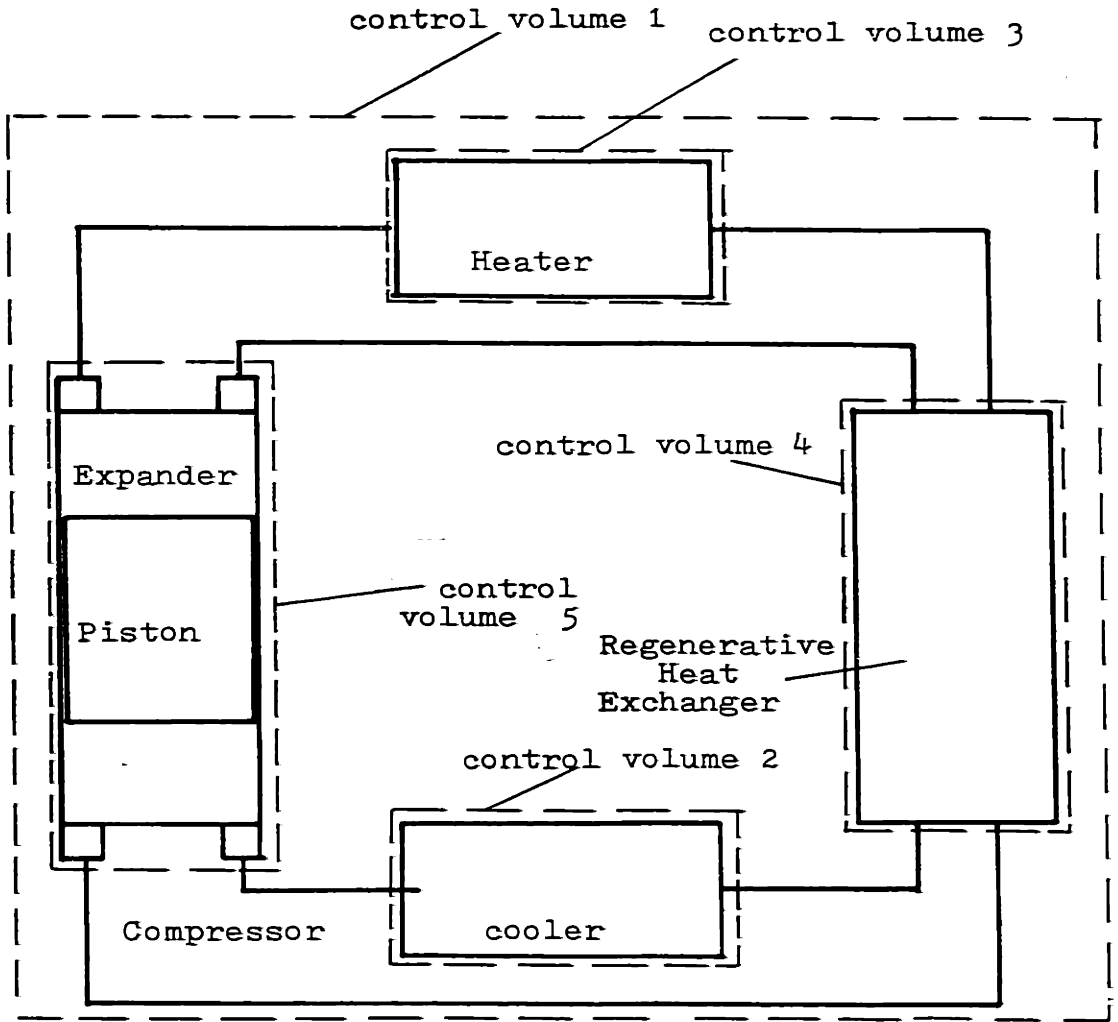
Fig. B-1 Control volumes for energy balance

114

Table B-1 Energy Balance for the Entire Engine

	Test #3	Test #5	H.T.F.Test
$\dot{Q}_{heater}$ (kW)	12.87	12.64	5.53
$\dot{Q}_{cooling\ water}$(kW)	8.26	8.08	6.14
$\dot{W}_{brake}$ (kW)	1.28	2.11	-2.30
$\dot{W}_{linkage}$ (kW)	0.44	0.44	0.44
$\dot{Q}_{environ,1}$(kW)	2.89	2.01	1.25

$\dot{Q}_{environ,1}$ can also be estimated from component surface temperatures and natural convection law. Hankard (3) thus estimated $\dot{Q}_{environ,1}$ to be about 1.20 kW for Test #1 which is similar to Test #3 and #5 in terms of surface temperatures of the engine components. The so-called unaccounted-for-energy mentioned in reference 1 and 3 is the underestimated portion of $\dot{Q}_{environ,1}$. As we check the energy balance of each components, it will be shown that most of the underestimation is from the heater and the regenerative heat exchanger.

(b) Control volume 2 (Cooler)

As mentioned earlier, the apparent mass flow rate of the cooler can be obtained from the cooler heat removal rate $\dot{Q}_{cooler}$, and gas temperature change ΔT between inlet and outlet. In the calculation, the heat loss to the environment from the cooler $\dot{Q}_{environ,2}$ was neglected because the temperature between

115

the cooler surface and the environment was negligible. Table B-2 summarizes the energy balance calculation for the cooler.

Table B-2 Cooler Energy Balance Calculations

	Test #3	Test #5	H.T.F.Test
$\dot{Q}_{cooler}$ (kW)	4.37	4.19	3.42
$\dot{Q}_{environ,2}$ (kW)	0	0	0
ΔT (C)	117	107	54
$\dot{m}_f$ (g/sec)	7.22	7.56	12.22

(c) Control volume 3 (Heater)

Given the mass flow rate $\dot{m}_f$ of Table B-2, gas temperature increase ΔT, electrical input to the heater $\dot{Q}_{heater}$, and the cooling water data for electrical feed through $\dot{Q}_{water}$, the heat loss to the environment from the heater $\dot{Q}_{environ,3}$ is calculated as shown in Table B-3.

Table B-3 Heater Energy Balance Calculations

	Test #3	Test #5	H.T.F.Test
$\dot{Q}_{heater}$ (kW)	12.87	12.64	5.53
$\dot{Q}_{water}$ (kW)	0.05	0.09	0.08
ΔT (C)	320	295	77
$\dot{Q}_{environ}$ (kW)	0.91	1.00	0.55

Hankard (3) estimated $\dot{Q}_{environ,3}$ to be 0.14 kW from

116

natural convection law and surface temperatures, which is far less than the values in Table B-3.

(d) Control volume 4 (Regenerative heat exchanger)

Given the temperature changes (ΔT) of both high pressure and low pressure stream, and the identical mass flow rate $\dot{m}_f$ for both stream, the heat leak to the environment from the regenerative heat exchanger $\dot{Q}_{environ,4}$ can be calculated as shown in Table B-4.

Table B-4 Regenerative Heat Exchanger Energy Balance
             Calculations

	Test #3	Test #5	H.T.F.Test
$\Delta T_{H.P.}$ (C)	299	300	430
$\Delta T_{L.P.}$ (C)	315	310	438
$\dot{Q}_{environ,4}$ (kW)	0.62	0.39	0.53

Hankard's (3) estimate for $\dot{Q}_{environ,4}$ from natural convection law was only 0.07 kW.

(e) Control volume 5 (Cylinder)

Knowing the brake engine power $\dot{W}_{brake}$, linkage loss $\dot{W}_{linkage}$, the average mass flow rate $\dot{m}_f$, temperature changes through compressor $\Delta T_{comp.}$ and expander $\Delta T_{exp.}$, cooling water heat removal rate $\dot{Q}_{water}$, the energy balance for the cylinder gives the rate of cylinder heat loss to the environ-

ment $\dot{Q}_{environ,5}$. Table B-5 summarizes the calculations.

Table B-5 Cylinder Energy Balance Calculations

	Test #3	Test #5	H.T.F.Test
$\Delta T_{comp.}$ (C)	104	83	5
$\Delta T_{exp.}$ (C)	279	254	20
$\dot{Q}_{water}$ (kW)	3.84	3.80	2.64
$\dot{Q}_{environ,5}$ (kW)	0.92	0.37	0.18

(f) Control volume 6 (Tubings between components)

Tubing heat loss is mostly from the tubing between compressor discharge and regenerative heat exchanger. It can be estimated from the mass flow rate $\dot{m}_f$ and the gas temperature drop ΔT along the tubing. Table B-6 shows the results.

Table B-6 Heat Loss Rate from Tubings

	Test #3	Test #5	H.T.F.Test
ΔT (C)	12	7	negligible
$\dot{Q}_{environ,6}$ (kW)	0.44	0.26	negligible

If all the test data are reasonably correct, the heat loss from the entire engine $\dot{Q}_{environ,1}$ should match the sum of $\dot{Q}_{environ}$'s of the control volumes 2 to 6. It turned out that

$\dot{Q}_{environ,1}$ and $\sum\limits_{i=2}^{6} \dot{Q}_{environ,i}$ is within 1% of each other which strengthens the energy balance argument in section II.2.

Appendix C   EXAMPLES OF CYCLIC HEAT TRANSFER CALCULATION

1. Equivalent Isentropic Method

As explained in section II . 3.4), this method estimates
the magnitude of cyclic heat transfer by approximating compressor
(or expander) processes with steady flow isentropic compressor
(or expander). Referring to Fig.II-3 , the equations for
compressor side are as follows.

Inlet temperature for steady flow compressor

$$T_{1i} = \dot{W}_c \: / \: (\dot{m}_f c_p (1 - P_r^{C_o}))$$

Outlet temperature for steady flow compressor

$$T_{2i} = T_{1i} \, P_r^{C_o} \quad ; \quad C_o = (\gamma - 1) \: / \: \gamma$$

Heat transfer rate into the gas

$$\dot{Q}_+ = \dot{m}_f c_p \: (T_{1i} - T_1)$$

Heat transfer rate out of the gas

$$\dot{Q}_- = \dot{m}_f c_p \: (T_2 - T_{2i})$$

Non-dimensional magnitude of cyclic heat transfer for compressor

$$X_c = (\, |\dot{Q}_+| + |\dot{Q}_-| \,) \: / \: (2\Delta H)$$

Total enthalpy change

$$\Delta H = \dot{m}_f c_p \: (T_2 - T_1)$$

The equations for expander side are as follows.

Inlet temperature for steady flow expander

$$T_{4i} = \dot{W}_e \: / \: \dot{m}_f c_p \: (1 - P_r^{C_o})$$

Outlet temperature for steady flow expander

$$T_{5i} = T_4 P_r^{C_o}$$

Heat transfer rate into the gas

$$\dot{Q}_+ = \dot{m}_f c_p \: (T_5 - T_{5i})$$

Heat transfer rate out of the gas

$$\dot{Q}_- = \dot{m}_f c_p \: (T_{4i} - T_4)$$

Non-dimensional magnitude of cyclic heat transfer for expander

$$X_c = (\left| \dot{Q}_+ \right| + \left| \dot{Q}_- \right|) \: / \: 2\Delta H$$

Total enthalpy change

$$\Delta H = \dot{m}_f c_p \: (T_4 - T_5)$$

Table C-1 shows the input data and results of Equivalent Isentropic Method for Test #1 through #6.

Table C-1 Input Data and Results of Equivalent Isentropic Method

	Test #1	Test #2	Test #3	Test #4	Test #5	Test #6
P_h/P_L	2.18	2.09	2.14	2.08	2.07	2.10
T_1 (K)	296	297	293	288	287	280
T_2 (K)	415	409	386	367	369	361
T_4 (K)	925	998	1004	993	957	973
T_5 (K)	686	733	726	724	703	713
$\dot{m}_f$ *	8.06	7.07	7.22	5.95	7.56	7.53
$\dot{W}_c$ (KW)	-7.71	-5.37	-5.58	-3.98	-4.61	-4.57
$\dot{W}_e$ (KW)	10.05	8.25	8.90	7.17	8.04	8.49
T_{1i} (K)	503	426	421	379	350	337
T_{2i} (K)	687	573	569	507	467	454
T_{4i} (K)	896	879	908	915	816	844
T_{5i} (K)	656	654	671	683	611	627
n_c (%)	58.9	69.7	69.8	75.9	81.9	83.0
n_e (%)	96.8	88.1	90.5	92.1	85.2	86.7
X_c	2.01	1.31	1.69	1.46	0.97	0.93
X_e	0.12	0.37	0.27	0.22	0.46	0.41

* In 10^{-3} Kg/sec

2. Equivalent Reversible Polytropic Method

As mentioned in section II.3.4, this method estimates
the cyclic heat transfer by approximating compressor processes
with reversible compression, reexpansion process, and constant
pressure intake, discharge process.   Referring to Fig. II-5
the equations used are:

$$\dot{Q}_+ = \dot{m}_f c_p \ (T_{ei} - T_{in}) + \dot{Q}_{rc}$$

$$\dot{Q}_- = \dot{m}_f c_p \ (T_{out} - T_{ed}) + \dot{Q}_{ct}$$

From equation II-2,   ignoring valve pressure drops, the
effective intake temperature

$$T_{ei} = \frac{P_L \ (V_1 - V_4)}{(\dot{m}_f/RPS) \ R} \quad ;$$

the effective discharge temperature

$$T_{ed} = \frac{P_h \ (V_2 - V_3)}{(\dot{m}_f/RPS) \ R} \quad ,$$

where RPS is the rotational frequency.   The heat transfer rates
$\dot{Q}_{ct}$ and $\dot{Q}_{rc}$ are

$$\dot{Q}_{ct} = (\frac{1}{1-n_1} - \frac{1}{1-\gamma}) \ (P_h V_2 - P_L V_1) \ RPS$$

123

$$\dot{Q}_{rc} = \left(\frac{1}{1-n_2} - \frac{1}{1-\gamma}\right) (P_L V_4 - P_h V_3) \text{ RPS}$$

where $n_1 = -\log(P_h/P_L) / \log(V_2/V_1)$,

$n_2 = -\log(P_L/P_h) / \log(V_4/V_3)$.

Non-dimensional cyclic heat transfer of the compressor X_c is defined as in the previous section. Table C-2 shows input data and results for Test #1 through #6.

Table C-2 Input Data and Results of Equivalent Reversible Polytropic Method

	Test #1	Test #2	Test #3	Test #4	Test #5	Test #6
P_h(MPa)	3.69	3.55	3.83	3.24	3.43	3.45
P_L(MPa)	1.69	1.70	1.79	1.56	1.66	1.64
V_1*	8.741	8.741	8.741	10.22	10.33	10.33
V_2	5.788	5.563	5.303	6.332	6.522	6.545
V_3	2.950	2.950	2.950	4.425	4.542	4.542
V_4	4.621	4.905	5.003	7.384	7.330	7.418
$\dot{m}_f$**	8.06	7.07	7.22	5.95	7.56	7.53
T_{in}(K)	296	297	293	288	287	280
T_{out}(K)	415	409	386	367	369	361
$\dot{Q}_+$(kW)	7.38	5.22	5.67	3.00	2.58	2.35
$\dot{Q}_-$(kW)	-9.63	-6.65	-7.48	-4.21	-3.89	-3.87
ΔH(kW)	4.98	4.10	3.89	2.45	3.25	3.15
X_c	1.71	1.45	1.69	1.47	0.99	0.99

* volumes in 10^{-4} m^3.   ** in 10^{-3} kg/sec

Appendix D   FLOWMETER CALCULATIONS

1.   Orifice Sizing

The two square edged orifices made of stainless steel 300 for measuring instantaneous mass flow rates during compressor intake and discharge had to be properly sized in order not to introduce too much pressure drop in the engine, and to limit the error due to non-linearity of orifice meter. Flange taps were used for pressure taps : the centers of the inlet and out-let pressure taps are 2.54 cm from the inlet and outlet faces of the orifice plates respectively (see Fig. III-2).

The equations for calculation of gas flow rate $\dot{m}$ (kg/sec) are as follows (6) :

$$\dot{m} = \frac{\pi d^2 \ Fa \ E_f}{4} \ \frac{C}{\sqrt{1-\beta^4}} \ \sqrt{2 \ g_c \ \rho_1 \ (\ P_1 - P_2 \ )} \qquad (D-1)$$

where d = diameter of the orifice (m),

   Fa = thermal expansion factor of the orifice metal,

   C = discharge coefficient,

   β = orifice diameter d (m) / tube diameter D (m),

   E_f = expansion factor due to compressibility,

   g_c = gravitational proportionality constant,

   ρ_1, ρ_2 = density of the gas (kg / m^3),

   P_1, P_2 = Pressure of the gas (Pa).

Subscript 1 refers to the upstream section, and subscript 2 refers to the downstream section.

125

The discharge coefficient C is computed from the following relations :

$$C = Ke \sqrt{1-\beta^4} \; (1+\frac{Z}{R_d}) \; (\frac{10^6 \, d}{10^6 d + 15 \, A}) \qquad (D-2)$$

where $Ke = 0.5993 + 1.778 \times 10^{-4} / D + (0.364 + 4.769 \times 10^{-1}/ D)\beta^4$

$+ 0.4 (1.6 - 2.54 \times 10^{-2}/D)^5 ((0.07 + 1.27 \times 10^{-2}/D-)^{2.5}$

$- (0.009 + 8.636 \times 10^{-4}/D) (0.5 - \beta)^{1.5}$

$+ (1.008 \times 10^5 + 3) (\beta - 0.7)^{1.5},$

$Z = 1000d \; (32.68 - 196.9\beta + 354.3\beta^2 - 165.4\beta^3 + 3.326/ D).$

The expansion factor E is evaluated from

$$E_f = 1- (0.41 + 0.35 \beta^4) \cdot \frac{\Delta P}{P_1} \cdot \frac{1}{\gamma} \; ; \; \Delta P = P_1 - P_2 \qquad (D-3)$$

when the reference pressure is measured at the inlet pressure tap, and from

$$E_f = \sqrt{1+ (\Delta P/P_2)^2} - (0.41 + 0.35 \beta^4) \frac{(\Delta P/P_2)^2}{\gamma} \; \frac{1}{1 + (\Delta P/P_2)^2}$$

$$(D-4)$$

when the reference pressure is measured at the outlet pressure tap.

The maximum flow rate during intake or discharge can be estimated from the piston velocity $v_{p,max}$ and inlet or outlet density.

126

$$\dot{m}_{max} = A_c \, v_{p,max} \, , \qquad\qquad\qquad\qquad (D-5)$$

where A_c is compressor volume per unit displacement. From geometry, the piston velocity v_p is given by

$$v_p = \frac{d}{dt} \left(-r \cos \theta - L_c \sqrt{1-(r/(L_c \sin\theta))^2} \right) \qquad (D-6)$$
$$\approx r \, \sin \, (1 +(\cos \theta) \, O(r/L_c))$$

where θ is crank angle, L_c is connecting rod length, and r is half the engine stroke. The maximum piston velocity $v_{p,max}$ is approximated by $v_{p,max} = r\omega$ within reasonable accuracy. Substituting values $r = 5.715$ cm, $L_c = 20.32$ cm, and $\omega = 20$ radian/sec, $v_{p,max} = 3.6$ m/sec.

From equation D-5, typical inlet density (Test #5) 2.789 kg /m^3, and outlet density 4.463 kg/m^3 give the maximum mass flow rate of 5.10×10^{-2} kg/sec during intake and 7.69×10^{-2} kg/sec during discharge. In the temperature range being considered (15 C $\sim$ 120 C) the thermal expansion factor F_a in equation D-1 can be regarded as 1.0 for stainless steel 300.

The diameter of the orifice plate d can be obtained from equation D-1 by solving for d after substituting appropriate values for ρ_1, P_1, P_2, F_a, D, and $\dot{m}$. For intake side, $\rho_1 = 2.789$ kg/m^3, $\dot{m} = 5.10 \times 10^{-2}$ kg/sec. For discharge side, $\rho_1 = 4.463$ kg/m^3, $\dot{m} = 7.69 \times 10^{-2}$ kg/sec. D $= 3.25 \times 10^{-2}$ m, Fa = 1.0 .

To be used with the $\pm$0.1 MPa differential pressure transducers, orifice diameters were sized so that β = 0.40 (d=1.3 cm), ΔP_{max} = 0.068 kPa for the intake side, and β = 0.45 (d=1.46 cm), ΔP_{max} = 0.065 kPa for the discharge side. The maximum pressure drops were designed to be less than 0.1 MPa to provide enough room in case the pressure drops were under-estimated.

2. Resonance Frequency of Pressure Taps

As shown in Fig. III-2, the differential pressure transducer adapter has almost equal void volume at each side. This was necessary to match the acoustic characteristics of the inlet pressure tap and outlet pressure tap. In order to estimate the resonance frequency of the pressure taps, it is assumed that the wave form inside the pressure tap is the plane wave. Referring to Fig. D-1, the acoustic pressure p and volume velocity q is expressed as follows (12).

$$p_1(x_1,t) = j \omega \rho c (A_1 e^{-jkx_1} + B_1 e^{jkx_1}) e^{j\omega t}$$

$$p_2(x_2,t) = j \omega \rho c (A_2 e^{-jkx_2} + B_2 e^{jkx_2}) e^{j\omega t}$$

$$q_1(x_1,t) = j \omega S_1 (A_1 e^{-jkx_1} - B_1 e^{jkx_1}) e^{j\omega t}$$

$$q_2(x_2,t) = j \omega S_2 (A_2 e^{-jkx_2} - B_2 e^{jkx_2}) e^{j\omega t},$$

(D-7)

where coordinates x_1 and x_2 are as shown in Fig. D-1, S_1 and S_2 are the cross-sectional areas of the chamber, and the tube
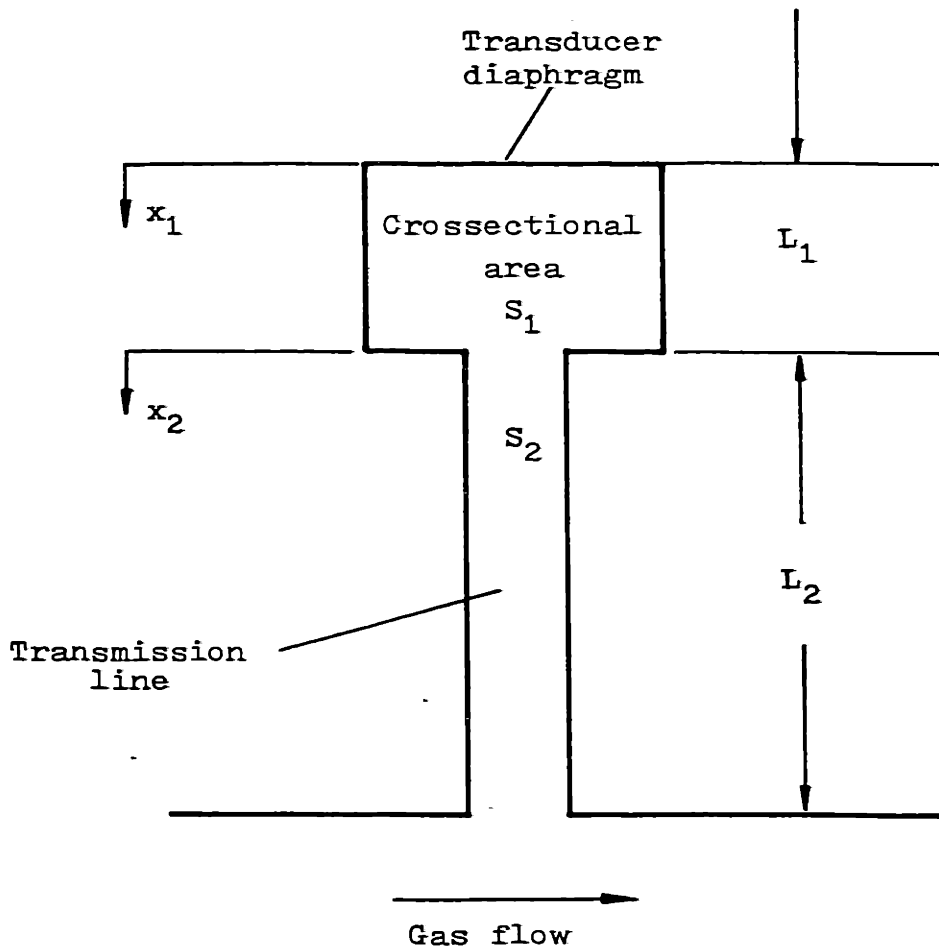
Fig. D-1 Pressure tap for differential pressure
transducer (schematic)

respectively, ω is the angular speed, A and B are the co-efficients to be decided by boundary conditions, t is time, and k is the wavelength constant defined by

$$k = \omega / c = 2\pi f / c \quad ; \quad c = \text{speed of sound} \qquad (D-8)$$

The boundary conditions are the continuity of acoustic pressure and volume velocity at the junction between the chamber and the tube, zero volume velocity at the end of chamber, and zero acoustic pressure at the tube entrance :

$$p_1 (L_1, t) - p_2 (0, t) = 0$$
$$q_1 (L_1, t) - q_2 (0, t) = 0$$
$$q_1 (0, t) = 0$$
$$p_2 (L_2, t) = 0$$

(D-9)

From equations D-6 and D-7, the boundary condition becomes

$$
[D]
\begin{bmatrix} A_1 \\ B_1 \\ A_2 \\ B_2 \end{bmatrix}
=
\begin{bmatrix}
f(L_1) & f(-L_1) & -1 & -1 \\
S_1 f(-L_1) & -S_1 f(L_1) & -S_2 & -S_2 \\
0 & 0 & f(-L_2) & f(L_2) \\
1 & -1 & 0 & 0
\end{bmatrix}
\begin{bmatrix} A_1 \\ B_1 \\ A_2 \\ B_2 \end{bmatrix}
= 0
$$

(D-10)

where $f(x) = e^{jkx}$. For non-trivial solution, the determinant |D| has to be equal to zero. This condition leads to the following relation :

$$\tan k\, L_1 \cdot \tan k\, L_2 = S_2/S_1. \tag{D-11}$$

Substituting values $L_1 = 1.59$ cm, $L_2 = 10$ cm, $S_1 = 2.52 \times 10^{-2}$ cm^2, $S_2 = 8.23 \times 10^{-3}$ cm^2, the wave length constant k can be calculated from equation D-11. Then from equation D-5, the resonance frequency is calculated to be about 1400 Hz. The orifice pressure drop data in Fig. III-5, and III-6 show the presence of 1400 Hz resonance.

Appendix E COMPUTER CODES FOR EVALUATION OF COMPRESSOR PERFORMANCE

```
C     THIS IS THE COMPUTER PROGRAM FOR THE FIRST LAW INTEGRAL ANALYSIS.
C     IT COMPUTES MASS FLOW RATE OF THE ENGINE FROM THE ORIFICE PRESSURE
C     DROP DATA.  USING THE COMPUTED MASS FLOW RATE, AND PRESSURE VOLUME
C     DATA, THE MIXED MEAN TEMPERATURE, HEAT TRANSFER RATE, AND SPECIFIC
C     ENTROPY ETC.  ARE CALCULATED.
C
C     ORADL, ORADH, ORPDL, ORPDH, ORAIL, ORATH, ORPIL, ORPIH ARE ORIFICE
C     FLOW RATE MEASUREMENT DATA.  THIRD LETTERS A AND P DENOTE CRANK
C     ANGLE IN DEGREES AND ORIFICE PRESSURE DROP IN INCHES REPECTIVELY.
C     THE FOURTH LETTERS D AND I DENOTE DISCHARGE SIDE AND INTAKE SIDE
C     RESPECTIVELY.  THE FIFTH LETTERS L AND H MEAN THE DATA WAS FROM
C     THE LOWER ENVELOPE AND THE HIGHER ENVELOPE OF THE ORIFICE PRESSURE
C     DROP CURVE RESPECTIVELY.
C
C     PIH, AIH, PIL, AIL, PDH, ADH, PDL ARE COMPRESSOR PRESSURE VS.
C     CRANK ANGLE DATA.  THE FIRST LETTERS P AND A DENOTE COMPRESSOR
C     PRESSURE IN INCHES AND CRANK ANGLE RESPECTIVELY.  THE SECOND
C     LETTERS I AND D DENOTE INTAKE AND DISCHARGE PERIOD.  ORFIL, ORFIH
C     ARE ARRAYS OF ORIFICE DATA FOR PLOTTING.
C
C     SENLD, SENHD, SENLI, SENHI; SENTI ARE ARRAYS FOR SMOOTHING
C     OUT ENTROPY CURVE.  THE FOURTH LETTERS L AND H MEAN THE LOWER AND
C     THE HIGHER ENVELOPE OF THE ENTROPY CURVE.  THE FOURTH LETTER T
C     MEANS CUMULATIVE ENTROPY.  THE FIFTH LETTERS D AND I MEAN
C     DISCHARGE AND INTAKE RESPECTIVELY.
C     TREF, AND PREF ARE THE REFERENCE TEMPERATURE AND PRESSURE FOR
C     ENTROPY CALCULATION.  PCALD, PCALI ARE THE CONVERSION FACTORS FOR
```

```
C     ORIFICE DATA INTO PSL FOR DISCHARGE AND INTAKE SIDE RESPECTIVELY.
C
C     PH IS THE EXPANDER INTAKE PRESSURE AND PL IS THE COMPRESSOR INTAKE
C     PRESSURE.  YSPA IS THE CONVERSION FACTOR FOR COMPRESSOR PRESSURE
C     DATA.  CFLR IS THE APPARENT MASS FLOW RATE OF COOLER.  VCL IS THE
C     CLEARANCE VOLUME OF THE COMPRESSOR, CSV, CSP ARE SPECIFIC HEAT OF
C     THE GAS AT CONSTANT VOLUME  AND CONSTANT PRESSURE RESPECTIVELY.
C
C     R IS THE GAS CONSTANT.  TINT AND TDIS ARE THE AVERAGE INTAKE AND
C     DISCHARGE TEMPERATURE OF COMPRESSOR.  TROC IS THE TEMPERATURE AT
C     THE BEGINNING OF COMPRESSION.  ZI AND ZD ARE THE CRANK ANGLE AT
C     THE BEGINNING OF INTAKE AND DISCHARGE.  NDIV IS THE NO. OF OUTPUT
C     DATA PER CYCLE.  RPM IS ENGINE REVOLUTION PER MINUTE.
C
C     IN THIS PROGRAM, ALL THE COMPUTATION WILL BE DONE IN BRITISH UNITS
C     AND THE RESULTS WILL BE CONVERTED TO S.I. UNITS AT THE END.
C
      INTEGER*2 XLAB(40)
      DIMENSION ORADL(29),ORADH(29),ORPDL(29),ORPDH(29),ORAIL(38),
     C          ORAIH(41),ORPIL(38),ORPIH(41),ORFIL(2,38),XSCL(4),
     C          PIH(12),AIH(12),PIL(14),AIL(14),PDH(11),ADH(11),PDL(14),
     C          SENID(2,7),SENHD(2,6),SENTD(2,21),NEHD(6),NFLD(7),
     C          SENLI(2,7),SFNHI(2,12),SENTI(2,12),NEHI(12),NFLI(7),
     C          ADL(14),ORFIH(2,41),AFRAY(12,91),ORFDL(2,29),ORFDH(2,29)
      COMMON DELTA,ADJD,ADJI,ORAIL,ORPIL,ORATH,ORPIH,ORADI,ORPDL,
     C       ORADH,ORPDH,ARRAY
      DATA PCALD,PCALI/2.1871,2.3438/
      DATA PH,PL,YSPA,CFLR /497.,241.,2.945,60./
      DATA VCL,CSV,CSP,R,TINT,TDIS /27.72,.7462,1.2405,.4943,516.,665./
```

134

```
      DATA TBOC,ZI,ZD,NDIV,NPTS/531.,276.,100.2,360.,91/
      DATA RPM,PCALI,PCALD /600.,2.3438,2.1871/
      DATA PIH/0.0,-.075,-.074,-.078,-.086,-.07,-.012,.0,.0,.0,.0,.0/
      DATA AIH/276.,279.,282.6,297.,311.4,322.2,343.8,347.4,351.0,354.6,
     .         358.2,360./
C
      DATA PIL/0.0,-.075,-.090,-.098,-.102,-.102,-.094,-.070,-.066,
     .         -.060,-.055,0.0,0.0,0.0,0.0/
C
      DATA AIL/276.,279.,286.2,289.8,293.4,304.2,315.,325.8,329.4,333.,
     .         336.6,354.6,358.2,360./
C
      DATA PDH/2.945,3.055,3.055,3.039,2.980,2.973,2.965,2.965,2.969,
     .         2.961,2.945/
C
      DATA ADH/100.2,102.6,109.8,113.4,120.6,124.2,145.7,149.4,174.6,
     .         178.2,180./
C
      DATA PDL/2.945,3.055,3.055,3.039,2.977,2.949,2.945,2.945,2.947,
     .         2.944,2.943,2.943,2.946,2.945/
C
      DATA ADL/100.2,102.6,109.8,113.4,117.,127.8,135.,138.6,142.2,153.,
     .         156.6,163.8,167.4,180./
C
      DATA TWAV,TWAM,PHAS/590.,40.,45./
      DATA TREF,PREF/537.,14.7/
      DATA NEHI /1,4,5,6,8,9,11,12,13,14,20,22/
      DATA NELI /1,3,7,10,17,18,22/
      DATA NEHD /1,4,8,15,20,21/
      DATA NELD /1,2,3,12,18,19,21/
      ADJT=1.
      ADJD=1.

      READ DATA FROM ORIFICE MEASUREMENT

      READ(8,2) (ORADL(I),I=1,29)
      READ(8,2) (ORADH(I),I=1,29)
      READ(8,3) (ORPDL(I),I=1,29)
      READ(8,3) (ORPDH(I),I=1,29)
      READ(8,2) (ORAIL(I),I=1,38)
```

```
      READ(8,2) (ORAIH(I),I=1,41)
      READ(8,3) (ORPIL(I),I=1,38)
      READ(8,3) (ORPIH(I),I=1,41)
    2 FORMAT((12F6.1))
    3 FORMAT((12F6.3))
    4 FORMAT((10F7.1))

C
C     SET UP COMPRESSOR PRESSURE ARRAY(1,J1)
C
      DO 500 TI=1,12
      DO 500 JJ=1,NPTS
  500 ARRAY(TI,JJ)=0.0
      COOL=CFLR/(RPM*60.)
      DELTA=360./(FLOAT(NPTS)-1.)
      PCAL=(PH-PL)/YSPA
      I1=IFIX(ADH(1)/DELTA)+1
      I2=IFIX(ADH(11)/DELTA)+1
      I3=IFIX(AIH(1)/DELTA)+1
      I4=IFIX(AIH(12)/DELTA)+1

C
C.....COMPRESSION
C
  100 DO 150 I=1,I1
      FI=FLOAT(I-1)
      ANG=FI*DELTA

C
C.....P*V**1.57291=EXP(12.0032)
  150 ARRAY(1,I)=163276./CYLV(ANG,VCL)**1.57291

C
C.....REEXPANSION
C.....P*V**1.51261OO82=EXP(B)
C.....B=11.2472733-9034283305*SIN((.05+(X-3.32215 )*.9/.478506)*PI)**.45
C
```

136

```
200   DO 250 I=I2,I3
      FI=FLOAT(I-1)
      ANG=FI*DELTA
      VX=CYLV(ANG,VCL)
      BX1=(.05+(ALOG(VX)-3.32215)*.9/.478506)*3.1415926
      BY2=3.4283305E-02*SIN(BX1)**.45
      BX3=11.2472733-BX2
250   ARRAY(1,I)=EXP(BX3)/VX**1.512610082
C
C.....DISCHARGE
C
      KDL=14
      KDLF1=KDL-1
      KDH=11
      KDHF1=KDH-1
      I1P1=I1+1
      DO 320 J=I1P1,I2
      JF1=J-1
      THETA=DELTA*FLOAT(JF1)
      DO 300 I=1,KDLF1
      IP1=I+1
      IF(THETA.GE.ADL(I).AND.THETA.LT.ADL(IP1)) GO TO 305
300   CONTINUE
305   SLOPE=(PDL(IP1)-PDL(I))/(ADL(IP1)-ADL(I))
      TPL=(PDL(I)+SLOPE*(THETA-ADL(I)))*PCAL+PL
      DO 310 I=1,KDHF1
      IP1=I+1
      IF(THETA.GE.ADH(I).AND.THETA.LT.ADH(IP1)) GO TO 315
310   CONTINUE
315   SLOPE=(PDH(IP1)-PDH(I))/(ADH(IP1)-ADH(I))
      TPH=(PDH(I)+SLOPE*(THETA-ADH(I)))*PCAL+PL
320   ARRAY(1,J)=(TPL+TPH)/2.
C
```

137

```
C.....INTAKE
C
      KIL=14
      KILF1=KIL-1
      KIH=12
      KIHF1=KIH-1
      I3P1=I3+1
      DO 350 J=I3P1,I4
      JF1=J-1
      THETA=DELTA*FLOAT(JF1)
      DO 330 I=1,KILF1
      IP1=I+1
      IF(THETA.GE.AIL(I).AND.THETA.LT.AIL(IP1)) GO TO 335
  330 CONTINUE
  335 SLOPE =(PIL(IP1)-PIL(I))/(AIL(IP1)-AIL(I))
      TPL=(PIL(I)+SLOPE*(THETA-AIL(I)))*PCAL+PL
      DO 340 I=1,KIHF1
      IP1=I+1
      IF(THETA.GE.ATH(I).AND.THETA.LT.AIH(IP1)) GO TO 345
  340 CONTINUE
  345 SLOPE=(PIH(IP1)-PIH(I))/(AIH(IP1)-AIH(I))
      TPH=(PIH(I)+SLOPE*(THETA-AIH(I)))*PCAL+PL
  350 ARRAY(1,J)=(TPL+TPH)/2.
C
C     CALCULATE CLEARANCE VOLUME MASS CLMS
C
      G=386.25*TBOC*12.
      TOMA=PL*CYLV(0.0,VCL)/G
      CLMS=TOMA-COOL
C
C     CONSTRUCT A PART OF COMPRESSOR MASS ARRAY(2,I)
      I1=IFIX(ZD/DELTA)+1
      I2=JFIX(180./DELTA)+1
```

138

```
        I3=IFIX(ZI/DELTA)+1
        DO 2000 I=1,I1
2000    ARRAY(2,I)=TOMA
        DO 2200 I=I2,I3
2200    ARRAY(2,I)=CLMS
C
C       CALCULATE INTAKE AND DISCHARGE MASS FLOW RATE. COMPARE WITH COOL.
C
C       DECIDE ADJUSTING CONSTANTS ADJI, ADJD.
C
        XX=360./FLOAT(MDIV)
        XX=1.0
        K=IFIX(DELTA/XX)
        MM=IFIX((360.-ZT)/XX)
        NN=IFIX((180.-ZD)/XX)
        WRITE(5,112) I1,I2,I3,K,MM,NN
112     FORMAT(1H ,6I10)
        CALL MASI(ZI,MM)
        MI=MM/K+I3
        ADJI=(ARRAY(2,MI)-ARRAY(2,I3))/COOL
        CALL MASD(ZD,NN)
        MD=NN/K+I1
        ADJD=-(ARRAY(2,MD)-ARRAY(2,I1))/COOL
C
        WRITE(5,222) ADJI,ADJD
222     FORMAT(1H ,2E10.4)
C
C       COMPLETE COMPRESSOR MASS ARRAY(2,I)
C
        CALL MASI(ZI,MM)
        CALL MASD(ZD,NN)
C       CONSTRUCT VOLUME AND TEMPERATURE ARRAYS
        DO 2300 L=1,NPTS
```

```
      D=(FLOAT(L)-1.)*DELTA
      ARRAY(3,L)=CYLV(D,VCL)
      ARRAY(4,L)=ARRAY(1,L)*ARRAY(3,L)*2.1575E-04/ARRAY(2,L)
 2300 CONTINUE
C     THE FIRST LAW OF THERMODYNAMICS FOR THE COMPRESSOR
      DO 5000 IS=1,2
      DO 2350 I=1,NPTS
      D= FLOAT(I-1)*DELTA
 2350 ARRAY(5,I)=HTRA(D)
      PDV=0.0
      NPT=NPTS-1
      QSUM=0.0
      XMULT=RPM*60.*360./DELTA
      K1=IFIX(ZD/DELTA)+1
      K2=IFIX(180./DELTA)+1
      K3=IFIX(ZI/DELTA)+1
      DO 3000 I=1,NPTS
      IF(I.EQ.1) GO TO 3000
      IF1=I-1
      DFCV=(ARRAY(2,I)*ARRAY(4,I)-ARRAY(2,IF1)*ARRAY(4,IF1))*CSV
      DWCV=(ARRAY(1,I)+ARRAY(1,IF1))*(ARRAY(3,I)-ARRAY(3,IF1))/(2.*777.9
     *12.)
C
      IF (I.LT.K1) GO TO 2400
      IF (I.LT.K2) GO TO 2500
      IF (I.LT.K3) GO TO 2400
      GO TO 2600
 2400 DMT=0.0
      DMD=0.0
      GO TO 2700
 2500 DMT=0.0
      DMD=ARRAY(2,IF1)-ARRAY(2,I)
      GO TO 2700
 2600 DMI=ARRAY(2,I)-ARRAY(2,IF1)
```

```
      DMD=0.0
 2700 HICV=DMI*CSP*TINT
      HOCV=DMD*CSP*TDIS
      PDV=PDV+DWCV
C
C     SET UP ARRAYS FOR DQ,UA,SUM OF DQ
C
      XX=DECV+DWCV-HICV+HOCV
      ARRAY(6,I)=XX*XMULT
      ARRAY(7,I)=ARRAY(6,I)/ARRAY(5,I)
      QSUM=QSUM+XX*RPM*60.
      ARRAY(8,I)=QSUM
 3000 CONTINUE
C
C     THE SECOND LAW OF THERMODYNAMICS FOR THE COMPRESSOR
C
      ENTS=0.0
      DO 4000 I=1,NPTS
      IF1=I-1
      IF(I.EQ.1) GO TO 3950
      IF1=I-1
      DSC1=ARRAY(2,IF1)*(CSP*ALOG(ARRAY(4,IF1)/TREF)-R*ALOG(ARRAY(1,IF1)
     C /PREF))
      DSC2=ARRAY(2,I)*(CSP*ALOG(ARRAY(4,I)/TREF)-R*ALOG(ARRAY(1,I)/
     C PREF))
      DSCV=DSC2-DSC1
      FI1=FLOAT(I)-1.
      X=FI1*DELTA
      IF(I.LT.K1)  TW=540.+X*100./100.2
      IF(I.GE.K1.AND.I.LT.K2)  TW=640.
      IF(I.GE.K2.AND.I.LT.K3)  TW=640.-(X-180.)*180./96.
      IF(I.GE.K3.AND.I.LE.NPTS)  TW=540.
      QSCV=ARRAY(6,I)/(TW*XMULT)
```

```
      IF(I.LT.K1) GO TO 3100
      IF(I.LT.K2) GO TO 3200
      IF(I.LT.K3) GO TO 3100
      GO TO 3300
3100  DMI=0.0
      DMD=0.0
      GO TO 3400
3200  DMI=0.0
      DMD=ARRAY(2,IF1)-ARRAY(2,I)
      GO TO 3400
3300  DMI=ARRAY(2,I)-ARRAY(2,IF1)
      DMD=0.0
3400  AVT=  (ARRAY(4,I)+ARRAY(4,IF1))/2.
      AVP=(ARRAY(1,I)+ARRAY(1,IF1))/2.
      AVM=.5*(ARRAY(2,I)+ARRAY(2,IF1))
      SICV=(CSP*ALOG(TINT/TREF)-R*ALOG(AVP/PREF))*DMI
      SDCV=(CSP*ALOG(AVT/TREF)-R*ALOG(AVP/PREF))*DMD
C
      XX= DSCV-QSCV-SICV+SDCV
      ARRAY(5,I)=ARRAY(6,I)/XMULT/(XX+QSCV)
      ARRAY(10,I)=XX/AVM
      ARRAY(11,I)=ARRAY(11,I)+ARRAY(10,I)
      ARRAY(11,I)=ARRAY(11,I)+ARRAY(10,I)
3950  ARRAY(9,I)=CSP*ALOG(ARRAY(4,I)/TREF)-R*ALOG(ARRAY(1,I)/PREF)
4000  CONTINUE
      ARRAY(5,1)=ARRAY(5,NPTS)
C
C     SET UP ARRAYS FOR CRANK ANGLE
      DO 4500 I=1,NPTS
      IF1=I-1
4500  ARRAY(12,I)=FLOAT(IF1)*DELTA
      IF(IS.EQ.1) GO TO 4890
C
C     ARRAY(1,I)=PRESSURE ARRAY
```

142

```
C     ARRAY(2,I)=MASS ARRAY
C     ARRAY(3,I)=VOLUME ARRAY
C     ARRAY(4,I)=TEMPERATURE ARRAY
C     ARRAY(5,I)=HEAT TRANSFER AREA ARRAY
C.....ARRAY(6,I)=HEAT TRANSFER RATE(BTU/HR)
C.....ARRAY(7,I)=HEAT TRANSFER RATE(BTU/SF-HR)
C.....ARRAY(8,I)=CUMULATIVE HEAT TRANSFER(BTU)
C.....ARRAY(9,I)=SPECIFIC ENTROPY(BTU/R-LB)
C.....ARRAY(10,I)=SPECIFIC INTERNAL ENTROPY GENERATION(BTU/R-LB)
C.....ARRAY(11,I)=CUMULATIVE INT.ENT.GENERATION(BTU/R-LB)
C     ARRAY(12,I)=CRANK ANGLE ARRAY
C     CONVERSION TO S.I. UNITS
C
      DO 4550 I=1,NPTS
      ARRAY(1,I)=ARRAY(1,I)*1.01325E-01
      ARRAY(2,I)=ARRAY(2,I)*0.4536
      ARRAY(3,I)=ARRAY(3,I)*1.6387E-05
      ARRAY(4,I)=ARRAY(4,I)/1.8
      ARRAY(6,I)=ARRAY(6,I)*2.9307E-04
      ARRAY(7,I)=ARRAY(7,I)*3.1546
      ARRAY(8,I)=ARRAY(8,I)*1.0551
 4550 ARRAY(9,I)=ARRAY(9,I)*4.1868
C
      WRITE(5,4600)
      WRITE(5,4650)
      WRITE(5,4700)   (ARRAY(12,J),(ARRAY(I,J),I=1,4),J=1,NPTS)
      WRITE(5,4800)
      WRITE(5,4950)
      WRITE(5,4700)   (ARRAY(12,J),(ARRAY(I,J),I=6,9),J=1,NPTS)
 4600 FORMAT(1H1,  2X,'CRANK ANGLE', 3X,'PRESSURE',8X,'MASS',9X,'VOLUME',
     C9X,'TEMP.')
 4650 FORMAT(1H ,4X,'(DEGREE)',6X,'(MPA)',9X, '(KG)',9X,'(CU-M)',7X,
     C'(DEGREE K)',//)
 4700 FORMAT((3X,F7.0,2X,4E14.5))
```

143

```
4800 FORMAT(1H1,2X,'CRANK ANGLE',3X,'H.T.RATE',6X,'H.T.COEFF',4X
     C,'H.T.SUM',6X,'SPEC.ENTROPY')
4850 FORMAT(1H ,4X,'(DEGREE)',5X,'(KW)',8X,'(KW/SQ-M)',7X,'(KJ)',8X,
     C'(KJ/KG-K)')

C
C  PLOT INPUT DATA AND OUTPUT
C
4855 DO 4860 I=1,29
     ORFDL(1,I)=ORPDL(I)*PCALD
     ORFDL(2,I)=ORADL(I)
     ORFDH(1,I)=ORPDH(I)*PCALD
4860 ORFDH(2,I)=ORADH(I)
     DO 4865 I=1,38
     ORFIL(1,I)=ORPIL(I)*PCALI
4865 ORFIL(2,I)=ORAIL(I)
     DO 4870 I=1,41
     ORFIH(1,I)=ORPIH(I)*PCALI
4870 ORFIH(2,I)=ORAIH(I)
     READ(8,1) XLAB
     CALL PICTR(ORFDH,2,XLAB,XSCL,1,29,2,-1,1004,2,0.0,1)
     CALL PICTR(ORFDL,2,XLAB,XSCL,1,29,2,0,1000,-2,0.0,1)
     DELA=(ORFDH(2,29)-ORFDH(2,1))/28.
     AA=ORFDH(2,1)
     DO 4875 I=1,29
     THETA=AA+DELA*FLOAT(I-1)
     ORFDH(1,I)=PDIS(THETA)
4875 ORFDH(2,I)=THETA
     CALL PICTR(ORFDH,2,XLAB,XSCL,1,29,2,0,0,-2,0.0,1)
     PAUSE
     READ(8,1) XLAB
     CALL PICTR(ORFIH,2,XLAB,XSCL,1,41,2,-1,1004,2,0.0,1)
     CALL PICTR(ORFIL,2,XLAB,XSCL,1,38,2,0,1000,-2,0.0,1)
     DELA=(ORFIH(2,41)-ORFIH(2,1))/40.
```

144

```
      AA=ORFIH(2,1)
      DO 4880 I=1,41
      THETA=AA+DELA*FLOAT(I-1)
      ORFTH(1,I)=PINT(THETA)
 4880 ORFIH(2,I)=THETA
      CALL PICTR(ORFIH,2,XLAB,XSCL,1,41,2,0,0,-2,0,0,1)
      PAUSE
      MOVE=-1
      LOOK=1
      LABEL=4
C
C     COMPRESSOR PRESSURE VS. VOLUME
C
      READ(8,1) XLAB
      CALL QPICTR(ARRAY,12, 91,QY(1),QX(3),QTSCL(1),QLABEL(LABEL),
     COXLAB(XLAB),QLOOK(LOOK),QMOVE(MOVE))
      PAUSE
      CALL QPICTR(ARRAY,12, 91,QY(1),QX(3),QTSCL(31),QLABEL(LABEL),
     CQXLAB(XLAB),QLOOK(LOOK),QMOVE(MOVE))
      PAUSE
C     COMPRESSOR TEMPERATURE VS. VOLUME
 4882 READ(8,1) XLAB
      CALL QPICTR(ARRAY,12, 91,QY(4),QX(3),QTSCL(1),QLABEL(LABEL),QXLAB
     C(XLAB),QLOOK(LOOK),QMOVE(MOVE))
      PAUSE
C     PLOT COMPRESSOR PRESSURE,MASS,VOLUME,TEMPERATURE,HEAT TRANSFER
C     RATE  (KW),HEAT TRANSFER RATE(KW/SQ-M),CUMULATIVE HEAT TRANSFER
C     (KJ),SPECIFIC ENTROPY VS. CRANK ANGLE
C
C
      DO 4885 LL=1,9
      IF(LL.EQ.3) GO TO 4885
      IF(LL.EQ.5) GO TO 4885
```

```
      READ(8,1) XLAB
    1 FORMAT(40A2)
C
      CALL QPICTR(ARRAY,12, 91,QY(LL),QX(12),QISCL(1),QLABEL(LABEL),
     COXLAB(XLAB),QLOOK(LOOK),QMOVE(MOVE))
      PAUSE
 4885 CONTINUE
      IF(IS.EQ.2) GO TO 5010
C
C     SMOOTHING OF SPECIFIC ENTROPY CURVE
 4890 DO 4900 II=1,6
      I=NEHD(II)
      IF1=I-1
      I1IF1=I1+IF1
      SENHD(1,II)=ARRAY(9,I1IF1)
 4900 SENHD(2,II)=ARRAY(12,I1)+FLOAT(IF1)*DELTA
      DO 4905 II=1,7
      I=NELD(II)
      IF1=I-1
      I1IF1=I1+IF1
      SENLD(1,II)=ARRAY(9,I1IF1)
 4905 SENLD(2,II)=ARRAY(12,I1)+FLOAT(IF1)*DELTA
      DO 4950 J=I1P1,I2
      JF1=J-1
      JJ=J-I1
      THETA=DELTA*FLOAT(JF1)
      DO 4930 I=1,5
      IP1=I+1
      IF(THETA.GE.SENHD(2,I).AND.THETA.LT.SENHD(2,IP1)) GO TO 4935
 4930 CONTINUE
 4935 SLOPE=(SENHD(1,IP1)-SENHD(1,I))/(SENHD(2,IP1)-SENHD(2,I))
      TSH=SENHD(1,I)+SLOPE*(THETA-SENHD(2,I))
      DO 4940 I=1,6
```

146

```
      IP1=I+1
      IF(THETA.GE.SENLD(2,I).AND.THETA.LT.SENLD(2,IP1)) GO TO 4945
4940  CONTINUE
4945  SLOPE=(SENLD(1,IP1)-SENLD(1,I))/(SENLD(2,IP1)-SENLD(2,I))
      TSL=SENLD(1,I)+SLOPE*(THETA-SENLD(2,I))
      TS=(TSH+TSL)/2.
      SENTD(1,JJ)=TS
      SENTD(2,JJ)=THETA
      ARRAY(9,J)=TS
      VX=(TS+R*ALOG(ARRAY(1,J)/PREF))/CSP
      ARRAY(4,J)=TREF*EXP(VX)
4950  ARRAY(2,J)=ARRAY(1,J)*ARRAY(3,J)/(386.25*ARRAY(4,J)*12.)
      DO 4960  II=1,12
      I=NEXT(II)
      IF1=I-1
      I3IF1=I3+IF1
      SENHI(1,II)=ARRAY(9,I3IF1)
4960  SENHI(2,II)=ARRAY(12,I3)+FLOAT(IF1)*DELTA
      DO 4965  IT=1,7
      I=NELI(II)
      IF1=I-1
      I3IF1=I3+IF1
      SENLI(1,II)=ARRAY(9,I3IF1)
4965  SENLI(2,II)= ARRAY(12,I3)+FLOAT(IF1)*DELTA
      DO 4990  J=I3P1,I4
      JF1=J-1
      JJ=J-I3
      THETA=DELTA*FLOAT(JF1)
      DO 4970  I=1,11
      IP1=I+1
      IF(THETA.GE.SENHI(2,I).AND.THETA.LT.SENHI(2,IP1)) GO TO 4975
4970  CONTINUE
4975  SLOPE=(SENHI(1,IP1)-SENHI(1,I))/(SENHI(2,IP1)-SENHI(2,I))
```

147

```
      TSH=SENHI(1,I)+SLOPE*(THETA-SENHI(2,I))
      DO 4980 I=1,6
      IP1=I+1
      IF(THETA.GE.SENLI(2,I).AND.THETA.LT.SENLI(2,IP1)) GO TO 4985
 4980 CONTINUE
 4985 SLOPE=(SENLI(1,IP1)-SENLI(1,I))/(SENLI(2,IP1)-SENLI(2,I))
      TSL=SENLI(1,I)+SLOPE*(THETA-SENLI(2,I))
      TS=(TSH+TSL)/2.
      SENTI(1,JJ)=TS
      SENTI(2,JJ)=THETA
      ARRAY(9,J)=TS
      VX=(TS+R*ALOG(ARRAY(1,J)/PREF))/CSP
      ARRAY(4,J)=TREF*EXP(VX)
 4990 ARRAY(2,J)=ARRAY(1,J)*ARRAY(3,J)/(386.25*ARRAY(4,J)*12.)
 5000 CONTINUE
      WRITE(5,4835) ADJI,ADJD,PDV
 4835 FORMAT(1H0,10X,3F15.6)
 5010 CONTINUE
      END


PROGRAM *MAIN* HAS    NO ERRORS
```

148

```
C
C      COMPRESSOR PRESSURE FUNCTION WRT THETA
C

       FUNCTION CYLP(THETA)
       DIMENSION ORAIL(38),ORPIL(38),ORAIH(41),ORPIH(41),ORADL(29),
      C         ORPDL(29),ORADH(29),ORPDH(29),ARRAY(12,91)
       COMMON DELTA,ADJD,ADJI,ORAIL,ORPIL,ORAIH,ORPIH,ORADL,ORPDL,
      C         ORADH,ORPDH,ARRAY
       M=IFIX(THETA/DELTA)
       FM=FLOAT(M)
       MP1=M+1
       SLOPE=(ARRAY(1,MP1)-ARRAY(1,M))/DELTA
       CYLP=ARRAY(1,M)+SLOPE*(THETA-DELTA*(FM-1.))
       RETURN
       END

PROGRAM  CYLP  HAS      NO ERRORS
```

149

```
C      COMPRESSOR VOLUME IN TERMS OF CRANK ANGLE AND CLEARANCE VOL VCl
       FUNCTION CYLV(THETA,VCL)
       THETR=THETA*1.745329E-02
       Z1=.28125*SIN(THETR)
       Z2=SQRT(1.-Z1*Z1)
       Z3=2.25*(1.+COS(THETR))
       Z4=8.*(-1.+Z2)
       CYLV=VCL+7.85398*(Z3+Z4)
       RETURN
       END

PROGRAM CYLV  HAS    NO ERRORS
```

150

```
C     HEAT TRANSFER AREA
      FUNCTION HTRA(THETA)
      DATA XR,XL,RORE,PISD/2.25,8.,3.25,.75/
      DATA GAP/2.9325/
      THETR=THETA*3.14159/180.
      A0=3.14159*(RORE*RORE-PISD*PISD)/4.+GAP*2.*3.14159*(BORE+PISD)
      X1=YR*SIN(THETR)/XL
      X2=SQRT(1.-X1*X1)
      X3=YR*(1.+COS(THETR))
      X4=XL*(-1.+X2)
      HTRA=(A0+2.*3.14159*(X3+X4)*(BORE+PISD))/144.
      RETURN
      END

PROGRAM  HTRA   HAS    NO ERRORS
```

151

```
C     INTAKE ORIFICE PRESSURE DATA INPUT
      FUNCTION PINT(THETA)
      DIMENSION ORAIL(38),ORPIL(38),ORAIH(41),ORPIH(41),ORADL(29),
     1   ORPDL(29),ORADH(29),ORPDH(29),ARRAY(12,91)
C     COMMON DELTA,ADJD,ADJI,ORAIL,ORPIL,ORATH,ORPIH,ORADL,ORPDL,
     1   ORADH,ORPDH,ARRAY
C
      PCALI=2.3438
      KL=38
      KLF1=KL-1
      DO 100 I=1,KLF1
      IP1=I+1
      IF(THETA.GE.ORAIL(I).AND.THETA.LT.ORAIL(IP1)) GO TO 150
100   CONTINUE
150   SLOPE=(ORPIL(IP1)-ORPIL(I))/(ORAIL(IP1)-ORAIL(I))
      PINTL=(ORPIL(I)+SLOPE*(THETA-ORAIL(I)))*PCALI
      KH=41
      KHF1=KH-1
      DO 200 I=1,KHF1
      IP1=I+1
      IF(THETA.GE.ORPIH( I ).AND.THETA.LT.ORAIH(IP1)) GO TO 250
200   CONTINUE
250   SLOPE=(ORPIH(IP1)-ORPIH(I))/(ORAIH(IP1)-ORAIH(I))
      PINTH=(ORPIH(I)+SLOPE*(THETA-ORAIH(I)))*PCALI
      PINT=(PINTL+PINTH)/2.
      RETURN
      END


PROGRAM  PINT   HAS     NO ERRORS
```

152

```
C
C
        DISCHARGE ORIFICE PRESSURE
        FUNCTION PDIS(THETA)
        DIMENSION ORATL(38),ORPTL(38),ORAIH(41),ORPIH(41),ORADL(29),
       ORPDL(29),ORADH(29),ORPDH(29),ARRAY(12,91)
C
        COMMON DELTA,ADJD,ADJT,ORAIL,ORPIL,ORATH,ORPIH,ORADL,ORPDL,
       ORADH,ORPDH,ARRAY
C
        PCALD=2.1871
        K=29
        KF1=K-1
        DO 100 I=1,KF1
        IP1=I+1
        IF(THETA.GE.ORADL(I).AND.THETA.LT.ORADL(IP1)) GO TO 150
100     CONTINUE
150     SLOPE=(ORPDL(IP1)-ORPDL(I))/(ORADL(IP1)-ORADL(I))
        PDISL=(ORPDL(I)+SLOPE*(THETA-ORADL(I)))*PCALD
        DO 200 I=1,KF1
        IP1=I+1
        IF(THETA.GE.ORADH(I).AND.THETA.LT.ORADH(IP1)) GO TO 250
200     CONTINUE
250     SLOPE=(ORPDH(IP1)-ORPDH(I))/(ORADH(IP1)-ORADH(I))
        PDISH=(ORPDH(I)+SLOPE*(THETA-ORADH(I)))*PCALD
        PDIS=(PDISL+PDISH)/2.0
        RETURN
        END

PROGRAM  PDIS  HAS     NO ERRORS
```

153

```
C      INTAKE ORIFICE MASS FLOW RATE(LB/SEC)
       FUNCTION DMTI(THETA)
       DIMENSION ORAIL(38),ORPIL(38),ORAIH(41),ORPIH(41),ORADL(29),
      .        ORPDL(29),ORADH(29),ORPDH(29),ARRAY(12,91)
C
       COMMON DELTA,ADJD,ADJI,ORAIL,ORPIL,ORAIH,ORPIH,ORADL,ORPDL,
      .        ORADH,ORPDH,ARRAY
C
       BETAI=.4038
       XK=1.662
       CNSTI=-(.41+.35*BETAI**4)/XK
       IF(PINT(THETA).LT.0.0) GO TO 100
       FY=1.+CNSTI*PINT(THETA)/CYLP(THETA)
       DMTI=FY*129.1*SORT(PINT(THETA))/3600./ADJI
       GO TO 200
100    FY=1.-CNSTI*PINT(THETA)/CYLP(THETA)
       DMTI=-FY*129.1*SQRT(-PINT(THETA))/3600./ADJI
200    RETURN
       END

PROGRAM   DMTI   HAS      NO ERRORS
```

154

```fortran
C     INTEGRATED MASS FLOW RATE(INTAKE)
      SUBROUTINE MASI(ZI,MM)
      DIMENSION ORAIL(38),ORPIL(38),ORAIH(41),ORPIH(41),ORADL(29),
     *     ORPDL(29),ORADH(29),ORPDH(29),ARRAY(12,91)
      COMMON DELTA,ADJD,ADJT,ORAIL,ORPIL,ORATH,ORPIH,ORADL,ORPDL,
     *     ORADH,ORPDH,ARRAY
C
      NDIV=360
      XX=360./FLOAT(NDIV)
      XX=1.
      II=IFIX(ZI/DELTA)+1
      K=IFIX(DELTA/XX)
      TCMI=ARRAY(2,II)
      DO 1000 I=1,MM
      DELT=XX*FLOAT(I)
      AVDM=(DMTI(ZI+DELT)+DMTI(ZI+DELT-XX))/2.
      TCMI=TCMI+AVDM*XX/3600.
      IF(I.EQ.(I/K)*K) GO TO 990
      GO TO 1000
  990 IX=I/K+II
      ARRAY(2,IX)=TCMI
 1000 CONTINUE
      RETURN
      END

PROGRAM MASI    HAS    NO ERRORS.
```

155

```
C
      DISCHARGE ORIFICE MASS FLOW RATE(LB/SEC)
      FUNCTION DMTD(THETA)
      DIMENSION ORAIL(38),ORPIL(38),ORAIH(41),ORPIH(41),ORADL(29),
     *            ORPDL(29),ORADH(29),ORPDH(29),ARRAY(12,91)
C
      COMMON DELTA,ADJD,ADJT,ORAIL,ORPIL,ORAIH,ORPIH,ORADL,ORPDL,
     *            ORADH,ORPDH,ARRAY
C
      RETAD=.45
      XK=1.662
      CNSTD=-(.41+.35*RETAD**4)/XK
      IF(PDIS(THETA).LT.0.0) GO TO 100
      FY=1.+CNSTD*PDIS(THETA)/CYLP(THETA)
      DMTD=FY*205.35*SQRT(PDIS(THETA))/3600./ADJD
      GO TO 200
  100 FY=1.-CNSTD*PDIS(THETA)/CYLP(THETA)
      DMTD=-FY*205.35*SQRT(-PDIS(THETA))/3600./ADJD
  200 RETURN
      END

PROGRAM  DMTD   HAS      NO ERRORS
```

156

```
C     INTEGRATED MASS FLOW RATE(DISCHARGE) PFR CYCLE
      SUBROUTINE MASD(ZD,NN)
      DIMENSION OPAIL(38),ORPIL(38),ORAIH(41),ORPIH(41),ORADL(29),
     *    ORPDL(29),ORADH(29),ORPDH(29),ARRAY(12,91)
C     COMMON DELTA,ADJA,ADJD,ADJI,ORAIL,ORPIL,ORAIH,ORPIH,ORADL,ORPDL,
     *    ORADH,ORPDH,ARRAY
C
      NDIV=360
      XX=360./FLOAT(NDIV)
      XX=1.0
      II=IFIX(ZD/DELTA)+1
      TCMD=ARRAY(2,II)
      K=IFIX(DELTA/XX)
      DO 1000 I=1,NN
      DELT=XX*FLOAT(I)
      AVDM=(DMTD(ZD+DELT)+DMTD(ZD+DELT-XX))/2.
      TCMD=TCMD-AVDM*XX/3600.
      IF(I.EQ.(I/K)*K) GO TO 990
      GO TO 1000
990   IX=I/K+II
      ARRAY(2,IX)=TCMD
1000  CONTINUE
      RETURN
      END

PROGRAM  MASD    HAS       NO ERRORS
```

157

CRANK ANGLE (DEGREE)	PRESSURE (MPA)	MASS (KG)	VOLUME (CU-M)	TEMP (DEGREE K)
0.	0.24421E 02	0.28010E-02	0.10334E-02	0.29502E 03
4.	0.24454E 02	0.28010E-02	0.10325E-02	0.29516E 03
8.	0.24555E 02	0.28010E-02	0.10298E-02	0.29561E 03
12.	0.24724E 02	0.28010E-02	0.10253E-02	0.29635E 03
16.	0.24962E 02	0.28010E-02	0.10191E-02	0.29738E 03
20.	0.25271E 02	0.28010E-02	0.10112E-02	0.29872E 03
24.	0.25651E 02	0.28010E-02	0.10016E-02	0.30035E 03
28.	0.26105E 02	0.28010E-02	0.99050E-03	0.30227E 03
32.	0.26636E 02	0.28010E-02	0.97791E-03	0.30450E 03
36.	0.27245E 02	0.28010E-02	0.96394E-03	0.30702E 03
40.	0.27937E 02	0.28010E-02	0.94870E-03	0.30983E 03
44.	0.28714E 02	0.28010E-02	0.93230E-03	0.31294E 03
48.	0.29580E 02	0.28010E-02	0.91486E-03	0.31635E 03
52.	0.30538E 02	0.28010E-02	0.89651E-03	0.32004E 03
56.	0.31591E 02	0.28010E-02	0.87738E-03	0.32402E 03
60.	0.32744E 02	0.28010E-02	0.85761E-03	0.32828E 03
64.	0.34000E 02	0.28010E-02	0.83733E-03	0.33281E 03
68.	0.35362E 02	0.28010E-02	0.81669E-03	0.33760E 03
72.	0.36833E 02	0.28010E-02	0.79580E-03	0.34265E 03
76.	0.38415E 02	0.28010E-02	0.77481E-03	0.34794E 03
80.	0.40109E 02	0.28010E-02	0.75383E-03	0.35346E 03
84.	0.41917E 02	0.28010E-02	0.73300E-03	0.35918E 03
88.	0.43836E 02	0.28010E-02	0.71243E-03	0.36508E 03
92.	0.45867E 02	0.28010E-02	0.69221E-03	0.37115E 03
96.	0.48003E 02	0.28010E-02	0.67246E-03	0.37736E 03
100.	0.50241E 02	0.28010E-02	0.65326E-03	0.38367E 03
104.	0.51327E 02	0.27611E-02	0.63469E-03	0.38634E 03
108.	0.51327E 02	0.26867E-02	0.61693E-03	0.38586E 03
112.	0.51241E 02	0.26138E-02	0.59973E-03	0.38498E 03
116.	0.50895E 02	0.25392E-02	0.58345E-03	0.38308E 03
120.	0.50641E 02	0.24693E-02	0.56803E-03	0.38145E 03
124.	0.50545E 02	0.24088E-02	0.55352E-03	0.38031E 03
128.	0.50493E 02	0.23536E-02	0.53994E-03	0.37930E 03
132.	0.50476E 02	0.23047E-02	0.52722E-03	0.37817E 03
136.	0.50462E 02	0.22598E-02	0.51566E-03	0.37706E 03
140.	0.50459E 02	0.22194E-02	0.50502E-03	0.37598E 03
144.	0.50456E 02	0.21831E-02	0.49539E-03	0.37491E 03
148.	0.50449E 02	0.21509E-02	0.48675E-03	0.37392E 03
152.	0.50445E 02	0.21231E-02	0.47913E-03	0.37276E 03
156.	0.50443E 02	0.20998E-02	0.47253E-03	0.37170E 03
160.	0.50445E 02	0.20808E-02	0.46694E-03	0.37066E 03
164.	0.50449E 02	0.20663E-02	0.46237E-03	0.36963E 03
168.	0.50464E 02	0.20566E-02	0.45881E-03	0.36864E 03
172.	0.50465E 02	0.20499E-02	0.45628E-03	0.36781E 03
176.	0.50452E 02	0.20465E-02	0.45476E-03	0.36709E 03

180.	0.50359E 02	0.20450E-02	0.45425E-03	0.36627E 03
184.	0.50193E 02	0.20450E-02	0.45476E-03	0.36547E 03
188.	0.49901E 02	0.20450E-02	0.45629E-03	0.36456E 03
192.	0.49425E 02	0.20450E-02	0.45881E-03	0.36309E 03
196.	0.48777E 02	0.20450E-02	0.46237E-03	0.36111E 03
200.	0.47975E 02	0.20450E-02	0.46694E-03	0.35868E 03
204.	0.47034E 02	0.20450E-02	0.47252E-03	0.35585E 03
208.	0.45971E 02	0.20450E-02	0.47913E-03	0.35257E 03
212.	0.44804E 02	0.20450E-02	0.48675E-03	0.34919E 03
216.	0.43551E 02	0.20450E-02	0.49539E-03	0.34544E 03
220.	0.42229E 02	0.20450E-02	0.50503E-03	0.34148E 03
224.	0.40857E 02	0.20450E-02	0.51568E-03	0.33735E 03
228.	0.39450E 02	0.20450E-02	0.52732E-03	0.33309E 03
232.	0.38025E 02	0.20450E-02	0.53994E-03	0.32873E 03
236.	0.36596E 02	0.20450E-02	0.55352E-03	0.32434E 03
240.	0.35177E 02	0.20450E-02	0.56803E-03	0.31994E 03
244.	0.33780E 02	0.20450E-02	0.58345E-03	0.31556E 03
248.	0.32414E 02	0.20450E-02	0.59973E-03	0.31126E 03
252.	0.31090E 02	0.20450E-02	0.61683E-03	0.30705E 03
256.	0.29814E 02	0.20450E-02	0.63469E-03	0.30298E 03
260.	0.28592E 02	0.20450E-02	0.65326E-03	0.29907E 03
264.	0.27432E 02	0.20450E-02	0.67246E-03	0.29536E 03
268.	0.26338E 02	0.20450E-02	0.69221E-03	0.29191E 03
272.	0.25317E 02	0.20450E-02	0.71243E-03	0.28879E 03
276.	0.24387E 02	0.20450E-02	0.73300E-03	0.28622E 03
280.	0.23751E 02	0.20637E-02	0.75383E-03	0.28408E 03
284.	0.23716E 02	0.21129E-02	0.77481E-03	0.28477E 03
288.	0.23673E 02	0.21624E-02	0.79580E-03	0.28527E 03
292.	0.23640E 02	0.22122E-02	0.81669E-03	0.28577E 03
296.	0.23629E 02	0.22639E-02	0.83733E-03	0.28616E 03
300.	0.23619E 02	0.23148E-02	0.85761E-03	0.28654E 03
304.	0.23609E 02	0.23653E-02	0.87738E-03	0.28677E 03
308.	0.23612E 02	0.24145E-02	0.89651E-03	0.28708E 03
312.	0.23621E 02	0.24622E-02	0.91486E-03	0.28738E 03
316.	0.23666E 02	0.25101E-02	0.93230E-03	0.28783E 03
320.	0.23732E 02	0.25560E-02	0.94870E-03	0.28842E 03
320.	0.23732E 02	0.25560E-02	0.94870E-03	0.28842E 03
324.	0.23806E 02	0.25996E-02	0.96394E-03	0.28904E 03
328.	0.23882E 02	0.26402E-02	0.97791E-03	0.28965E 03
332.	0.23955E 02	0.26756E-02	0.99050E-03	0.29027E 03
336.	0.24023E 02	0.27092E-02	0.10016E-02	0.29089E 03
340.	0.24125E 02	0.27391E-02	0.10112E-02	0.29152E 03
344.	0.24227E 02	0.27641E-02	0.10191E-02	0.29248E 03
348.	0.24331E 02	0.27940E-02	0.10253E-02	0.29341E 03
352.	0.24384E 02	0.27957E-02	0.10298E-02	0.29411E 03
356.	0.24419E 02	0.28020E-02	0.10325E-02	0.29464E 03
360.	0.24419E 02	0.28010E-02	0.10334E-02	0.29500E 03

CRANK ANGLE (DEGREE)	H.T.RATE (KW)	H.T.COEFF (KW/SQ-M)	H.T.SUM (KJ)	SPEC.ENTROPY (KJ/KG-K)
0.	0.00000E 00	0.00000E 00	0.00000E 00	-0.58466E 01
4.	-0.18793E 00	-0.14978E 04	-0.75174E 01	-0.58468E 01
8.	-0.56146E 00	-0.44871E 04	-0.29977E 02	-0.58475E 01
12.	-0.94124E 00	-0.75564E 04	-0.67628E 02	-0.58488E 01
16.	-0.13193E 01	-0.10659E 05	-0.12040E 03	-0.58505E 01
20.	-0.16947E 01	-0.13803E 05	-0.18820E 03	-0.58526E 01
24.	-0.20729E 01	-0.17050E 05	-0.27112E 03	-0.58553E 01
28.	-0.24535E 01	-0.20416E 05	-0.36926E 03	-0.58584E 01
32.	-0.28222E 01	-0.23798E 05	-0.48215E 03	-0.58620E 01
36.	-0.32131E 01	-0.27503E 05	-0.61068E 03	-0.58660E 01
40.	-0.35749E 01	-0.31111E 05	-0.75369E 03	-0.58705E 01
44.	-0.39637E 01	-0.35126E 05	-0.91224E 03	-0.58754E 01
48.	-0.43317E 01	-0.39150E 05	-0.10855E 04	-0.58806E 01
52.	-0.47050E 01	-0.43431E 05	-0.12737E 04	-0.58863E 01
56.	-0.50643E 01	-0.47811E 05	-0.14763E 04	-0.58923E 01
60.	-0.54191E 01	-0.52383E 05	-0.16930E 04	-0.58987E 01
64.	-0.57694E 01	-0.57191E 05	-0.19232E 04	-0.59054E 01
68.	-0.61093E 01	-0.62164E 05	-0.21682E 04	-0.59124E 01
72.	-0.64299E 01	-0.67226E 05	-0.24254E 04	-0.59196E 01
76.	-0.67395E 01	-0.72467E 05	-0.26950E 04	-0.59271E 01
80.	-0.70158E 01	-0.77643E 05	-0.29757E 04	-0.59348E 01
84.	-0.72922E 01	-0.83116E 05	-0.32674E 04	-0.59426E 01
88.	-0.75304E 01	-0.88445E 05	-0.35686E 04	-0.59506E 01
92.	-0.77283E 01	-0.93567E 05	-0.38777E 04	-0.59586E 01
96.	-0.79086E 01	-0.98724E 05	-0.41941E 04	-0.59667E 01
100.	-0.80554E 01	-0.10369E 06	-0.45163E 04	-0.59748E 01
104.	-0.11125E 02	-0.14765E 06	-0.49613E 04	-0.59831E 01
108.	-0.12235E 02	-0.16737E 06	-0.54508E 04	-0.59896E 01
112.	-0.13376E 02	-0.18855E 06	-0.59858E 04	-0.59980E 01
116.	-0.15789E 02	-0.22918E 06	-0.66174E 04	-0.60097E 01
120.	-0.14421E 02	-0.21539E 06	-0.71943E 04	-0.60214E 01
124.	-0.13212E 02	-0.20288E 06	-0.77228E 04	-0.60331E 01
128.	-0.12374E 02	-0.19514E 06	-0.82178E 04	-0.60448E 01
132.	-0.14002E 02	-0.22648E 06	-0.87779E 04	-0.60595E 01
136.	-0.13307E 02	-0.22048E 06	-0.93102E 04	-0.60743E 01
140.	-0.12665E 02	-0.21460E 06	-0.98168E 04	-0.60890E 01
144.	-0.12119E 02	-0.20968E 06	-0.10302E 05	-0.61037E 01
148.	-0.11581E 02	-0.20421E 06	-0.10765E 05	-0.61184E 01
152.	-0.11150E 02	-0.19999E 06	-0.11211E 05	-0.61331E 01
156.	-0.10784E 02	-0.19635E 06	-0.11642E 05	-0.61478E 01
160.	-0.10441E 02	-0.19258E 06	-0.12060E 05	-0.61624E 01
164.	-0.10199E 02	-0.19014E 06	-0.12468E 05	-0.61770E 01
168.	-0.10045E 02	-0.18885E 06	-0.12870E 05	-0.61916E 01
172.	-0.79293E 01	-0.14997E 06	-0.13187E 05	-0.62033E 01
176.	-0.65870E 01	-0.12504E 06	-0.13450E 05	-0.62130E 01

160

180.	-0.78300E 01	-0.14881E 06	-0.13764E 05	-0.62208E 01
184.	-0.30040E 01	-0.57024E 05	-0.13884E 05	-0.62253E 01
188.	-0.56982E 00	-0.10777E 05	-0.13906E 05	-0.62262E 01
192.	-0.74989E 00	-0.14098E 05	-0.13936E 05	-0.62273E 01
196.	-0.69583E 00	-0.12972E 05	-0.13964E 05	-0.62284E 01
200.	-0.43490E 00	-0.80218E 04	-0.13982E 05	-0.62292E 01
204.	-0.29961E-02	-0.54556E 02	-0.13982E 05	-0.62293E 01
208.	0.52926E 00	0.94932E 04	-0.13961E 05	-0.62296E 01
212.	0.11571E 01	0.20404E 05	-0.13914E 05	-0.62270E 01
216.	0.18409E 01	0.31850E 05	-0.13841E 05	-0.62243E 01
220.	0.25621E 01	0.43414E 05	-0.13738E 05	-0.62204E 01
224.	0.33379E 01	0.55305E 05	-0.13605E 05	-0.62153E 01
228.	0.41321E 01	0.66839E 05	-0.13439E 05	-0.62088E 01
232.	0.49277E 01	0.77709E 05	-0.13242E 05	-0.62009E 01
236.	0.57634E 01	0.88500E 05	-0.13012E 05	-0.61916E 01
240.	0.65861E 01	0.98372E 05	-0.12748E 05	-0.61807E 01
244.	0.74214E 01	0.10772E 06	-0.12451E 05	-0.61683E 01
248.	0.82541E 01	0.11635E 06	-0.12121E 05	-0.61543E 01
252.	0.90750E 01	0.12415E 06	-0.11758E 05	-0.61386E 01
256.	0.99053E 01	0.13146E 06	-0.11362E 05	-0.61212E 01
260.	0.10743E 02	0.13829E 06	-0.10932E 05	-0.61021E 01
264.	0.11645E 02	0.14537E 06	-0.10466E 05	-0.60811E 01
268.	0.12688E 02	0.15362E 06	-0.99589E 04	-0.60579E 01
272.	0.14043E 02	0.16493E 06	-0.93972E 04	-0.60319E 01
276.	0.16535E 02	0.18847E 06	-0.87357E 04	-0.60009E 01
280.	0.82686E 01	0.91508E 05	-0.84050E 04	-0.59853E 01
284.	0.79949E 01	0.85966E 05	-0.80852E 04	-0.59696E 01
288.	0.68518E 01	0.71637E 05	-0.78111E 04	-0.59567E 01
292.	0.65854E 01	0.67009E 05	-0.75477E 04	-0.59447E 01
296.	0.46193E 01	0.45790E 05	-0.73629E 04	-0.59366E 01
300.	0.45529E 01	0.44017E 05	-0.71808E 04	-0.59290E 01
304.	0.31892E 01	0.30108E 05	-0.70532E 04	-0.59239E 01
308.	0.34811E 01	0.32133E 05	-0.69139E 04	-0.59186E 01
312.	0.32722E 01	0.29574E 05	-0.67830E 04	-0.59139E 01
316.	0.29143E 01	0.25826E 05	-0.66665E 04	-0.59098E 01
320.	0.36716E 01	0.31952E 05	-0.65196E 04	-0.59048E 01
324.	0.37024E 01	0.31691E 05	-0.63715E 04	-0.59001E 01
328.	0.35144E 01	0.29636E 05	-0.62309E 04	-0.58958E 01
332.	0.39645E 01	0.32989E 05	-0.60723E 04	-0.58910E 01
336.	0.40343E 01	0.33183E 05	-0.59110E 04	-0.58862E 01
340.	0.41223E 01	0.33575E 05	-0.57461E 04	-0.58814E 01
344.	0.53638E 01	0.43334E 05	-0.55315E 04	-0.58750E 01
348.	0.62984E 01	0.50564E 05	-0.52796E 04	-0.58672E 01
352.	0.61328E 01	0.49013E 05	-0.50342E 04	-0.58595E 01
356.	0.49644E 01	0.39567E 05	-0.48356E 04	-0.58531E 01
360.	0.46931E 01	0.37371E 05	-0.46479E 04	-0.58467E 01

```
┌─────────────────────────────────┐
│  Input data P(θ), V(θ), TBOC    │
│                                  │
│        ΔP(θ) of orifices        │
└─────────────────────────────────┘
              │
┌─────────────────────────────────┐
│     Calculate mass flow rate     │
│      using orifice equation      │
│                                  │
│        ṁ(θ) = f (ΔP(θ))         │
└─────────────────────────────────┘
              │
┌─────────────────────────────────┐
│  Integrate ṁ(θ) during intake   │
│ and discharge to get mass flow   │
│       per cycle m_f from         │
│                                  │
│      m_f(θ) = ∫ ṁ(θ) dθ/ω       │
└─────────────────────────────────┘
              │
┌─────────────────────────────────┐
│  Calculate clearance mass m_c from │
│                                  │
│    m_c = PV / (R TBOC) - m_f(θ_o) │
└─────────────────────────────────┘
              │
┌─────────────────────────────────┐
│ Calculate mixed mean temperature T(θ) from │
│                                  │
│      T(θ) = P(θ) V(θ) / M(θ)    │
└─────────────────────────────────┘
              │
┌─────────────────────────────────┐
│     Calculate specific entropy s │
│         of the gas from          │
│                                  │
│  s = s_ref. + c_p log (T/T_ref.) │
│                                  │
│        - R log (P/P_ref.)        │
└─────────────────────────────────┘
              │
┌─────────────────────────────────┐
│   Smoothe out the entropy curve  │
│ In order to decrease the mismatch │
│       among P,V,m,T data         │
└─────────────────────────────────┘
              │
┌─────────────────────────────────┐
│ Calculate  new mixed mean temperature │
│      heat transfer rate etc.     │
│      from the new entropy valve  │
└─────────────────────────────────┘
```

Fig. E-1   Flow chart for the First Law Integral
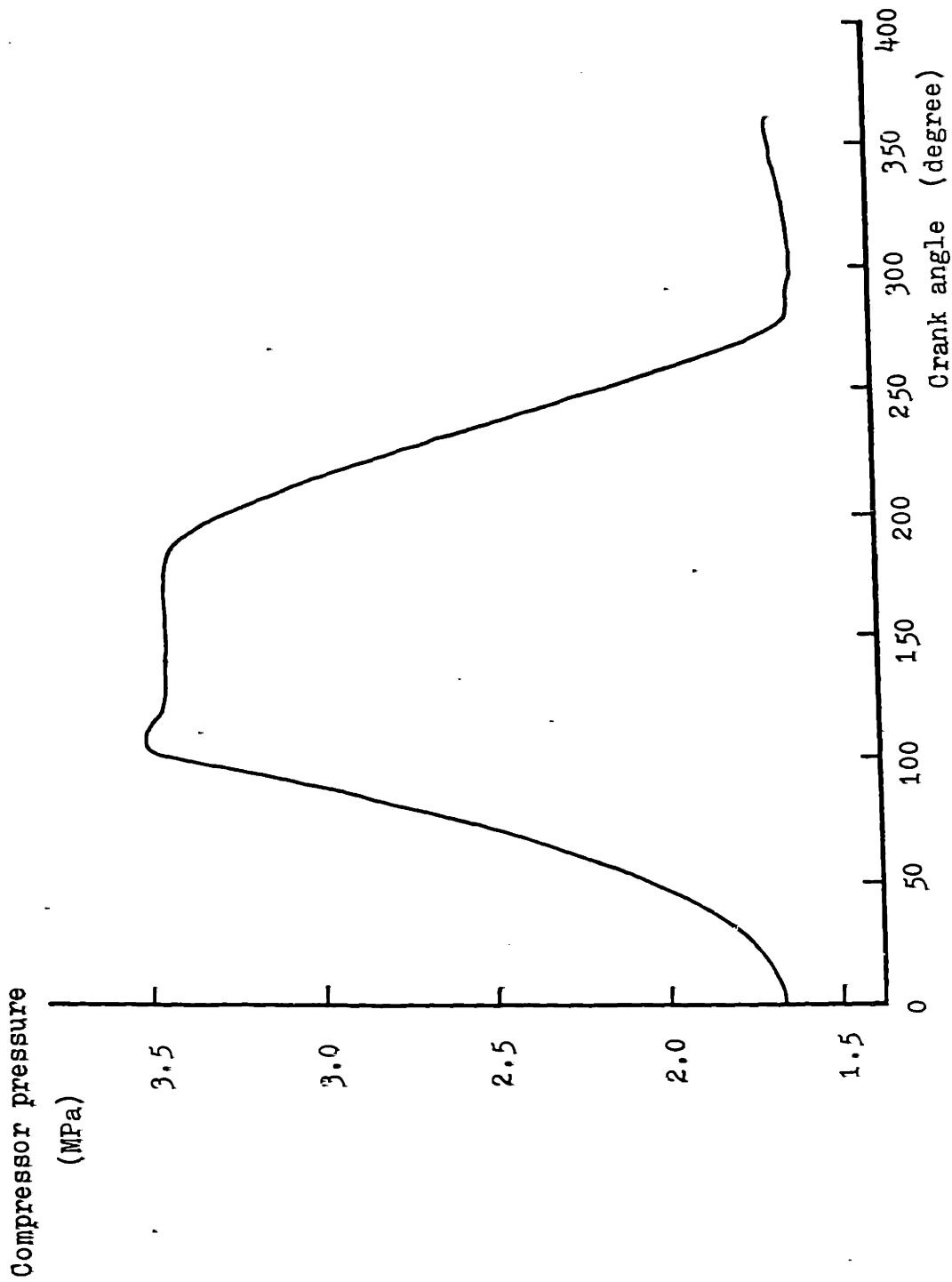Analysis program

162

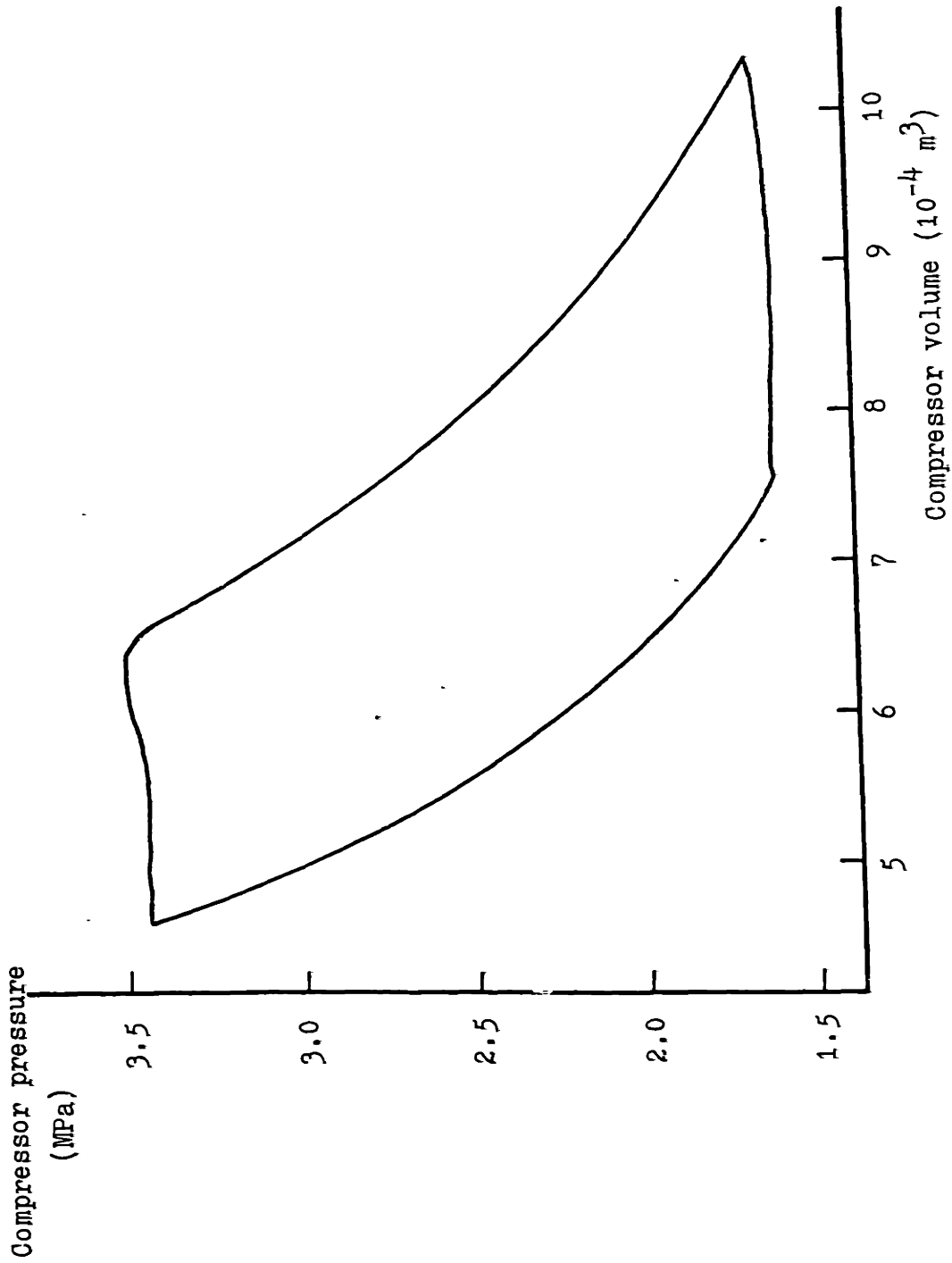Fig. E-2 Compressor pressure vs. crank angle - input data

163

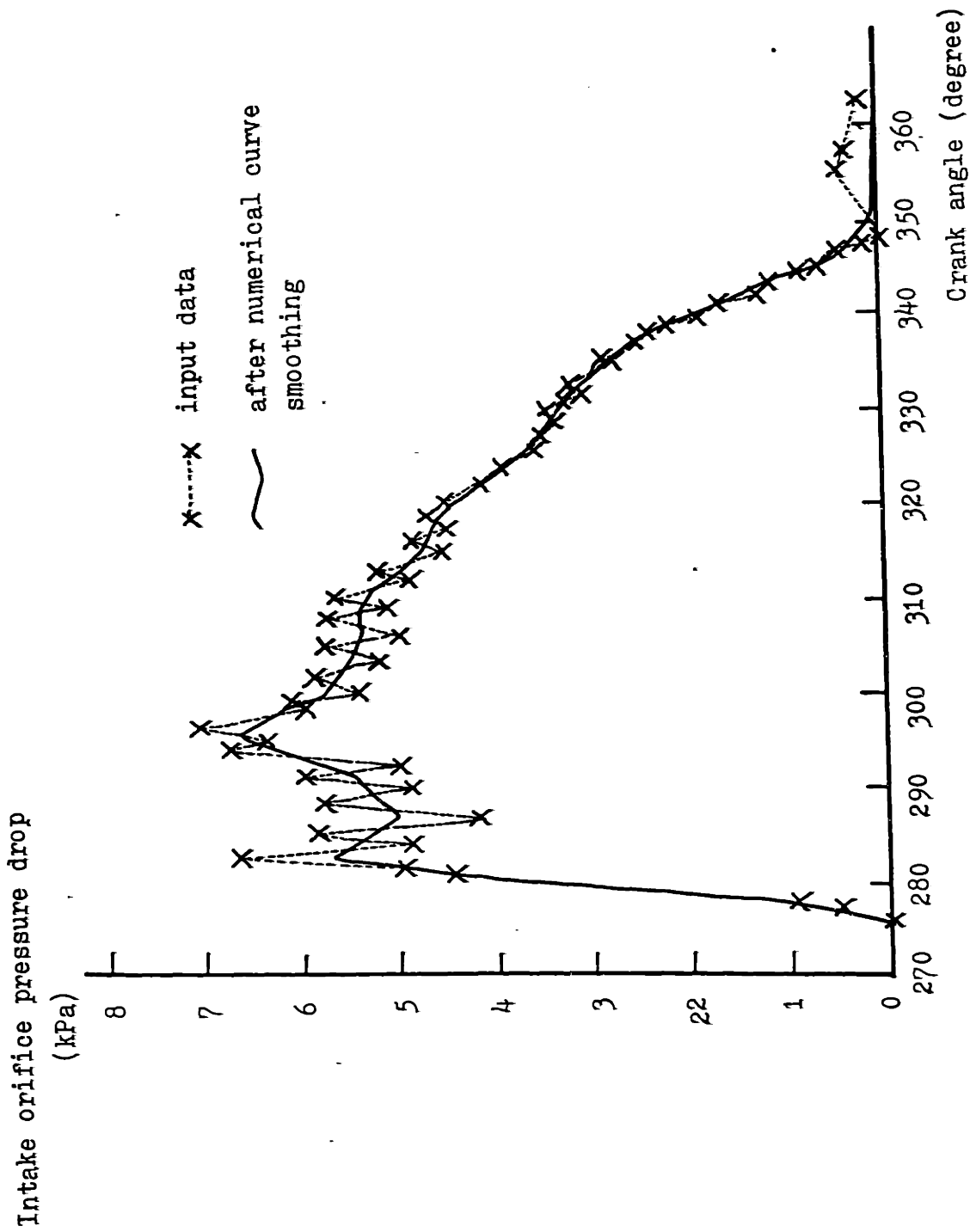Fig. E-3 Compressor pressure vs. volume - input data

164

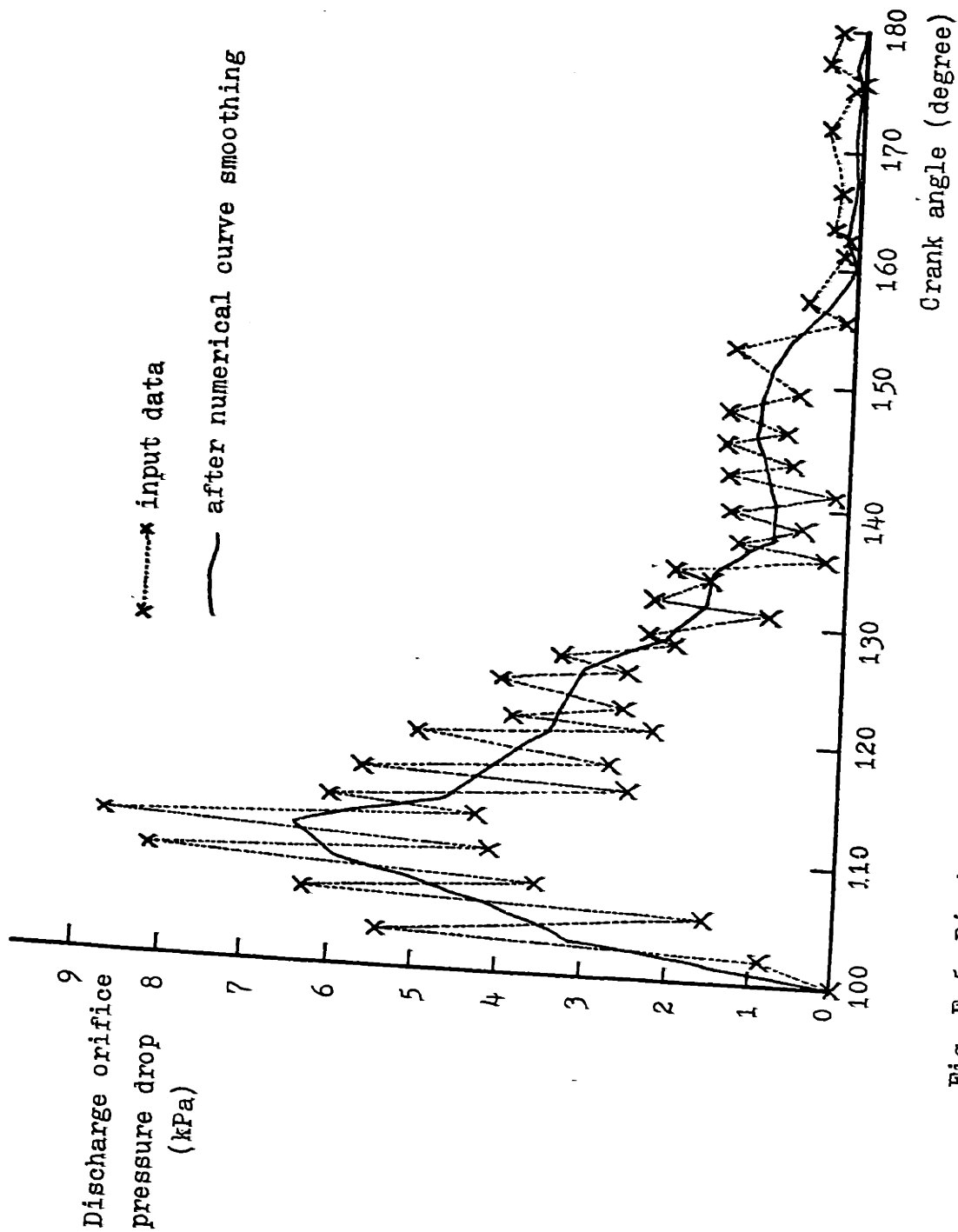Fig. E-4 Intake orifice pressure drop vs. crank angle
– input data

Fig. E-5 Discharge orifice pressure drop vs. crank angle - input data
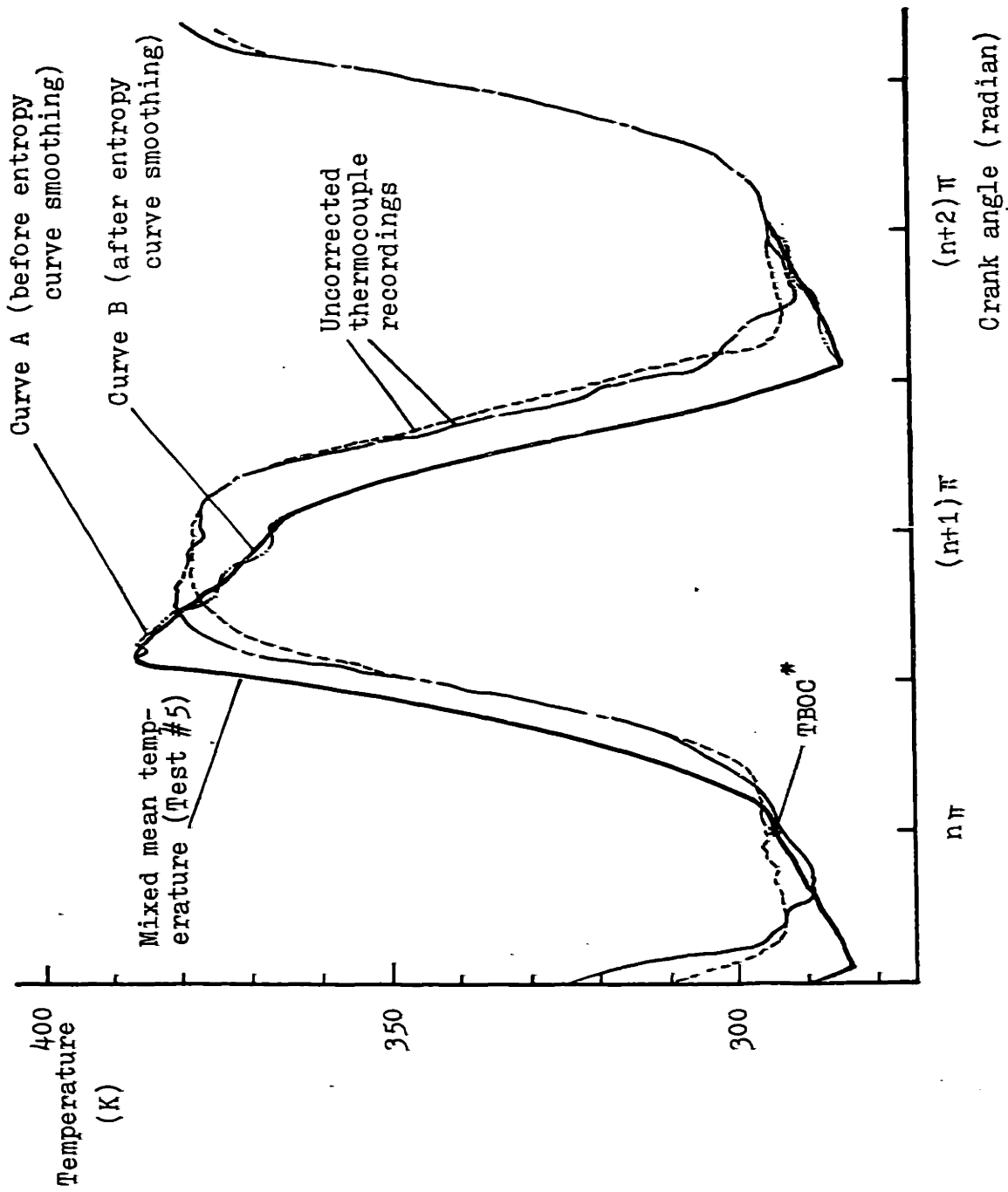
166

Fig. E-6 Comparison of calculated mixed mean temperature and thermocouple recordings.
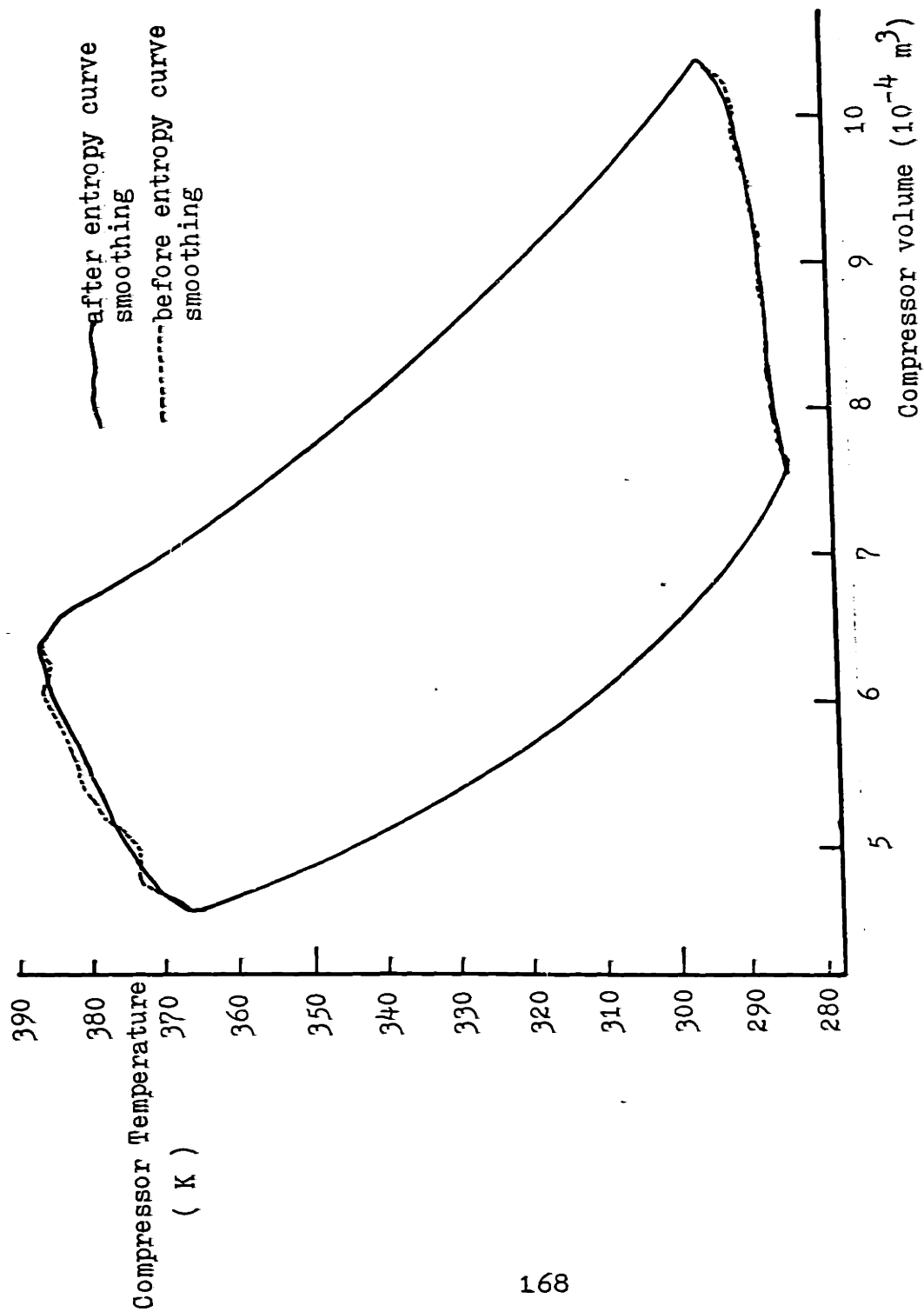
* See Appendix E

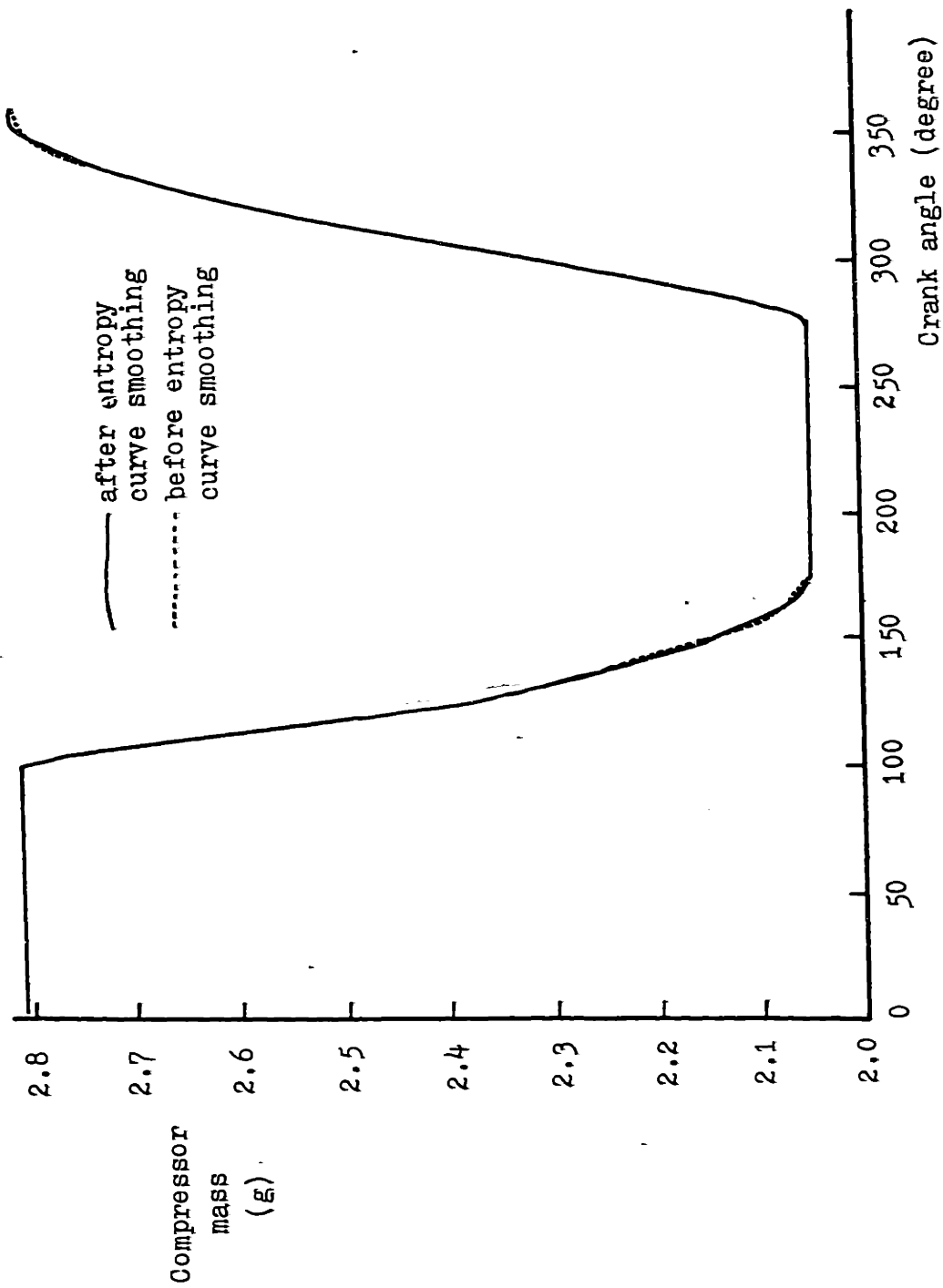Fig. E-7 Compressor gas temperature vs. volume
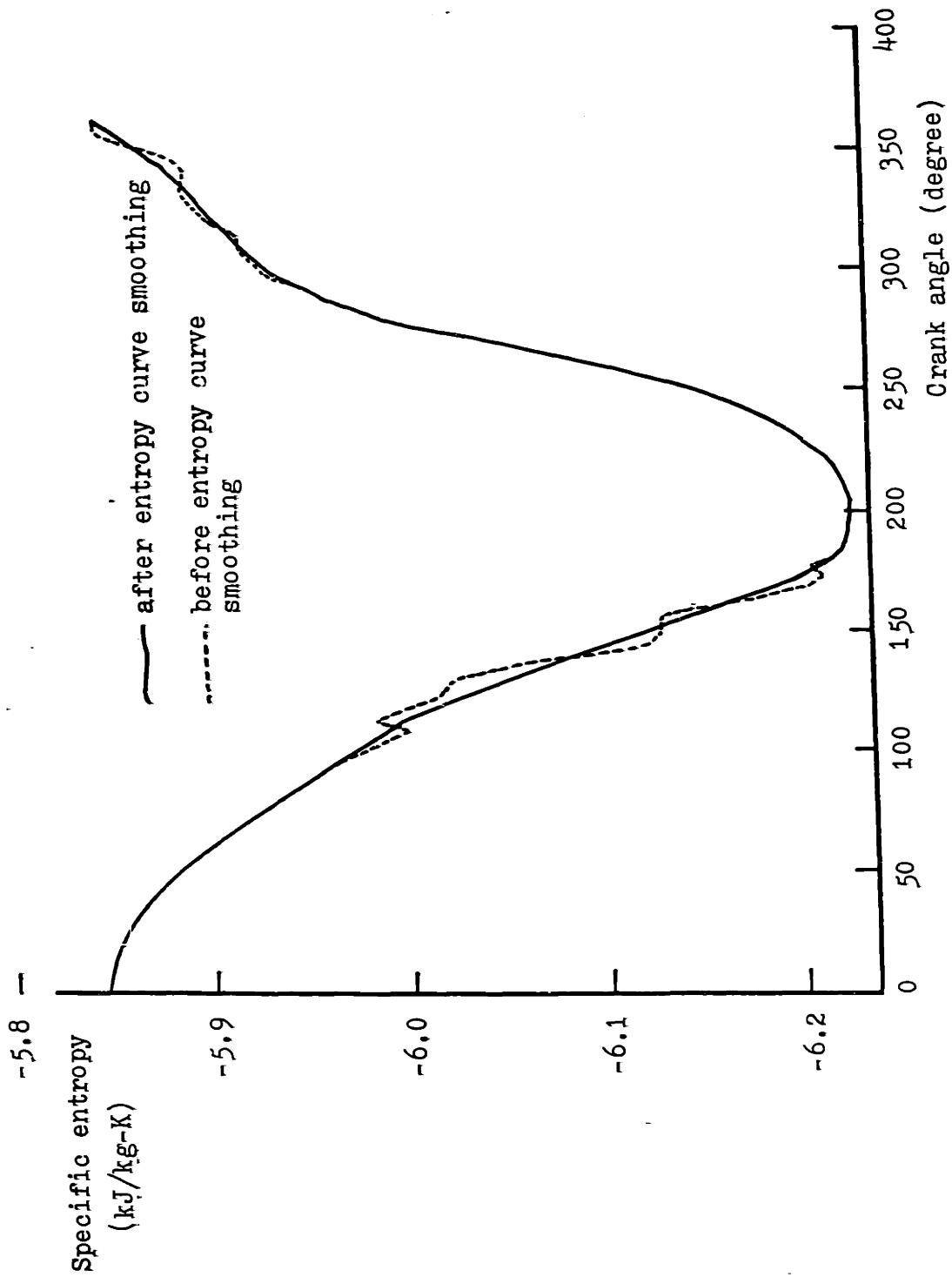
168

Fig. E-8   Mass of the gas vs. crank angle for compressor

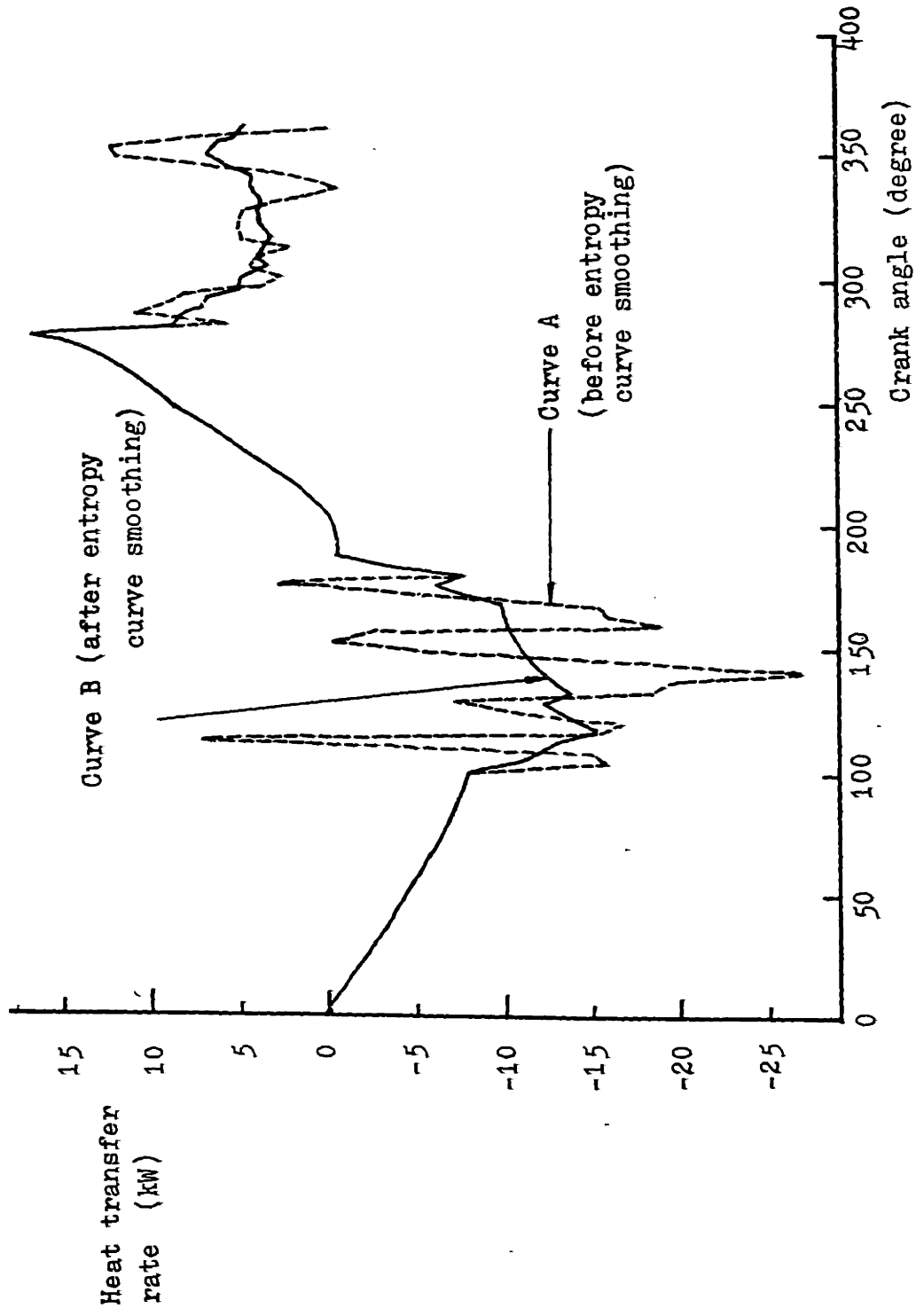Fig. E-9 Specific entropy of the gas vs. crank angle for compressor

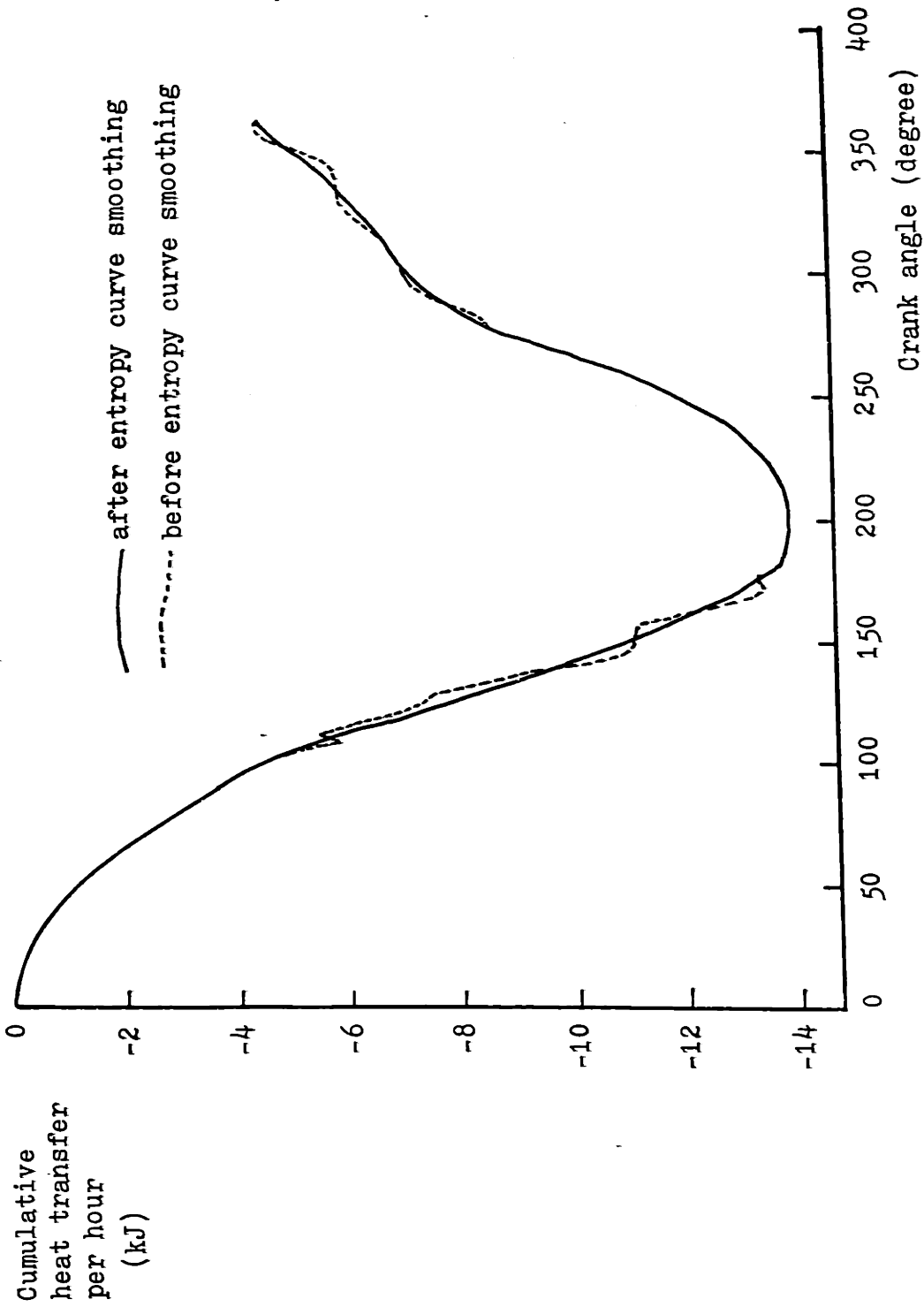Fig. E-10 Heat transfer rate vs. crank angle for compressor

171

Fig. E-11 Cumulative heat transfer vs. crank angle for compressor

BIOGRAPHICAL NOTE

The author was born in Kyunggi do, Korea on January 9, 1945. He attended Kyunggi Middle School, and Kyunggi High School in Seoul, Korea.

In 1964, he entered Seoul National University, and received B.S. in mechanical engineering in 1972. Between 1965 and 1968, he served in the army of the Republic of Korea.

In 1972, he came to the United States and entered Clarkson College of Technology, Potsdam, N.Y., and took graduate courses for one year. He entered M.I.T. in 1973, and received S.M. degree in 1974, specializing in Acoustics. He held research assistantships for four and half years at M.I.T.

The following paper was co-authored by him :
K.P. Lee and H.G. Davies, "Nomogram for estimating noise propagation in urban areas", J. Acoust. Soc. AM. Vol. 57, No. 6, Part II, June 1975, pp. 1477-1480.